Spring 5-2022

Mechanistic Undrestanding Of Amorphization In Iron-Based Soft Magnetic Materials

Taban Larimian

MECHANISTIC UNDRESTANDING OF AMORPHIZATION IN IRON-BASED SOFT MAGNETIC MATERIALS

TABAN LARIMIAN

Bachelor of Science in Mechanical Engineering-Manufacturing Engineering

Arak University

MARCH 2016

Master of Science in Mechanical Engineering

Cleveland State University

MAY 2021

Dissertation Prepared for the Degree of

DOCTOR OF PHILOSOPHY IN MECHANICAL ENGINEERING

At the

CLEVELAND STATE UNIVERSITY

MAY 2022

ACKNOWLEDGEMENTS

I express my deep gratitude and appreciation to my advisor Dr. Tushar Borkar, for giving me the biggest opportunity of my life by accepting me as his first Ph.D. student. I thank him for his patience and guidance throughout the years and for teaching me everything I know about doing research.

I would like to thank my committee, Dr. Majid Rashidi, Dr. Petru Fodor, Dr. Maryam Younessi, and Dr. Somnath Chattopadhyay, for lending me their precious time and providing me with guidance.

I thank Dr. Varun Chaudhary, Dr. Raju Ramanujan, and Dr. Rajeev Gupta for their valuable comments and for helping me with some of the experiments. I also thank my friends Jijo and Farooq from North Carolina State University for helping me in various stages of my research. I thank Mr. Miroslav Bogdanovski for teaching me how to use the SEM and let me use it many, many times in the past five years.

I thank my lab mates and dear friends, Amit, Ganesh, Adarsh, Prashanth, Calvin, Brad, Mahesh, Anthony, Evodia, Manoj, Amit Jr., and Sanoj for making going to the lab so much fun. Thank you, guys, for the great memories.

I thank my high school teachers, Mr. Hadi Farshi and Ms. Leila Akhlaghi, who were the reason I decided to be an engineer, and my college professors, who helped me become one.

Last but not least, I would like to thank my family for their emotional support and for always helping me get through the hard times. Maman, baba, Mobi, I could not have done it without you. Arash and Taimaz, you have always been my best source of guidance and words cannot describe how grateful I am. And Timi, this is for you.

MECHANISTIC UNDRESTANDING OF AMORPHIZATION IN IRON-BASED SOFT MAGNETIC MATERIALS

TABAN LARIMIAN

ABSTRACT

Iron-based magnetic alloys possess very good magnetic and mechanical properties. Among these alloys Fe-Si-B-based alloys show outstanding saturation magnetization and coercivity which makes them great candidates for many industrial applications.

Addition of certain elements to the Fe-Si-B base is proven to improve the homogeneity and fineness of microstructure as well as enhance the magnetic behavior of these alloys. In this research work, we have studied the effect of adding copper and niobium to the Fe-Si-B base alloy.

Previous studies have shown that magnetic alloys show better magnetic properties when their microstructure consists of nanocrystals embedded in an amorphous matrix. In order to reach amorphization, magnetic alloys are traditionally melted and then cooled down very fast to prevent crystallization and grain growth in their microstructure. However, there are several disadvantages associated with this method of fabrication, such as the limitation in thickness of the products.

To solve this issue, we proposed a new method of fabrication for magnetic alloys where amorphization occurs through mechanical alloying, and the amorphous powder alloy that is produced by this process is then consolidated using a technique called spark plasma sintering

finding appropriate mechanical alloying processing parameters to get an amorphous structure. Many different processing parameters were investigated, and the mechanical properties, microstructure, and magnetic properties of all samples were examined. The effect of spark plasma sintering processing parameters on samples sintered from the amorphous powders was then studied.

Finally, the amount of energy introduced to the powder from the milling balls during the mechanical alloying process was calculated. We were able to find a trend between the energy introduced to the powder during the milling process and the amorphous structure of the milled powders. From our data, we draw an energy map that shows the window of total energy in which the powder, regardless of the mechanical alloying processing parameters under which it was milled, will show an amorphous structure. This area has not been explored for these magnetic alloys before, and this data can be used by researchers who are trying to obtain amorphization via the mechanical alloying process.

TABALE OF CONTENT

Page

LIST OF TABLES

LIST OF FIGURES

CHAPTER I

LITERATURE REVIEW

1.1. Iron-based magnetic materials and FeSiB based magnetic alloy system

Amorphous alloys are a type of alloy with no crystal segregation or specific atomic configuration [1]. Materials with amorphous structures usually exhibit better mechanical properties such as higher yield and tensile strength, better corrosion and wear resistance, and lower elastic modulus in comparison to their crystalline counterparts [2-6]. The main reason for the better mechanical properties observed in materials with amorphous structures is the lack of crystal defects such as grain boundaries and dislocations in the structure of these materials. Due to these mechanical advantages and many practical applications, metallic materials with amorphous structures have been the subject of interest in many fundamental studies [7].

Among the amorphous metallic materials with different compositions, iron-based amorphous alloys have gained a lot of attention. The iron-based amorphous alloys not only possess the excellent mechanical properties associated with the amorphous metallic materials but also have the advantage of being cheap and easy to access and handle [8-9]. Additionally, iron-based amorphous alloys are great candidates for the fabrication of magnetic alloys. Studies have shown some magnetic alloys with iron as the base/main

element (matrix) with Fe(Si) nanocrystals dispersed in the matrix show outstanding magnetic properties.

One of the major advantages of Fe-based amorphous magnetic alloys is having fast-flux reversal and low magnetic loss, which makes these alloys great candidates for applications in energy-efficient transformers, power electronics, and sensing devices. Iron-based magnetic alloys also have applications in everyday used devices such as mobile phones, hearing devices, and computer hard disks [10-12]. According to Alben et al. [13], amorphous iron-based magnetics have high permeability and low coercivity values due to the magnetization vectors being parallel to each other in such materials. Due to these good magnetic properties and their relatively high hardness and strength, iron-based magnetic alloys have application in industries such as aerospace and defense [14-16]. Additionally, iron-based magnetic alloys are great candidates for applications in sensors and inductive devices due to their ability to exhibit high permeability while maintaining a high saturation magnetization [17-19]. Some of the most critical applications of iron-based magnetic alloys are in magnetic components that are used in wind power generators and converting inductors in hybrid and electric vehicles. Due to the recent problems of increased air pollution from vehicles and demands for cleaner and more sustainable energy, finding new techniques for optimizing the mechanical and magnetic properties and increasing the efficiency of these magnetic components is an absolute necessity.

Among the iron-based magnetic alloys, the ones made of the three main elements of iron, silicon, and boron possess outstanding magnetic properties such as high permeability while maintaining high saturation magnetization along with low coercivity

[20-21].We chose FeSiB-based alloys for our investigations due to these outstanding magnetic properties which according to past research is due to the embedment of Fe(Si) nanocrystals in the iron matrix [22-24].

Higher saturation magnetization and lower coercivity can be obtained in FeSiB-based alloys by the addition of small quantities of other elements to the base composition [25]. The addition of copper and niobium elements to the FeSiB-based magnetic alloys can affect their mechanical and magnetic properties, microstructure, and transformation of phases present. Studies have shown the addition of these two elements mostly has a positive effect on FeSiB-based magnetic alloys and improves the mechanical and magnetic properties of these alloys [26].

When copper is added to the composition, it can act as a nucleation site for α-Fe(Si) nanocrystals which can increase the presence of these nanocrystals in the amorphous matrix [27]. On the other hand, the addition of niobium can help prevent or reduce excessive growth of grains and retain a fine microstructure in the alloy. Marin et al. [27] stated that since copper is insoluble in iron in the early stages of alloying, This insolubility will result in the creation of Cu clusters in the amorphous matrix, which can act as nucleation sites for α-Fe(Si) nanocrystals [28]. However, Marin et al. [27] realized that the addition of only copper to the FeSiB alloy composition would destabilize the amorphous phase by decreasing the crystallization temperature and increasing the chance of crystallite formation and growth. The result of research done on the addition of niobium to the amorphous matrix showed that niobium has the exact opposite effect on the crystallization temperature [29]. Studies have shown that the addition of niobium to the FeSiB-based alloys can aid the stabilization of the glassy phase and delay or hinder

crystallization [30]. Therefore, the addition of copper can help in the nucleation of the Fe(Si) nanocrystals which are responsible for the good magnetic properties of Fe-based magnetic alloys, and the addition of niobium can help in preventing excessive grain growth and preserving the amorphous microstructure. The influence of the addition of copper and niobium on laser devitrification of FeSiB-based alloys was studied by Alam et al. [22], who observed an increase in the saturation magnetization and coercivity of copper-containing FeSiB samples as compared to niobium containing FeSiB sample due to finer scale Fe(Si) nanocrystals being homogeneously distributed in the amorphous matrix . This increase in coercivity value of the Cu-containing sample compared to the Nb-containing sample was explained by Marin et al. [27], who stated that the addition of Cu to the amorphous matrix destabilizes it and, as a result, coercivity values begin to rise at lower temperatures. Even though the main influence of copper is enhancing the crystallization of α-Fe_3Si crystallites and niobium to control the growth of the nanocrystals, but studies have shown copper can affect crystal growth, and niobium can impact the nucleation kinetics as well [31]. The advantages of the addition of each element to the Fe-based magnetic alloys attracted the attention of researchers to the addition of both elements to the mix. Simultaneous addition of copper and niobium to the FeSiB alloy can decrease the stabilizing effect of niobium on the amorphous phase [32], however, it has been proven by Drbohlav [33] that this simultaneous addition of the two elements will aid the dispersion of α-Fe_3Si nanocrystalline in the amorphous iron matrix and therefore improve the magnetic properties. Yoshizawa et al. [28] also studied the addition of copper and niobium to the FeSiB magnetic alloys and concluded that the simultaneous addition of Cu and Nb to the alloy can improve the magnetic properties of

the FeSiB alloys due to the appearance of certain alloy-phases that occur when these two elements are added to the mix. Other studies on the effect of the addition of copper and niobium to magnetic alloys with similar compositions that are processed using different processing methods have been done, which can be helpful in understanding the effect of these two elements more in depth [34-36].

Based on the previous research done on magnetic alloys, it has been established that superior magnetic properties can be achieved in magnetic alloys when nanocrystalline are embedded in an amorphous metal matrix [37-42]. Studies done on iron-based magnetic alloys have shown that the microstructure of these alloys mainly consists of precipitates such as α-Fe(Si) in the scale of nanometer distributed in an iron matrix [43-45]. The embedment of these α-Fe(Si) nanocrystals in the amorphous iron matrix gives the Fe-based magnetic alloys their excellent magnetic properties [46-48].

Fe73.5Si13.5B9Cu1Nb3 (Finemet) is an amorphous Fe-based alloy invented by Yoshizawa et al. [28], which exhibits high permeability and saturation polarization (1.2-1.3 T) along with low coercivity values of usually less than 1 A/m [27]. The finement alloy, which was processed by the addition of copper and niobium to the amorphous FeSiB alloy, shows an excellent combination of permeability and saturation flux in comparison to other magnetic alloys such as Si-steel or Co-based alloys when it is in the amorphous state [28].

1.2. Different processing routes of iron based amorphous alloys

Until recent years the main way of fabricating amorphous metallic alloys was rapid cooling. Rapid cooling processes are capable of producing metallic material with amorphous structure from metals that are typically in crystalline state [49-50]. In rapid

cooling, the melted metal was either cooled to a temperature below its crystallization temperature with a very high cooling speed of 10^5 to 10^6 k/s, or it was prepared by condensing the vapor into a cold substrate [51]. Due to the requirement of special safety measures associated with the condensation of hot vapor into a cold substrate and the cost that accompanies these safety measures, processes such as melt spinning, which are based on fast cooling of metallic material in liquid form, are mostly used for fabrication of amorphous magnetic alloys.

In the melt spinning process alloys are melted inside a container and are then flushed out of a nozzle with the help of an inert gas onto a rotating wheel made of copper. The melted alloy is then instantly solidified in order to avoid crystallization [52]. The reason for choosing copper for the wheel is its high thermal conductivity which can absorb and transfer the heat quickly. The wheel is constantly rotating at a high rotation speed and being cooled down by a water-cooling system to avoid overheating.

Even though the melt spinning process is perfectly capable of producing alloys with amorphous structure, it has its own drawbacks, such as amorphization of only the side of the ribbon that in contact with the wheel and its incapability to produce magnetic material with a high thickness which means it is only capable of fabricating magnetic materials in the shape of thin ribbons or wires. The thickness of these amorphous ribbons is typically less than 50 μm with width of up to 30mm [5], and they need to get stacked on top of each other in order to make bigger magnetic components. For certain magnetic components, thousands and sometimes even tens of thousands of these thin ribbons need to get stacked in order to reach the desired thickness. Stacking this large number of ribbons, especially for applications where both mechanical and magnetic properties are of

importance (such as permeability engineering), is not practical. Another important drawback of the melt spinning process is that the ribbons fabricated by rapid cooling are quite brittle and require further heat-treating steps, which makes the fabrication of magnetic components with complex shapes using these ribbons more difficult [53]. Furthermore, the shapes of the magnetic parts produced with the rapid cooling technique are only limited to the shapes and sizes that can be machined out of the stack of ribbons. Therefore, it is important to come up with a technique to not only increase the efficiency of the produced magnetic alloys but also miniaturize them for applications in electric and electronic equipment.

1.3. Application of mechanical alloying/milling for processing amorphous materials

The drawbacks associated with the rapid cooling processes have attracted the attention of some researchers to mechanical alloying as a powerful alternative for the fabrication of amorphous magnetic alloys. Mechanical alloying (MA) is a powder processing technique that is capable of fabricating amorphous and crystalline alloys. Mechanical alloying or powder metallurgy was established over three decades ago and is capable of producing homogeneous material from elemental blend powders. This non-equilibrium technique is capable of processing materials in large quantities and has a relatively low cost compared to some of the other alloy production techniques. Moreover, conventional methods of alloy production, which depend on the melting and mixing of metals, require the melting points of the alloying materials to be close to each other. However, the mechanical alloying process has the ability to process various metals with different melting temperatures to form alloys.

During the mechanical alloying process, the elemental powders are placed inside a high energy ball mill along with the grinding media; when two milling balls collide, the powder particles that are placed in between them get flattened and fractured and then fused back together due to a competing cold-welding process. During the MA process, alloying takes place due to these continuous and repeated fracturing and rewelding of particles [54].

Other than making an alloy out of elemental blend powders, the mechanical alloying technique is also capable of amorphization of the alloy. Generally, the amorphization process during the mechanical alloying technique happens as a result of diffusion along with the constituent interfaces of primary components at relatively low temperatures Weeber et al. [55] proposed three different routes by which amorphization takes place during the MA of elemental powders. First, continuous broadening of the peaks in the XRD patterns. Second, decrease in the intensity of the Bragg reflection, and third, the formation of crystalline intermetallic products and later transformation of these products into amorphous alloys.

According to Hu et al. [56] there are two main factors that can drive the amorphization process: changes in the free energy of the system and increase of defect concentration or instability of the lattice. As for the concentration of defects and instability of the lattice, there are a number of lattice defects involved with the mechanical alloying process, such as dislocations, grain boundaries, vacancies, and interstitials, that occur during the MA process and can all affect the kinetics (different diffusion coefficients as well as large negative heat of mixing) and thermodynamics of the amorphization process during milling [57-59]. As for the free energy of the system,

during the mechanical alloying process, the free energy of the crystalline phase can rise due to the defects, which means this phase will become unstable in comparison to the amorphous phase.

The thermodynamics of the alloy system and the amount of energy that is provided to the powder during the mechanical alloying process governs the phase formation and amorphization of the powder being milled. Koch et al. [18], who studied the amorphization process during the mechanical alloying of different powder compositions, stated that amorphization during the milling process increases the free energy of crystals which means the amorphous phase will be thermodynamically favorable. The driving force of the amorphization reaction depends on the enthalpy of the mixing of the elemental powders. If the enthalpy is positive, the solid-state reaction will not happen therefore, the system needs to have a negative enthalpy of mixing for amorphization to take place [18] (the work of Schwarz et al. [60] can help in finding the free enthalpy diagrams of solid-state reaction systems). Schwarz et al. [60] stated that solid-state amorphization involves the diffusion of components into the matrix in a way that produces a lot of negative heat of mixing. As a result, the free energy of the amorphous phase would be lower than that of the crystalline phase, and therefore amorphization would be favored.

Generally solid state amorphization (SSA) can happen by mechanically alloying of elemental powders in crystalline or amorphous state or by milling of intermetallic compounds [60]. In case of mechanical milling of intermetallic compounds amorphization takes place due to lattice defects as well as chemical disordering in the lattice, however, in case of mechanical alloying of elemental powders solid state

amorphization happens due to diffusion and negative heat of mixing [61]. Schultz [62] who studied the amorphization of metallic material by mechanical alloying stated that during the MA process the particles that are placed in between the colliding milling balls get flattened and form ultra-thin layers. The fusion reaction then starts at these new interfaces and since the fusion-related growth selection favors the amorphous phase, this phase grows faster than the crystalline intermetallic phase and the amorphous phase eventually takes over. Hu et al. [56] who also studied amorphous materials, stated that for pure metals to be able to amorphized, other than a large negative mixing heat, a big difference between mutual diffusion is also required which can both be obtained by the mechanical alloying process [56]. Therefore, the MA process is chosen for alloying of the elemental powders as well as to obtain a powder alloy with amorphous structure.

1.4. Spark plasma sintering of soft magnetic alloys

After the powder alloy is processed by the mechanical alloying technique it then needs to be consolidated into a bulk magnetic part. The mechanical alloying process is capable of producing alloy powders in amorphous or crystalline state which are both suitable for consolidation and compaction into various shapes. Consolidation of the mechanically alloyed powders is done by the spark plasma sintering (SPS) process. The SPS process uses a uni-axial press to densify the powder and then utilizes a pulsed direct current in order to heat the powder up. The reason for choosing the SPS process for consolidating the powders is the fact that SPS can process a wide range of materials such as metals, ceramics, and composite powders, and it can process the powders at a higher speed and lower temperature compared to conventional sintering techniques such as hot pressing. The higher speed in sintering and lower sintering temperature will preserve the

microstructure of the sintered parts, prevents grain growth, and retains the nanocrystalline structure [63]. Other than the capability to process different types of material SPS technique is also capable of processing powders in a wide range of particle sizes. Additionally, SPS is capable of fabricating bulk parts that are near-net shape and are fully dense, which has attracted a lot of attention to the process. The pulsed direct current that is used in the SPS process produces sparks which instantaneously heats up the powder, and the uni-axial pressure that is induced to the powder during the sintering process helps in homogenizing the microstructure of the consolidated alloy. When the spark discharges in the gaps in between the powder particles during the spark plasma sintering process, a high local temperature is generated, which causes evaporation and melting on the grain boundaries of the particles, which will bound the particles together and form a fully dense part without the need to actually melt the powder alloys completely. Joule's law states that the current has a tendency to go through the pass of least resistance. In the case of powder being spark plasma sintered, the areas with the least resistance for the current to pass through are the grain boundaries, which is why the electric field is generated in these areas, melting and connecting the grain boundaries and making the sintering process possible [64]. The speedy heating process associated with SPS and its capability in heating the sample simultaneously and homogeneously from inside and out prevents grains from aggressive growth and preserves the nanocrystalline structure which is why SPS is a great technique for processing nanocrystalline material. [65]. SPS is also capable of processing parts with uniform grain structures in a single step and without the need for any post-processing. Processing amorphous alloys using the mechanical alloying

technique followed by the spark plasma sintering process can be the new route for the fabrication of bulk magnetic alloys with great magnetic and mechanical properties.

Spark plasma sintering processing parameters can affect the magnetic and mechanical properties of the fabricated parts. There is only a little research done on the sintering of soft magnetic alloys, and therefore the effect of the sintering processing parameters on the sintered alloys is not yet fully understood. Among the SPS processing parameters sintering temperature is the most important parameter which can affect both mechanical and magnetic properties of the fabricated part. A few researchers have studied the effect of temperature on sintered alloys with similar compositions. Xiao et al. [66] have experimented on FeSiCuNb composition and proven that the sintering temperature is indeed effective on the magnetic properties of this alloy. According to their findings, sintering temperature affects both saturation magnetization as well as coercivity. They discovered that increasing the sintering temperature increases the saturation magnetization while the coercivity decreases with higher temperatures. Due to the presence of boron and the possibility of formation of boron phases in our samples, and the fact that boron phases such as Fe2B, Fe3B, or Fe23B6 can negatively affect the saturation magnetization and increase the coercivity values, tuning the SPS processing parameters in order to get the best mechanical and magnetic properties for our samples is more challenging. Other than the sintering temperature there are other SPS processing parameters such as holding time and maximum pressure that can also affect the fabricated part. Neamtu et al. [67] studied the role of holding time on SPS-processed Fe-based alloys sintered at low pressures. In this study in order to achieve full densification at low pressure, Neamtu et al. [67] increased the sintering temperature (up to 800°C) and

holding time and concluded that as a result of better densification at higher temperatures and holding time, the magnetic properties of the alloy improved. Gheiratmand et al. [68] worked on the sintering of Finemet at low pressures and long holding times. One of their discoveries was that the density of the fabricated part depends on whether the initial powder was amorphous or partially crystallite (higher density in the case of amorphous powder due to placement of smaller powder particle in between bigger particles). Additionally, they realized that longer holding times help in increasing the saturation magnetization of the alloy, however, it will also increase the chance of crystallization and create a coarse and completely un-amorphous microstructure in the sintered sample.

As mentioned before, pressure is another factor that can affect the properties of the SPS-fabricated parts. Xio et al. [66] studied the effect of maximum pressure and holding time on the microstructure of SPS-fabricated samples and found that if the loading pressure is less than 500 MPa, the powders would not be consolidated or may require longer holding times to achieve full densification. Neamtu et al. [67] did SPS on FeSiB composition with holding time of 1 to 15 minutes with varying temperatures from 450 °C to 900 °C and maximum pressure of 30 MPa. As the pressure that was chosen for the experiments was too low, Neamtu et al. only achieved full compactions at temperatures over 800 °C. This high sintering temperature can cause grains to grow excessively and since our goal for our experiments was to achieve fully dense parts while avoiding crystallization and grain growth, we chose a high pressure for our SPS experiments (600 MPA) in order to avoid having to increase the holding time or sintering temperature to be able to achieve full densification.

1.5. Different processing parameters affecting amorphization of iron-based alloys

During the mechanical alloying process certain amount of kinetic energy is introduced to the powder. This energy that is induced to the powder as a result of a continuous collision with the rotating milling balls will affect the amorphization process. During the mechanical alloying process, each milling ball, depending on its size, rotation speed, etc., has a certain amount of energy which is called the energy of a single ball. This energy is calculated by the assumption that there is only one ball present in the milling bowl, and there are no interactions between that particular ball with the rest of the milling balls during the milling process. However, in reality, the interaction between the milling balls affects their energy which is why there is another energy that should be taken into consideration, called the total energy of the process. The total energy of the process is the entire energy introduced to the powder particles by all the milling balls in throughout the process of mechanical alloying. There are several different mechanical alloying processing parameters that can affect the total energy involved in the process, the energy of each single milling ball as well as the amorphization process during milling. The milling processing parameters such as the size of the balls, the ball to powder weight ratio, the rotation speed, the milling duration, and even the process control agent, which prevents the powder from cold welding during the process, can affect the amorphization. Yang et al. [69] studied the amorphization of SiBCN powders via high-energy ball milling and observed that the amorphous phase is easier to obtain with milling balls with smaller sizes. Yang et al. [69] also studied the effect of milling duration and ball to powder weight ratio on the structure of SiBCN powders and came to the conclusion that longer milling durations and higher BPR aid the amorphization

process. This observation from this study is interesting since Yang et al. [69] did not get a fully amorphous microstructure until a BPR of 100:1; however, they were able to obtain amorphization in a relatively short time of 30 hours. In comparison, in our studies we got the best amorphization results with a fairly low BPR of 10:1 and milling duration between 30 and 120 hours depending on the rotation speed. Aydinbeyli et al. [70] studied mechanically alloyed Mg-Ni alloys and observed various amorphization times for different mechanical alloying processes. Aydinbeyli et al. [70] were able to obtain a fully amorphous powder with milling durations ranging from as low as 5 hours up to 60 hours of milling. The only varying factor in their experiments was the ball to powder weight ratio, which changed from 5:1 to 20:1. This proves the importance of the role of BPR in obtaining a fully amorphous structure since changing it can increase the required time for amorphization by more than ten times. Other than the amorphization, mechanical alloying processing parameters such as milling duration and ball to powder weight ratio greatly affect the crystallite size of the milled powders [71]. Studies have shown that a higher ball to powder ratio usually reduces the grain size of the powder. Suryanarayana [72] stated that the reduction of crystallite size as a result of higher BPR is mainly due to the fact that at higher BPRs, the number of collisions per unit time increases, and therefore, the energy that is transferred to the power increases as well. They introduced a formula that directly correlates the energy of milling to the size of the crystallites and surface area of the grains during the alloying process. The reason for the importance of studying the effect of mechanical alloying processing parameters on the particle size is that it has a direct effect on the magnetic properties of the magnetic alloys. According to the Herzer model, the grain size has a strong influence on *Hc*, and when grain sizes are

less than 40 nm, the coercivity drastically drops as a result of the ferromagnetic exchange interactions [73]. Moreover, magneto-crystalline anisotropy is the primary factor determining coercivity; the reduction in magneto-crystalline anisotropy due to reduced grain size leads to low coercivity values. Raja et al. [74] found this size to be ~ 10 nm for Finemet type alloys which is less than 35 nm which is the ferromagnetic exchange length of Fe–Si alloys. Tong et al. [75] also studied the effect of crystallite size (D) on coercivity and observed a proportional relationship between the two variables. Other researchers have done similar experiments on the effect of crystallite size on the magnetic properties of magnetic alloys. Carr et al. [76] who studied the crystallite size of melt-spun Fe-Nb-B magnetic alloys, Hartridge et al. [77] who investigated the magnetic properties of nanocrystalline magnetic material and their dependence on crystallite size, Berkowitz et al. [78] who studied the magnetic properties of ferromagnets and Passamani et al. [59] who studied the magnetic and thermal behavior of iron-boron alloys observed similar results as Tong et al. [75]. In this research work we have studied the effect of mechanical alloying processing parameters on FeSiB-based magnetic alloys processed via mechanical alloying and spark plasma sintering and have investigated the effect of these parameters on particle size, amorphization and mechanical and magnetic properties of these alloys.

1.6. Critical issues discovered

The principal objective of this research work was to identify the factors affecting the amorphization of iron-based softmagnetic materials during the mechanical alloying process. Amorphization during the mechanical alloying process occur due to high density of defects such as vacancies, dislocations and grain boundaries which affect the kinetics

of the process and favor the amorphization reaction over crystallization. The energy introduced to the powder as a result of constant collision between the milling balls and powder particles increases the defect density produced during mechanical alloying and aids the diffusion processes and therefore the amorphization reaction. Mechanical alloying processing parameters play an important role in defining the kinetic energy introduced to the powder during the milling process and as a result affect the glass forming ability of blend of elemental powder composition.

In this study alloys with full amorphous structures were defined based on the microstructural studies of the mechanically alloyed powders milled with different processing parameters. The total energy introduced to the powder during these milling processes were then defined and an energy map was created which shows the correlation between the energy of the process and the amorphous structure of FeSiB-based alloys. Additionally, effect of spark plasma sintering temperature on mechanical and magnetic properties of the sintered FeSiB-based alloys was identified.

CHAPTER II

PROCESSING TOOLS AND EXPERIMENTAL DETAILS

2.1. Alloy composition

Iron, silicon, boron, copper and niobium elemental powders were used for producing FeSiB, FeSiBNb, FeSiBCu and FeSiBCuNb magnetic alloys. Iron powder with purity of 99.9% and size of 1–9 μm, silicon with purity of 99.99% and mesh size of − 325, amorphous boron with purity of 97%, copper with purity of 99.9% and size of 1–5 μm, and niobium: with purity of 99.8% and size of 1–5 μm were obtained from Carpenter Technology. The Fe, Si, B, Cu and Nb elemental powders were combined with atomic weight percentages mentioned in table 2.1 in order to process the following compositions: compositions $Fe_{77.5}Si_{13.5}B_9$, $Fe_{76.5}Si_{13.5}B_9Cu_1$, $Fe_{74.5}Si_{13.5}B_9Nb_3$ and $Fe_{73.5}Si_{13.5}B_9Cu_1Nb_3$.

Table 0-1 Chemical composition of FeSiB, FeSiBCu, FeSiBNb and FeSiBCuNb

Composition	Content (at.%)				
	Fe	Si	B	Cu	Nb
FeSiB	77.5	13.5	9	0	0
FeSiBCu	76.5	13.5	9	1	0
FeSiBNb	74.5	13.5	9	0	3
FeSiBCuNb	73.5	13.5	9	1	3

2.2. Mechanical alloying

Fritsch Pulverisette 7 high energy planetary ball mill was used for ball milling the above-mentioned alloy compositions. The milling media, including the milling balls and milling bowls/vials, were made out of tungsten carbide. The process of milling was done under an argon atmosphere. The elemental powders as well as the milling media were placed inside a standard glove box and after placing the appropriate powder composition and number of milling balls inside the bowls the milling bowls were sealed to prevent oxidation during the process specially at higher rotation speeds. In order to prevent agglomeration of powder particles, cold welding and bonding between powder particles and the milling media 2 wt% stearic acid/ benzene were added to the elemental powder mix as a process control agent (PCA). PCAs can be in solid (stearic acid) or liquid (benzene) form and should be between 1-5 wt% for best result [79]. Mechanical alloying processing parameters such as the weight ratio of milling balls to the powder that is being milled, the size of the milling balls, the rotation speed of the milling machine, the duration of milling and different PCAs were studied. The ball to powder weight ratios (BPR) for the mechanical alloying experiments in this project are as follows: 5:1, 10:1, 15:1. This means that if we use 10 g of powder for instance, in case of BPR 5:1 we need to add 50 grams of milling balls, 100 g of milling balls in case of BPR 10:1 and 150 g of milling balls in case of BPR 15:1. The milling durations used for this project ranged from 10-120 hours. Several experiments were done with milling durations of 10, 20, 30, 60, 90 and 120 hours with different alloy compositions and mechanical alloying processing parameters. The rotation speeds used in our experiments were: 350 rpm, 500 rpm and 700 rpm. The kinetic energy released from the collision between the milling balls can convert into heat during the

alloying process therefore the milling process needs to be interrupted in order to give the powder and the milling media time to cool down. In order to prevent the milling media from overheating during the mechanical alloying process and the powder getting cold welded, especially in case of powders being milled with high rotation speed of 700 rpm, we put 10 minutes pauses in between the 10 minutes milling periods. The resultant powder alloy from the mechanical alloying process was then consolidated using the spark plasma sintering technique.

2.3 Spark plasma sintering

Spark plasma sintering process was done under controlled argon filled atmosphere. The powder was pre-compacted with 20 MPa pressure and the maximum pressure during the sintering process was at 600 MPa. The pre-compact pressure is the initial pressure by which the powder is kept in place inside the die and in between the punches (20 MPa in this case). This pressure will ramp up to the maximum pressure chosen for the sintering process (600 MPa in this case) at a rate of 100 MPa/min. At the next stage temperature ramps up to the sintering temperature at the heating rate of 30°C/min while the powder is kept under the maximum pressure. After reaching the maximum temperature the powder is kept under the sintering temperature and the maximum pressure for a certain amount of time which is referred to as the holding time. The holding time of 5 minutes was used for all the experiments in this research work. Dies and punches with diameter of 10 mm were made of tungsten carbide. Tungsten carbide dies and punches were chosen due to their ability to endure higher pressures and moderately high temperatures. The dies and punches were covered with graphite foil in order to prevent direct contact between the powder alloy and the dies and punches as well

as for better electrical conductivity. Different sintering temperatures were selected in order to study the role of sintering temperature on microstructure, mechanical properties and magnetic behavior of the samples. Three different temperatures of 470, 510 and 550 °C were used for different experiments. For the first set of experiments (chapters 3 and 4) 550 °C was selected as the sintering temperature. Differential scanning calorimetry (DSC) was performed with heating rate of 10 °C/min with maximum temperature of 800 °C under argan atmosphere in order to find the crystallization temperatures of different phases in the alloy powder. A major exothermic peak which indicated the crystallization temperature for this particular alloy was observed at around 500 °C and 2 temperatures of 470 °C and 510 °C were chosen, one bellow and one above the crystallization temperature of the alloy, for the next set of experiments (chapter 5).

2.4 Heat treatment

The annealing heat treatment was done in an oven furnace at the temperature of 200 °C for duration of 2 hours in order to relieve the residual stress induced to the powder during the mechanical alloying process. The oven furnace was not inert atmosphere therefore in order to prevent the alloy from oxidizing a glove box with argon atmosphere was used. After the milling process the milling vials were placed inside the glovebox and powder was taken out of the vial, weighed, and placed in a secure container for annealing. The mechanical and magnetic properties as well as the microstructure of the sample sintered from the annealed powder were then compared with sample sintered from the same powder batch (milled with the same parameters) but un-annealed.

2.5 Microhardness

The microhardness values of the SPS consolidated samples were measured using a standard Wilson Vickers microhardness tester. The measurements were taken under a load of 5N and dwell time of 10 seconds. For each sample microhardness readings of 10 different were taken into account and the average value was reported.

2.6 Microstructural analysis

For microstructural analysis, the spark plasma sintered samples were mounted using an Allied TECHPRESS 3 mounting press and polished using an automatic Fritsch polisher. Polishing was done on different grit polishing papers ranging from rough to soft 250 to 1200 grit. The roughest polishing paper with 250 grit was used to remove the graphite left on the surface of the sample after mounting. Polishing papers 400, 600, 800 and 1200 grit (roughest to softest) were then used to further smoothen the surface. The sample was rotated 90° clockwise every 5 minutes of polishing in order to prevent leaving marks on the surfaces. Final polishing was done using colloidal silica on a micro cloth. While the samples were polished by each of the 400-1200 grit polishing papers for 10-15 minutes, they were polished for 30-45 on the micro cloth and only 5 minutes on 250 grit paper. After final polishing on the automatic polisher on a micro cloth a vibrometer was used for the final polishing stage in order to get the clearest view of the microstructure.

After the polishing steps the samples were viewed and characterized with a FEI-Quanta Nova-SEM. Both secondary and backscattered images were taken at magnifications ranging from 100x to 5000x.

2.7 X-ray diffraction and crystallite size analysis

The structure and phases of powder and consolidated samples were determined with an X-ray diffraction (XRD) using a Rigaku Ultima III X-Ray diffractometer (Cu Kα radiation, 1.54 Å). The 2θ range for all the powder and sintered samples of all the milling conditions were 30 ° to 90°. The crystallite size of the sintered samples was measured based on the X-ray diffraction data by using the Scherrer equation [80]. In the Scherrer formula $B=K\lambda/(L\cos(\theta))$, K is the shape factor which was considered 0.94. λ is the wavelength of the x-ray which in our case is 0.1542 nm. L is the peak at Full Width at Half Maximum (FWHM) (linear dimension of the particle which is line broadening at FWHM minus the instrumental line broadening) and θ is the Bragg angle (in radians).

2.8 Magnetic properties

Magnetic properties of the mechanically alloyed powder as well as spark plasma sintered alloys were measured using a magnetometer (VSMLakeshore 7404) with maximum magnetic field of 1T.

CHAPTER III

INFLUENCE OF COPPER AND NIUBIUM ON AMORPHIZATION OF FeSiB-BASED ALLOYS

3.1 Abstract

Addition of elements such as copper and niobium to iron-based magnetic alloys affects their microstructure as well as their magnetic properties. In this chapter [1]effect of addition of these 2 elements to the FeSiB-based magnetic alloys is studied. Alloys with the following compositions were considered: $Fe_{77.5}Si_{13.5}B_9$, $Fe_{76.5}Si_{13.5}B_9Cu_1$, $Fe_{74.5}Si_{13.5}B_9Nb_3$ and $Fe_{73.5}Si_{13.5}B_9Cu_1Nb_3$.

Magnetic and mechanical properties as well as the microstructure and crystallite sizes of these compositions were studied. It was found that addition of copper or (and) niobium to the FeSiB-base alloy improves the magnetic properties of the alloy and results in higher saturation magnetization and lower coercivity values. The higher saturation magnetization obtained can be attributed to the larger volume fraction of α-Fe_3Si nanocrystals which is due to the presence of copper particles that act as nucleation cites

for these nano particles. The lower coercivity values can be attributed to the presence of niobium which prevents excessive grain growth and consequently reduces the coercivity values. Grain sizes and homogeneity of the sintered alloys was studied using SEM images and microhardness values of the samples were obtained using a standard Vickers microhardness tester. Finer microstructure was observed for sample containing niobium from SEM images. An increase in the micro hardness of the sintered FeSiBCuNb alloy was observed with increasing the milling duration primarily due to a decrease in crystallite sizes. Moreover, the micro hardness of FeSiB alloys were also found to increase monotonically with longer milling durations due to a more uniform microstructure and smaller grain sizes. Furthermore, x-ray diffraction was also done on samples containing each element in order to study their effect on phase transformation and crystallite size of the magnetic alloys.

3.2 Introduction

Iron, silicon and boron-based (FeSiB) alloys are a group of magnetic alloys with outstanding magnetic properties such as high permeability and saturation magnetization as well as low coercivity values [81-82]. The good magnetic properties of these alloys are mostly attributed to the formation of nanocrystalline α-Fe(Si) grains that are dispersed in an amorphous Fe matrix [83]. FeSiB-based magnetic alloys possess good magnetic properties however, adding elements such as niobium and copper to the mix can further improve the magnetic and mechanical properties of these alloys. When copper is added to the base FeSiB alloy it acts as a nucleation site for α-Fe(Si) nanocrystal particles while addition of niobium is proven to reduce the growth of the nanocrystals [27][73]. Effects of copper and niobium on iron-based magnetic alloys was confirmed in the studies done

by Marin et all [27]. In their experiments Marin et al. [27] made the observation that copper tends to cluster in the iron matrix. This tendency in copper is due to the fact that Cu does not dissolve in iron and therefore tends to cluster. The copper clusters in the alloy then act as nucleation sites for Fe(Si) nano crystals. These nucleation cites then aid the crystallization of α-Fe_3Si which consequently enhances the magnetic properties of the alloy. Youshizawa et al [49], who studied the microstructure of ultrafine iron-based magnetic alloys, also stated that insolubility of copper in the iron matrix creates Cu-clusters which act as nucleation cites specially during the initial stages of mechanical alloying. Youshizawa et al [49] also discovered that addition of niobium to the magnetic alloys increases the crystallization temperature which as a result delays crystallization and aids stabilization of the glassy phase. Finemet ($Fe_{73.5}Si_{13.5}B_9Cu_1Nb_3$) which is an amorphous iron-based magnetic alloy was first processed by adding the 2 elements of copper and niobium to the traditional composition of iron, silicon and boron [84-86]. This new composition showed promising magnetic properties such as high permeability and saturation magnetization along with low coercivity and as a result attracted a lot of attention in research and industry [87-88]. In the past researchers have studied the effect of addition of copper and niobium to the traditional FeSiB magnetic alloys. Duhaj et al. [34] studied the formation of copper crystalline phases in amorphous ribbons with similar compositions to $Fe_{76.5}Si_{13.5}B_9Cu_1$ and $Fe_{73.5}Si_{13.5}B_9Cu_1Nb_3$. They realized that the crystallization of copper-based phases takes place very quickly in the beginning and decreases significantly after the initial stages. They also concluded that different contents of niobium can affect the crystallization behavior of the alloy with more niobium content decreasing the sizes of FeSiCu clusters. Jha et al. [35], studied the growth of copper

clusters in finemet alloys. From their experiments they realized that increased temperature increases the speed by which copper clusters are formed. Marin et al. [27], studied amorphous wires made of FeSiB(Cu and Nb) alloys obtained from rotating water quenching technique and effect of copper and niobium on their crystallization. They stated that when Cu and Nb are added to the base composition individually they significantly change the thermal stability and crystallization dynamic of the amorphous matrix. They concluded that copper has a destabilizing effect on the FeSiB alloy and forms its first clusters at a low temperature. These initial clusters include αFe(Si) crystals which consequently results in magnetic hardening due to increasing size of the Fe(Si) grains. Addition of niobium on the other hand enhances the thermal stability of the FeSiB alloy however, it does not have the same nucleation effect that copper has with niobium having much less density of nuclei. Addition of Nb also has the effect of decreasing the coarsening of the grains which in turn decrease the magnetic hardening. Jiang et al. [36] studied soft magnetic finemet type alloys and tried to replace the element niobium with molybdenum in the composition. From the results of their experiments Jian et al. [36] realized that the thermal stability of the composition is reduced by substitution of niobium with molybdenum. They concluded that addition of molybdenum results in formation of nonmagnetic phases at early stages which deteriorates the soft magnetic properties of the alloy. Borrego et al. [89] studied the nano crystallization behavior of FeSiBCu alloys with addition of refractory elements such as Nb, Mo, Zr and V. They observed an enhancement in crystallization of Fe_3Si crystalline with the help of annealing process. They observed higher volume fractions of the phase with higher annealing

temperatures and longer times. They also observed a stabilizing effect on the amorphous matrix by addition of the refractory elements to the mix.

In this chapter we have focused on mechanically alloyed amorphous FeSiB-based magnetic alloys and the effect of addition of Cu and Nb separately and simultaneously on mechanical, microstructural and magnetic properties of the sintered and milled powder FeSiB-based alloys.

3.3 Experimental procedure

For this chapter FeSiB, FeSiBCu, FeSiBNb and FeSiBCuNb(finemet) magnetic alloys prepared from mechanical alloying of Fe, Si, B, Cu and Nb elemental powders were studied. Chemical compositions of the alloys used for the experiments done in this chapter are mentioned in Table 2.1 based on atomic weight percent. Mechanical alloying was done on Fritsch Pulverisette 7 high energy planetary ball mill under argon atmosphere using tungsten carbide milling balls and bowls. FeSiBCuNb alloy was milled using milling balls with 3mm diameters with ball to powder weight ratios of 10:1. The FeSiBCuNb alloy was milled for milling durations of 30, 60, 90 and 120 hours with rotation speed of 350 rpm. FeSiB, FeSiBCu and FeSiBNb compositions were mechanically alloyed with BPR 15:1, rotation speed of 350 rpm and milling duration of 90 hours using milling balls with 3mm diameters. 2 wt% Stearic acid was used as PCA for all the milling processes and 10-minute pauses were placed between 10-minute milling periods. Spark Plasma sintering was done under controlled argon atmosphere using 10mm tungsten carbide dies and punches that were covered by graphite foil (for better electrical conduction) and heating rate of 30°C/min. The packing pressure was at 20 MPa and the maximum pressure during the sintering process was at 600 MPa. The sintering temperature was 550°C and the holding

time was 5 minutes. One sample was sintered from each of the powder alloys prepared by mechanical alloying. FeSiBCuNb powder alloys milled for 30, 60, 90 and 120 hours were sintered using the said SPS parameters giving us a total of 5 finemet sitered samples. FeSiB, FeSiBCu and FeSiBNb powder alloys milled for 90 h with BPR 15:1 were spark plasma sintered using the same SPS processing parameters giving us another 3 sintered samples. The sintered samples were then mounted and polished using grinding papers 250-1200 grit followed by 30-45 minutes of polishing using colloidal silica on a micro cloth. Scanning electron microscopy was done on all the sintered and polished samples using a FEI-Quanta Nova-SEM. Both secondary and backscattered images were taken at magnifications ranging from 100x to 5000x. X-ray diffraction was done on powder as well as sintered alloys of all compositions and milling parameters in order to study their phase composition as well as their amorphous structures using an X-ray diffraction (XRD) machine using a Rigaku Ultima III X-Ray diffractometer (Cu Kα radiation, 1.54 Å) and 2θ range of 30° to 90°. Based on the XRD data the crystallite sizes of the samples were measured using the Scherrer Equation [80]. Microhardness of the sintered samples was measured using a standard Wilson Vickers microhardness tester. The measurements were taken under a load of 5N and dwell time of 10 seconds. For each sample microhardness readings of 10 different were taken into account and the average value was reported. Magnetic properties of the samples were measured using a magnetometer (VSMLakeshore 7404) with maximum magnetic field of 1T.

3.4 Results and discussion

3.4.1 X-ray diffraction of FeSiB alloys

Figure 3.1 depicts the XRD patterns of FeSiB magnetic alloy mechanically alloyed for durations of 30, 60 and 90 hours. From the XRD pattern we can see (111), (200), and (220) diffraction peaks of α-Fe(Si) phase which is an indication that all the samples exhibit α-Fe_3Si as the primary phase without presence of any secondary boron phases such as Fe_3B, Fe_2B and $Fe_{23}B_6$. A significant broadening of the Fe_3Si peaks can be observed as the milling duration increases from 30 hours to 90 hours. This broadening can be the result of decrease in the size of the grains (listed in table 3.1) as well as some level of amorphization taking place as the milling progresses. Another reason that can contribute to the peak broadening is the internal stress consequence of long milling durations. Therefore, it can be concluded that mechanical alloying processing parameters specially milling duration have significant effect on tailoring the size of the crystallites as well as the alloying process itself and the amorphization of the final alloy powder.

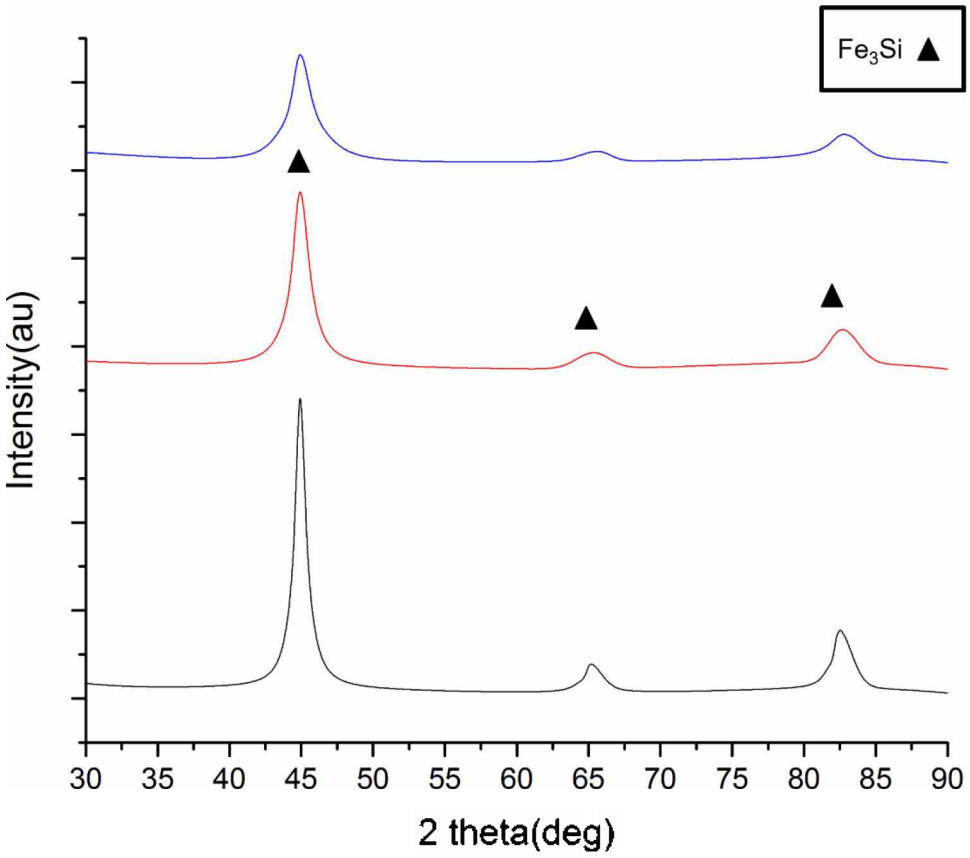

Figure 3.1 XRD pattern for FeSiB powder; 30h (black),60h (red) and 90h (blue)

Table 3.1 Grain sizes for FeSiBCu and FeSiBNb and FeSiB powder; 30h, 60h, 90h

Composition (Powder)	Grain size (nm)
FeSiB (30h)	9.26
FeSiB (60h)	6.14
FeSiB (90h)	4.73
FeSiBCu	6.86
FeSiBNb	4.75

Fig. 3.2 depicts the XRD patterns from spark plasma sintered FeSiB samples sintered from the powders milled for 30, 60 and 90 hours. similar to the milled powders the XRD patterns for the sintered samples also shows a large volume fraction of α-Fe(Si) phase. The primary Fe_3Si phase was detected in all the samples and minor peaks corresponding to secondary boron phases of Fe_2B and $Fe_{23}B_6$ were also detected in all 3 samples. When the alloy is heated above the crystallization temperature of these secondary phases during the SPS process, formation of these phase occurs from the amorphous phase. Among the secondary boron phases, $Fe_{23}B_6$ phase is a metastable phase. This means that the $Fe_{23}B_6$ phase can easily be broken down to the other boron phases such as Fe_2B and Fe_3B. In their research on the crystallization behavior of amorphous iron-based magnetic alloys Zhang et al. [90] stated that formation of boron phase Fe_3B is a result of secondary crystallization and occurs at temperatures above 550 °C and is followed by formation of the other secondary boron phase Fe_2B. Presence of small amounts of the $Fe_{23}B_6$ phase is expected after sintering the sample at 550 °C since this phase has a fairly low crystallization temperature of only 405 °C [91] which can explain why this phase is detected in all 3 sintered samples. Furthermore, crystallization

temperature of the other main boron phase Fe_2B is reported to be around 550 °C [59]. According to Passamini et al. [59] the α-Fe_2B phase forms at temperatures between 496 °C and 642 °C and γ-Fe_2B phase in temperatures between 642 °C and 901 °C. For the initial stages of this research work we chose 550 °C as the maximum sintering temperature in order to achieve full densifications for all our FeSiB-based alloys.

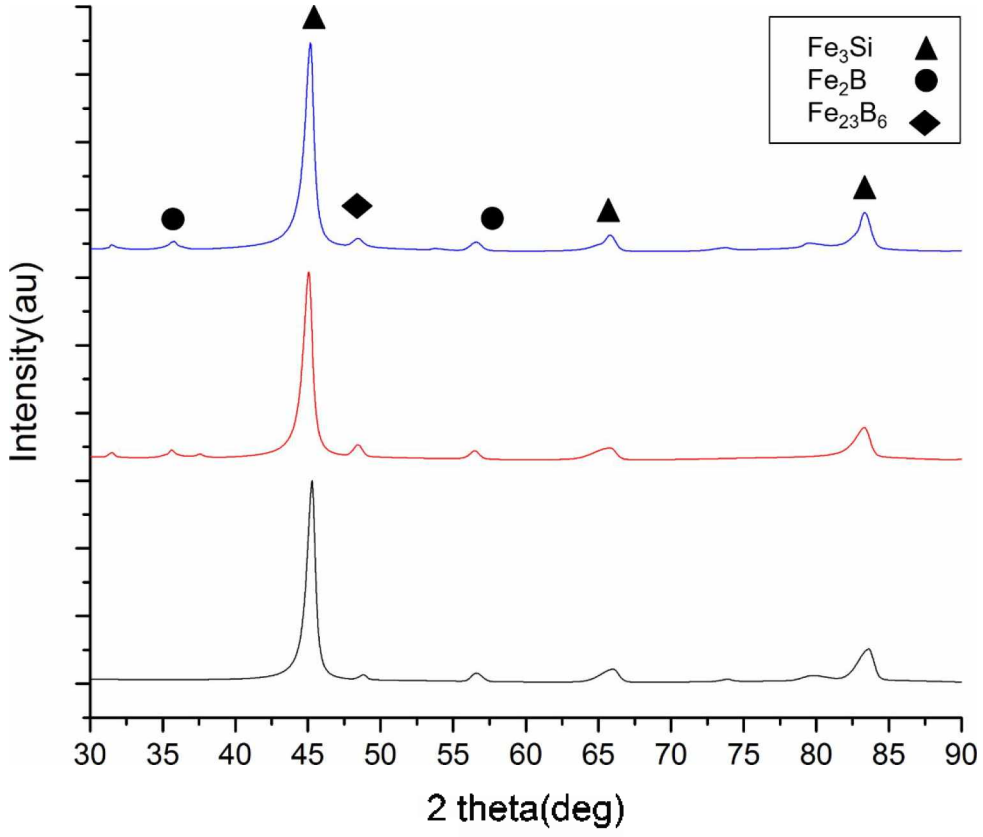

Figure 3.1 XRD patterns of FeSiB sintered samples;30h (black), 60h (red), 90h (blue)

3.3.2 Microhardness and crystallite size of FeSiB alloys

Figure 3.3 depicts the microhardness values of the spark plasma sintered FeSiB alloys. From this figure it can be observed that the microhardness values of the alloy increases as the crystallite sizes decreases due to the longer milling durations that reduces

the particle size. This observation is consistent with the Hall-Petch relationship which reports a reverse correlation between crystallite size and microhardness. The microhardness values of the sintered FeSiB alloy varies from 1000 HV in case of sample sintered from the 30h-milled powder to 1161 HV in case of sample sintered from the 90h-milled powder. From the x-ray diffraction patterns of the sintered FeSiB alloy we can see that the major phase present in the sample is α-Fe_3Si peaking at 2θ=45, 65 and 85 degrees. The broadening of these peaks as the milling duration increases is another indicator of decrease in the crystallite sizes of these alloys. This decrease in the crystallite size of the α-Fe_3Si phase plays a major role in increasing the microhardness of the FeSiB sintered alloys. Moreover, the increased number of defects that occur during the mechanical alloying process specially with longer milling durations has a hardening effect on the powder that is being milled. As a result, powders milled for longer periods of time experience more defects and therefore an increase in the microhardness value. The grain sizes of FeSiBCu and FeSiBNb powder alloys both with rotation speed of 350 rpm and milling duration of 90 hours and FeSiB powder alloys with rotation speed of 350 rpm and milling durations of 30, 60 and 90 hours are listed in table 3.1 and the crystallite sizes of spark plasma sintered FeSiB samples sintered from powder alloys milled with 30, 60 and 90 hours are depicted in figure 3.3. The grain sizes of the mechanically alloyed FeSiB powders as well as the crystallite sizes of the sintered FeSiB alloys decrease with longer milling duration. The FeSiB sample milled for the longest time (90 hours) exhibited the smaller grain size of 4.7 nm. The 30 h and 60 h milled samples showed grain sizes of 9.2 nm and 6.1 nm respectively. The spark plasma sintered samples show slight increase in the particle size as compared to as milled powders which is mainly due

to being subjected to high temperatures during the SPS process which consequently results in small coarsening in particles. The crystallite sizes of samples sintered from powders with different milling durations follow the same trend where the FeSiB sample sintered form the 90 h-milled powder exhibits the smallest crystallite size of 12.5 nm, followed by the sample sintered from the 60h-milled powder which exhibited crystallite size of 13.03 nm followed by the sample sintered from the 30 h-milled powder which shows the coarsest microstructure and biggest crystallite size of 14.92 nm.

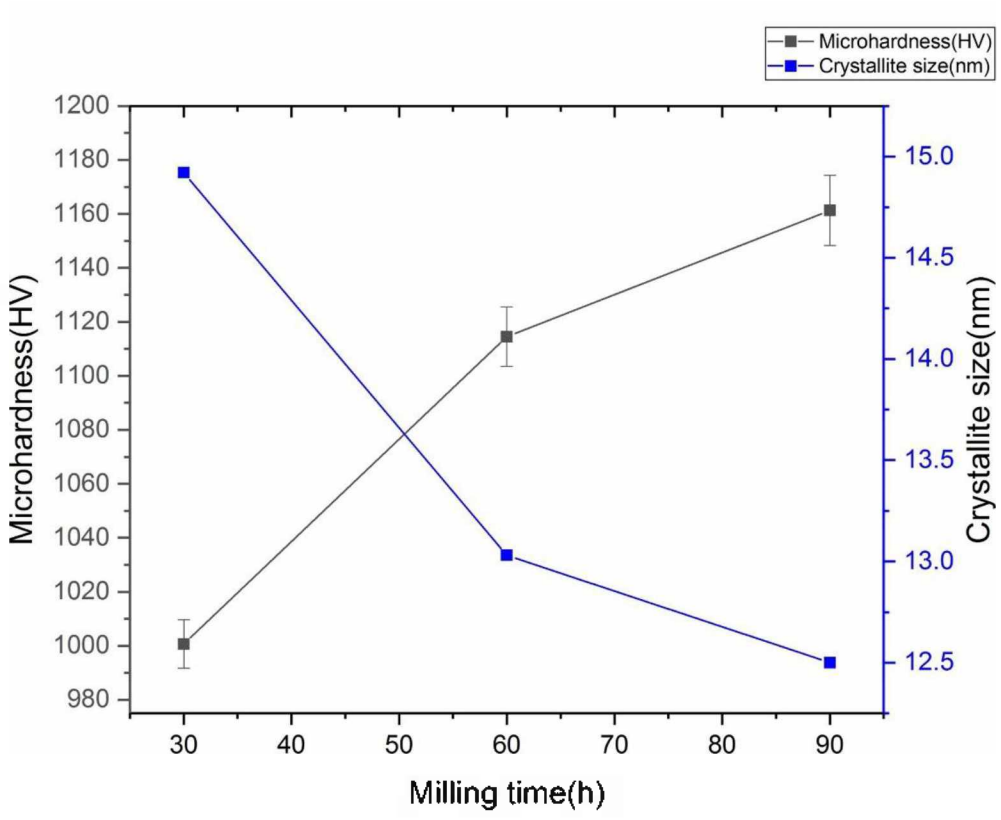

Figure 3.2 Microhardness values and crystallite size for FeSiB 30,60 and 90 h sintered samples

3.3.3 Scanning Electron Microscopy of FeSiB alloys

Figure 3.4 depicts the SEM images of the spark plasma sintered FeSiB alloys processed form powders milled for 30, 60 and 90 hours. For samples sintered form powders with longer milling times a more uniform and more refined microstructure

(smaller grain sizes) and higher levels of alloying is observed as compared to samples with shorter milling durations. The fact that only a small increase in the particle size occurs during the sintering process shows that spark plasma sintering is a promising process for consolidating magnetic alloys from mechanically alloyed powders without severe grain growth.

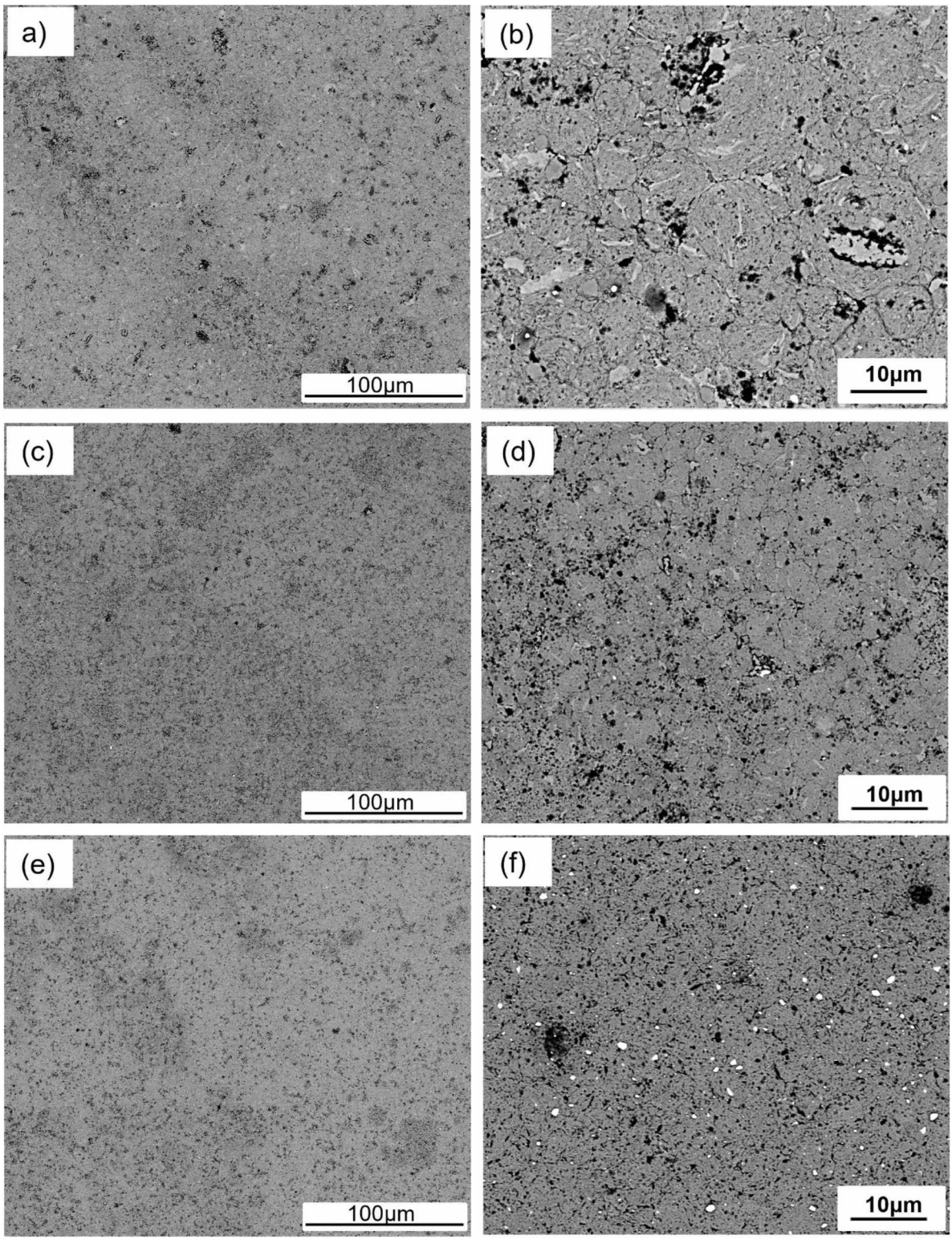

Figure 3.3 SEM images of FeSiB sintered samples; a) 30h, b) 60h and c) 90h

3.3.4 Magnetic properties of FeSiB alloys

Figure 3.5 and table 3.2 show the result of vibrating magnetometer test done on sintered FeSiB magnetic alloys. From the sample sintered from 30h-milled powder to the sample sintered from 90h-milled powder a slight increase in saturation magnetization and decrease in the coercivity value was observed. The increase in the saturation magnetization in case of the sample sintered from the 90h-milled powder can be attributed to the amorphization of the powder and decrease in the crystallite size which results in higher density values. An important observation from the magnetic tests is the difference between the shapes of the M-H curves for the 30-, 60- and 90-hour samples. In case of FeSiB alloy sintered from the 90h-milled powder the dM/dH which has a direct correlation with the magnetic permeability is higher than the FeSiB-30 hours and FeSiB-60 hours samples. As per the Herzer model, the coercivity value of magnetic alloys is strongly influenced by the size of their grains. This model states that when the average size of the grains drops below 40 nm the coercivity value decreases as well due to ferromagnetic exchange interactions [92]. Another important factor in determining the coercivity value is magneto-crystalline anisotropy. Reduction in grain size which results in reduction in magneto-crystalline anisotropy results in lower coercivity values.

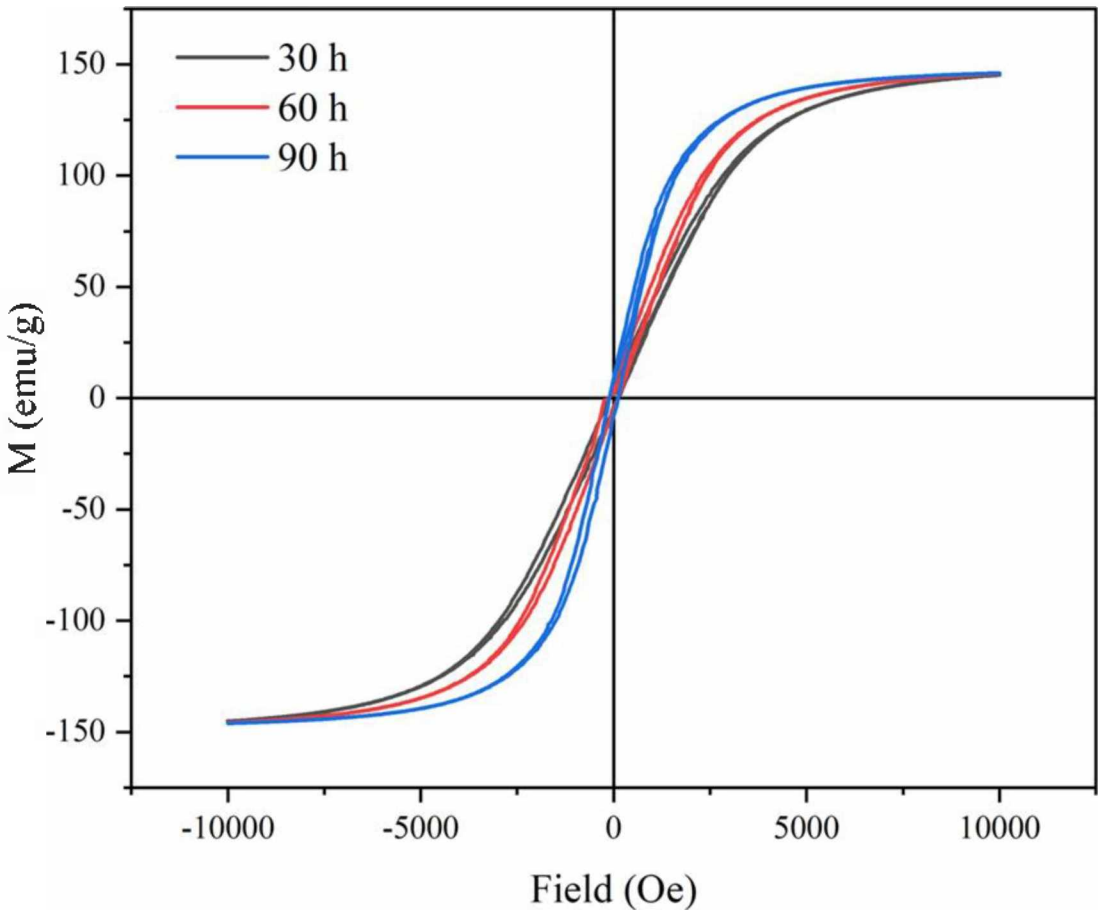

Figure 3.4 Magnetization and coercivity values for FeSiB 30,60 and 90h

Table 3.1 Magnetization and coercivity values for FeSiB 30,60 and 90h

Sample	Ms (emu/g)	Hc (Oe)
FeSiB-30h	145.2	117
FeSiB-60h	145.8	113
FeSiB-90h	146.1	113.4

3.3.5 X-ray diffraction of FeSiB, FeSiBCu and FeSiBNb alloys

Figure 3.6 depicts the XRD pattern of FeSiBNb, FeSiBCu and FeSiBCuNb alloy powders milled with rotation speed of 350 rpm and milling duration of 90 hours. Based on the XRD patterns the main phase observed in all 3 powder alloys is the α-Fe_3Si phase with no dominant secondary phases present. From Fig. 3.6 XRD patters it can be observed that the FeSiBCuNb sample exhibits a significant broadening of the Fe_3Si diffraction peak at 2θ of 45° as compared to the similar peak in FeSiBCu and FeSiBNb samples. This increase in full width at half maximum (FWHM) and more broadening of the peak in case of the FeSiBCuNb sample can be attributed to the smaller size of its crystallite compared to the other 2 samples.

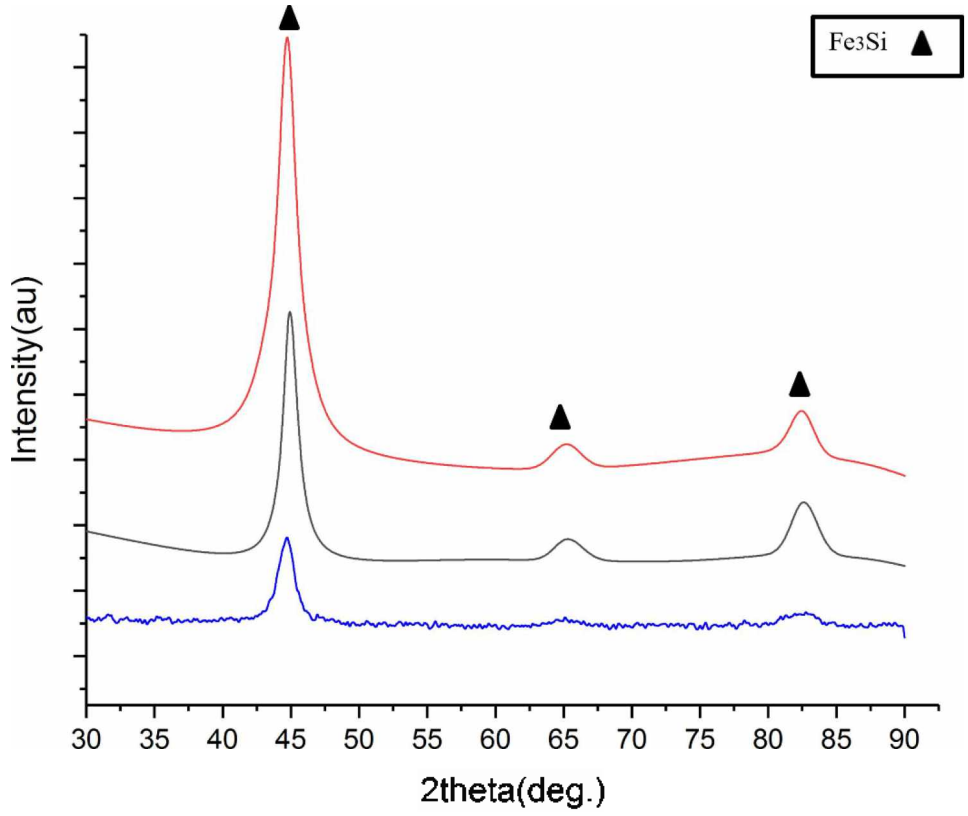

Figure 3.5 XRD pattern for Finemet, FeSiBNb and FeSiBCu alloy powder

Figure 3.7 depicts the XRD patterns of spark plasma sintered FeSiBNb, FeSiBCu and FeSiBCuNb samples sintered with the same SPS parameters. Presence of a large volume fraction of α-Fe_3Si phase can be clearly observed in all the sintered alloys. In addition to the main α-Fe_3Si phase minor secondary peaks from formation of Fe_2B and $Fe_{23}B_6$ boron phases were also spotted in the FeSiBCu and FeSiBNb samples. Secondary crystallization of Fe_3B phase usually happens at temperatures above 550°C and is followed by formation of the Fe_2B phase [93]. Addition of niobium to the composition along with copper results in formation of $Fe_{23}B_6$ phase in later stages of solidification. Ping et al. [94] discovered that addition of niobium changes the crystallization process and aids the formation of secondary $Fe_{23}B_6$ and Fe_3B phases along with the α-Fe_3Si phase. Formation of $Fe_{23}B_6$ phase precipitates occurs at the interface between the α-Fe_3Si phase crystalline and the Fe amorphous matrix.

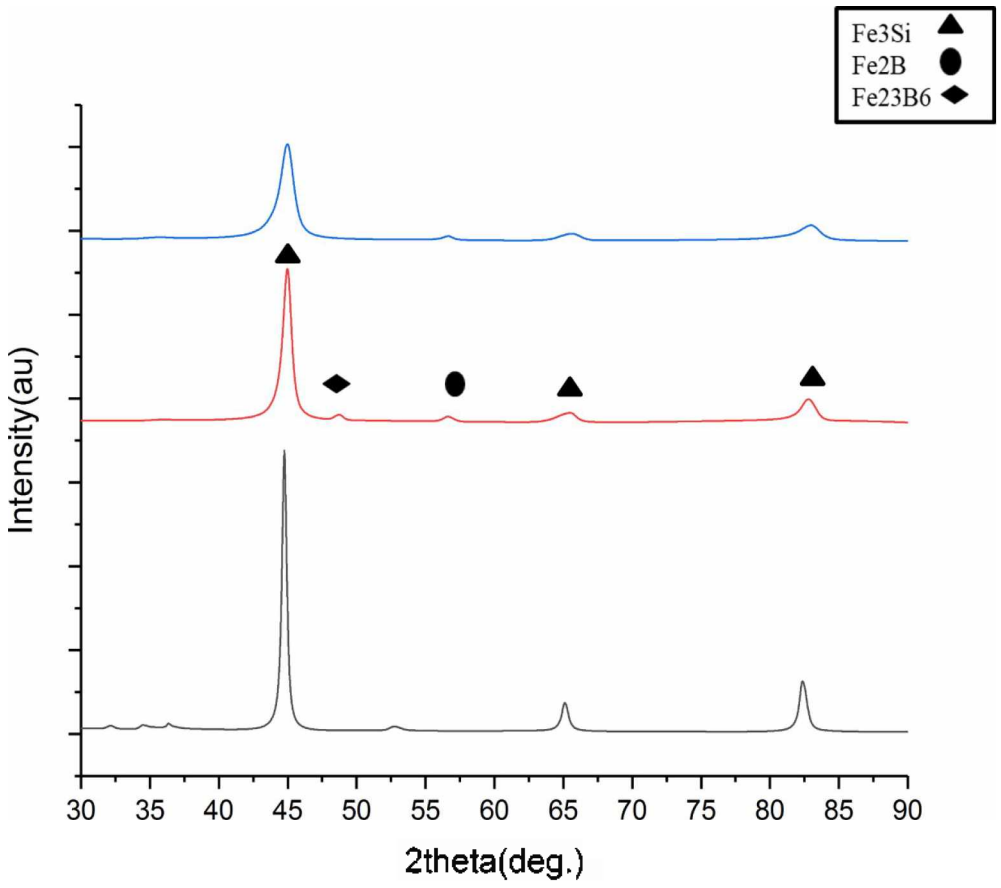

Figure 3.6 XRD pattern for Finemet, FeSiBNb and FeSiBCu sintered samples

3.3.6. Crystallite size and microhardness of FeSiNCu and FeSiBNb and Finemet alloys

The correlation between the crystallite size (calculated by the Scherrer Equation from the XRD results) and the microhardness values (obtained from a standard Vickers microhardness tester) of spark plasma sintered FeSiBCu, FeSiBNb and finemet alloys is depicted in figure 3.8. From fig. 3.8, it can be observed that the crystallite size and the microhardness values are inversely correlated. The mechanically alloyed FeSiBCu sample has the crystallite size of 6.8 nm and the sintered FeSiBCu has crystallite size of ~13 nm. The crystallite size of the mechanically alloyed FeSiBNb sample is 4.7 nm and the crystallite size of the sintered FeSiBNb sample is ~7.7 nm. In the case of both

FeSiBCu and FeSiBNb samples a slight increase in size of crystallites is observed after the sintering process at maximum temperature of 550 °C. Presence of niobium helped in preventing aggressive growth of crystallites and as a result the FeSiBNb alloy has smaller crystallites in comparison to the FeSiBCu alloy. However, in case of finemet alloy where both copper and niobium are present in the composition the crystallite size is higher than FeSiBCu and FeSiBNb samples which is why this alloy shows lower microhardness values as compared to the other two alloys. Moreover, even though copper helps in increasing the precipitation of Fe_3Si crystallites it has a negative effect on the grain growth in the sintering process. Copper decreases the crystallization temperature [95] and as a result the crystallization process takes place at lower temperatures during the sintering process. Magnetic alloys that contain copper will have sufficient time for grain growth during the sintering process and will therefore have larger grain sizes (as observed in the FeSiBCu sample). Furthermore, Martin et al [27] stated that simultaneous addition of both copper and niobium to the FeSiB-base alloy results in reduction of the stabilizing affect that niobium has on the amorphous FeSiB phase.

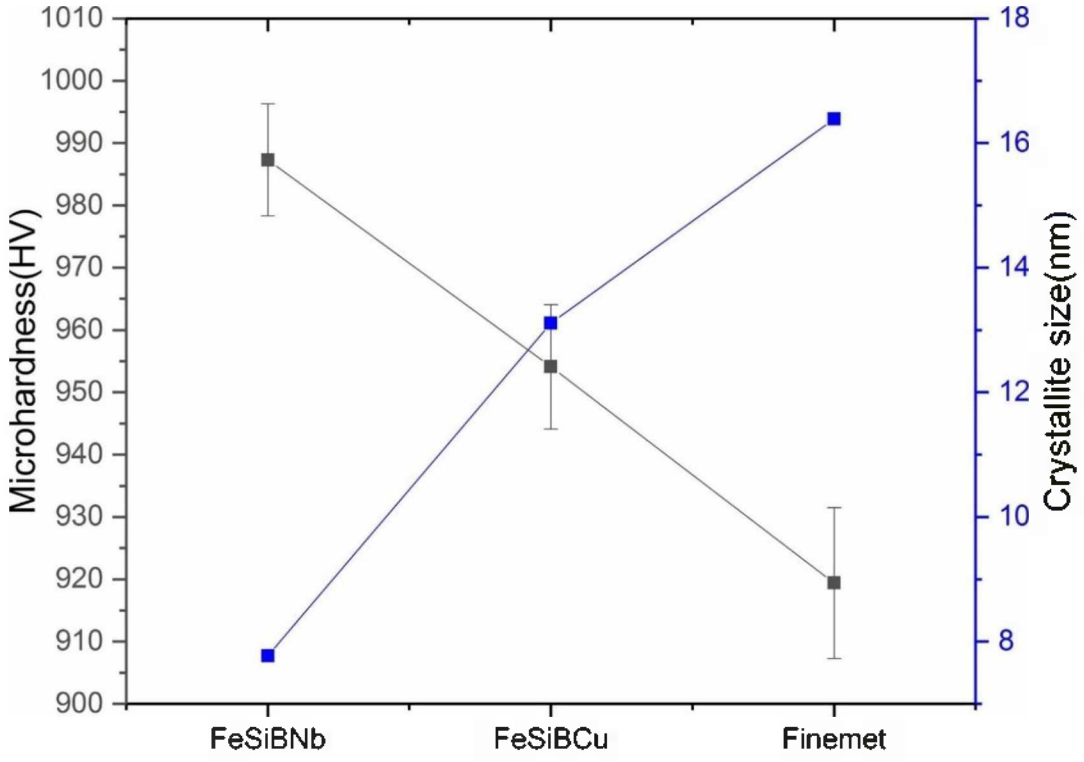

Figure 3.7 Microhardness values for Finemet, FeSiBCu and FeSiBNb sintered samples

3.3.7 Scanning electron microscopy of FeSiBN, FeSiBCu and Finemet alloys

Fig. 3.9 depicts the SEM images of FeSiBCu alloy sintered from 90 hours-milled powder, FeSiBNb alloy sintered also from 90 hours-milled powder and FeSiBCuNb alloy sintered from 120 hours-milled powder in 2 different magnifications. It can be observed that the sintered FeSiBNb alloy exhibits a more refined microstructure in comparison to both FeSiBCu and FeSiBCuNb samples. Size of the particles has a significant effect on the sintering behavior of the alloy. During the sintering process the smaller particles are capable of providing larger surface area per unit volume which results in better sintering

and a more homogeneous microstructure and higher levels of densification as a result. This can be seen in case of niobium containing alloys.

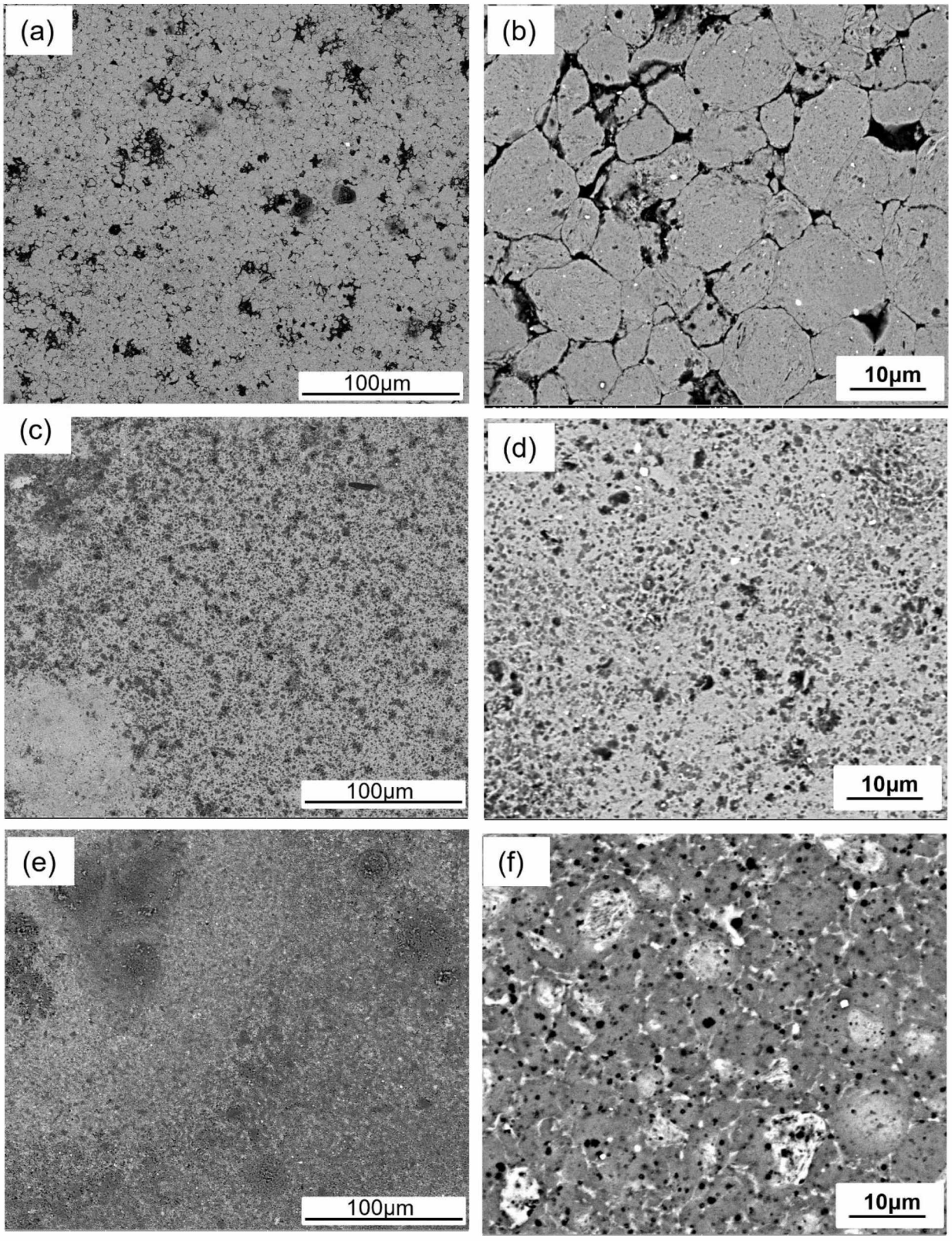

Figure 3.8 SEM images of a and b) FeSiBCu, c and d) FeSiBNb and e and f) Finemet sintered samples

3.3.9 Magnetic properties of FeSiBCu, FeSiBNb and Finemet alloys

The results from magnetic tests for sintered FeSiBCu, FeSiBNb and FeSiBCuNb alloys using vibrating magnetometer is depicted in figure 3.10 and table 3.3. The coercivity values of these magnetic alloys are reasonable while the saturation magnetization is high for all compositions. The finemet alloy shows the highest value for saturation magnetization as compared to both FeSiBCu and FeSiBNb alloys due to absence of any boron phases such as Fe_2B and $Fe_{23}B_6$ in the sample. Presence of these boron phases significantly affects the saturation magnetization therefore, due to presence of small volume fractions of Fe_2B and $Fe_{23}B_6$ phases, FeSiBCu and FeSiBNb samples exhibit lower saturation magnetization values. The reason for this deterioration in the magnetic properties of the alloys when boron phases are present in sample is due to the fact that these phases act as pinning sites for magnetic domains which consequently decreases the saturation magnetization values. The finemet alloy shows a higher coercivity value as compared to FeSiBNb and FeSiBCu samples. The reason for the higher coercivity value in case of the finemet alloy is the development of high internal strain during the mechanical alloying of this alloy, which was milled for longer milling duration of 120 hours, as compared to FeSiBCu and FeSiBNb which were both milled for 90 hours.

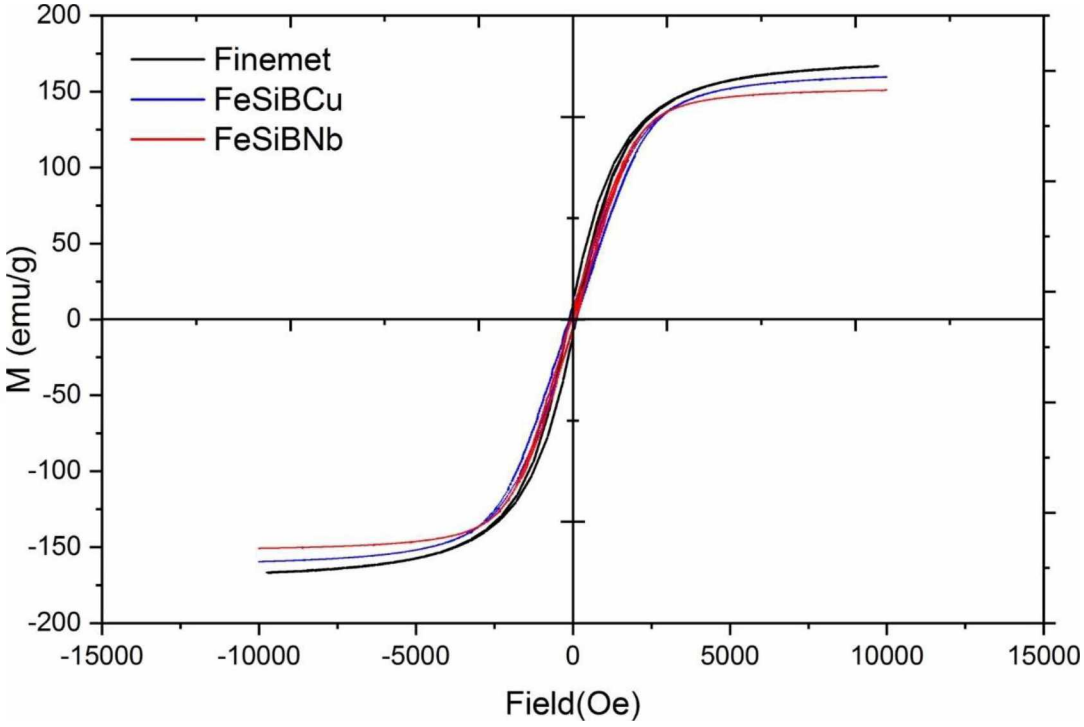

Figure 3.9 Magnetization and coercivity values for FeSiBCu, FeSiBNb and Finemet

Table 3.2 Magnetization and coercivity values for FeSiBCu, FeSiBNb and Finemet

Sample	Ms (emu/g)	Hc (Oe)
FeSiBCu	159.6	87
FeSiBNb	150.8	62.4
Finemet	166.8	109.2

Drbohlav [33] who studied the microstructure of nanocrystalline soft magnetic alloys stated that while simultaneous addition of copper and niobium is not necessary for

crystallization it will result in more effective dispersion of Fe_3Si nanocrystalline within the amorphous iron matrix which consequently improves the magnetic properties of the FeSiBCuNb alloys. Overall, addition of copper, niobium or a combination of the two (NbCu) to the base FeSiB alloy enhances the saturation magnetization and decreases the coercivity value in comparison to FeSiB alloys that were mechanically alloyed using the same processing parameters. From the results of our magnetic tests, we observed that the copper containing alloy (FeSiBCu) shows higher coercivity value of 87 Oe in comparison to the niobium containing alloy (FeSiBNb) which showed the coercivity value of 63.4 Oe. Marin et al. [27] stated that the copper enriched clusters in the copper containing alloy act as pining centers for domain wall displacement which results in an increase in the coercivity value. They did not observe such clusters in niobium containing samples which can be the reason for lower coercivity value in case of the FeSiBNb alloys [27]. Moreover, adding copper to the FeSiB-base alloy destabilizes the glassy/amorphous phase of FeSiB and results in higher coercivity values in comparison to niobium containing FeSiB alloys. Furthermore, individual addition of copper and niobium to the FeSiB alloy would decrease the coercivity compared to the base FeSiB alloy. Alam et al. [22] who studied the laser devitrification of amorphous FeSiB alloys and the role of addition of copper and niobium to them observed a higher saturation magnetization as well as higher coercivity values for copper containing alloy as compared to the niobium containing alloy. Yoshizawa et al. [49] who studied the microstructure of iron-based soft magnetic alloys observed that adding Cu and Nb to the amorphous FeSiB alloy causes a distinctive alloy-phases which is responsible for enhanced magnetic properties of the alloy.

As a part of this research work, we studied the mechanical alloying and spark plasma sintering processing parameters and optimized them for best mechanical and magnetic properties for our magnetic alloys. The magnetic alloys processed using the mechanical alloying and spark plasma sintering processing parameters resulted from this research work show magnetic properties on par or even better than FeSiB-based alloys processed using conventional methods. Our results were even superior to results observed from mechanical alloying of iron-based magnetic alloys in other research works. In their study on mechanical alloying of finemet-type magnetic alloys Alleg et al. [96] found saturation magnetization of the alloy to be 14.3 emu/g and coercivity to be 62 Oe for nanocrystalline finemet alloy milled for 150 hours. In the same study Alleg at al. [96] also investigated nanocrystalline FeSiB powder alloy that was milled under the exact condition as the finemet alloy and the highest saturation magnetization that they achieved was a little over 8 emu/g which is much lower than the results we observed from our experiments. Gheiratmand et al. [68] who tried to obtain amorphous finemet powder by mechanically alloying amorphous finemet ribbons and then consolidating the resultant powder alloy using the SPS process observed saturation magnetization of 124 emu/g as their highest value which is still lower than saturation magnetization values we obtained from mechanical alloying and spark plasma sintering of finemet alloy from elemental powders. Kang et al. [97] who studied the vacuum hot pressing of FeSiBNb composition found the saturation magnetization of their composition to be 127 emu/g. Neamt et al. [98] studied the mechanical alloyed FeSiB alloys and reported the saturation magnetization for the wet mechanically alloyed FeSiB alloy to be at about 131 emu/g and about 141 emu/g after the annealing process. In the present study mechanically alloyed

FeSiB sample with rotation speed of 700 rpm, BPR 5:1, milling duration 10h and ball size 5mm, which was processed by spark plasma sintering at temperature of 470°C with pressure of 600MPa and holding time of 5 minutes show saturation magnetization as high as 182.8 emu/g.

3.5 Conclusions

FeSiB-based alloys were processed using the mechanical alloying technique and consolidated via spark plasma sintering process. FeSiB alloys were mechanically alloyed for durations of 30, 60 and 90 hours in order to study the role of milling duration on mechanical and magnetic properties as well as microstructure of these alloys. The effect of addition of two new elements to the base FeSiB alloy was studied. Copper and niobium were added to FeSiB alloys separately and simultaneously making the following compositions: FeSiBCu, FeSuBNb and FeSiBCuNb in order to study the effects of each element on mechanical, microstructural and magnetic properties of FeSiB-based magnetic alloys. Results from the experiments are as follows:

- The main phase present in all the FeSiB-based powders after the mechanical alloying process was α-Fe_3Si. After the spark plasma sintering process other secondary boron phases were detected in the samples including Fe_2B and $Fe_{23}B_6$ due to the sintering temperature being higher than the crystallization temperature of these minor phases.
- The crystallite size of powders milled for longer times decreased in case of all the FeSiB samples
- FeSiB samples sintered from powders milled for longer time showed higher microhardness values due to decrease in the crystallite size (mainly α-Fe_3Si).

- X-ray diffraction patterns of FeSiB powder alloys show the beginning of amorphization process after milling duration of 90 hours.
- FeSiB-based alloys containing copper (FeSiBCu) showed higher saturation magnetization as well as higher coercivity values in comparison to FeSiB-based sample containing niobium (FeSiBNb). However, the sample containing niobium showed higher microhardness values and lower coercivity as well as finer microstructure in case of sintered FeSiBNb and smaller grain size in case of powder FeSiBNb as compared to FeSiBCu samples.
- Due to presence of high volume fractions of α-Fe(Si) crystallites, finemet alloy sintered from the powder that was mechanically alloyed for 120 hours showed the highest saturation magnetization
- Saturation magnetization of FeSiB samples increases with longer milling durations with FeSiB-90h sample showing the highest value; and coercivity value decreases with longer milling durations. Overall FeSiB alloys milled for longer times show better magnetic properties.

[2]CHAPTER IV

SPARK PLASMA SINTERING OF FeSiBCuNb/FINEMET BASED ALLOYS

4.1 Abstract

Mechanical alloying or powder metallurgy has been around for the past 3 decades, and it is a unique technique for processing powders which allows for homogeneous blending of elemental powders. Mechanical alloying process, also sometimes referred to as milling process, has several processing parameters which can influence the outcome of the alloying process. Processing parameters such as milling duration, size of the milling balls, the process control agent (to prevent the cold welding), the weight ratio of powder vs. the milling balls, the rotation speed and even the volume of the milling vials which is filled with the milling media (powder and milling balls) can affect the state of the final alloy. In this chapter we have introduced the mechanical alloying process and its influential processing parameters and how each of these parameters can affect the mechanical, microstructural and magnetic properties of the Finemet-based alloys. From our results increasing the milling duration to 120 hours resulted in full amorphization of the FeSiBCuNb powder alloy. Effect of BPR on

crystallite size of the finemet alloy was studied and higher BPR of 15:1 showed smaller crystallite size as compared to BPR 10:1. Microhardness and magnetic properties of the sintered finemet alloy improved with longer milling duration.

4.2 Introduction

Mechanical alloying is a solid-state powder processing technique in which the powder particles are repeatedly fractured and rewelded in a high energy ball mill [99-102]. This process was stablished over 30 years ago as a way for reducing the size of powder particles as well as to produce alloys with homogeneous structures from elemental blend powders. The mechanical alloying process has received significant attention in the past few years due to its ability to synthesize both nanocrystalline and amorphous material [103-105]. Mechanical alloying offers a non-equilibrium processing route for alloying material at relatively lower cost compared to some other fabrication techniques and is capable of processing material in large quantities [55][106]. Currently, most amorphous magnetic alloys are prepared by a process called melt spinning in which melted material is cooled down with very high cooling rates, in range of 10^6-10^8 °C/S, in order to prevent the microstructure from crystalizing [107-109]. The main disadvantage of the melt spinning process is that it only allows for the fabrication of very thin ribbons and wires of magnetic materials. In order to guarantee a fast cooling and prevention of crystallization (to keep the microstructure amorphous) the thickness of the ribbons fabricated by melt spinning is limited to 50 μm [5]. Therefore, in order to obtain bigger and more complex shapes a huge number of these ribbons need to be stacked on top of each other. Moreover, these ribbons are very thin and are quite brittle and therefore are not suitable for fabrication of certain magnetic components specially with more complex

shapes [110-111]. Additionally, the shapes of the magnetic components that are fabricated via this technique are limited to the shapes and sizes that can be carved or machined out of the stack of ribbons. This is where obtaining an amorphous powder alloy by mechanical alloying and consolidating it via a new technique, with the ability to fabricate samples in bulk format, becomes even more important. One great advantage that the mechanical alloying process has in regard to the amorphization process is its capability of amorphization of elemental powders by diffusion along primary component interfaces at relatively lower temperatures [112]. The mechanical alloying process also has the ability to permit different metals with varying melting temperatures form alloys which is a major advantage compared to conventional alloying processes that are based on melting and mixing of elements. Mechanical alloying process is also capable of producing amorphous material from material in variety of shapes and sizes. Opposite to magnetic components fabricated via melt spinning, mechanically alloyed powders milled from elemental powders can be compacted and consolidated using the spark plasma sintering method. The mechanical alloying followed by the spark plasma sintering process not only increases the efficiency of the magnetic components but also miniaturizes them for applications in electric and electronic equipment. The miniaturization is possible due to elimination of stacking of a large number of ribbons on top of each other and instead producing the alloy in bulk format. The magnetic products fabricated from the mechanical alloying and spark plasma sintering techniques can be specifically used in hybrid and electric cars due to smaller sizes. This is an extremely important application due to the recent increase in air pollution and need for cleaner energies. The two main routes to obtain amorphous powder via the mechanical alloying

process is milling of elemental powders that make up the powder composition of the alloy and milling of amorphous ribbons [113]. Most of the research done on FeSiB-based alloys have focused on obtaining the amorphous powder by mechanically alloying amorphous ribbons. However, in our research we have focused on obtaining the amorphous powder via milling of its elemental powders. During the mechanical alloying process, the amorphization is only achieved if obtaining the amorphous phase is kinetically faster than the crystalline phases [114]. Lattice defects such as interstitials, dislocations, and vacancies that occur during the mechanical alloying process can influence the thermodynamics and kinetics of the process (large negative heat of mixing) and raise the free energy of the crystalline phase as compared to the amorphous phase which will ultimately result in amorphization taking place [115-117]. Moreover, the energy that is released during the mechanical alloying process, due to crashes between the milling media, governs the formation of the amorphous phase [118]. One of the most important parameters that can affect the amorphization process is the milling duration. Previous studies on this subject have shown that in cases where other than the milling duration the rest of the milling parameters were kept constant; increasing the milling duration results in more amorphization. Raja et al. [74] who studied the microstructure of mechanically alloyed finemet alloys, observed starting of amorphization at stages as early as 6 hours of milling. However, based on their observations the full amorphization did not take place until a much longer milling time. During the mechanical alloying process the initial elemental powders first reach a nanocrystalline state; after this point increasing the milling duration results in appearance of the amorphous phase and the longer milling time (to a certain extent) will eventually result in full amorphization [74][119]. Schwartz

et al. [60], explained that during the amorphization reaction, mixing occurs in a way that the amorphous phase has lower free energy and is therefore more stable compared to the crystalline components. This difference in the free energies of the crystalline and amorphous phase is the reason why amorphization takes place during the mechanical alloying process [120]. According to Hellstern et al. [121], who studied the amorphization of alloys during the mechanical alloying process, the plastic deformation which occurs during the mechanical alloying process will consequently increase the free energy of the defected crystalline phases. This means that formation of the amorphous phase during high energy ball milling is favored due to the lower free energy. Furthermore, in their studies on amorphization of different alloys during the mechanical alloying process, Koch [18] also concluded that formation of defects during the mechanical alloying process is the reason why free energy of the crystallite phase increases during milling, which as a result makes this phase unstable in comparison to the amorphous phase.

One of the applications of the mechanical alloying process is reducing the size of the particles alongside the amorphization process. The elemental powders during the initial stages of the mechanical alloying are subjected to cold welding which results in an increase in their particle sizes [122]. At these early stages the particles go through plastic deformation and surface flattening that will consequently increase the grain boundaries which results in a higher tendency for particles to fuse together and form bigger particles [123]. At the next stages of mechanical alloying the particles that were fused together in the previous stage get fractured over and over again due to continues collision with the milling balls and therefore the overall diameter of the particles tends to decease at this

stage. The decrease and then increase in the particle size phenomenon during the mechanical alloying process was observed by Neamtu et al. [124] who witnessed the increase of the particle sizes in the first 5 hours of their MA process as a result of cold welding between the particles and at later stages a decrease in the diameter of the particles due to the repeated fractures associated with the ball milling process. Interestingly, at a certain point in the mechanical alloying process, the tendency of powder particles for fragmentation becomes equal to the cold-welding tendency. At this point the size of the particles usually do not change very drastically, or changes at a very low speed or even not at all. Our goal for this research work was to study the effect of each of the milling processing parameters including ball to powder ratio, milling duration, the process control agent, rotation speed and even the level by which the milling bowl is filled with the milling media on the microstructure, particle size, mechanical properties and magnetic properties of the resultant magnetic alloy.

4.3 Experimental procedure

$Fe_{73.5}Si_{13.5}B_9Cu_1Nb_3$ magnetic alloy was prepared from Fe, Si, B, Nb, Cu elemental powders using the mechanical alloying process. High energy planetary ball mill Fritsch Pulverisette 7 was used for the milling process. Milling balls and bowls were made of tungsten carbide and the process was done under argan atmosphere with lids on the milling bowls securely sealed in order to prevent oxidation. In order to prevent cold welding 2 wt% stearic acid/ benzene were added to the elemental powder mix as a process control agent (PCA). Ball to powder weight ratios (BPR) used in the mechanical alloying process were 10:1 and 15:1 in order to study the role of BPR on crystallite size and mechanical properties of the finemet alloys. The milling durations used for the

experiments in this chapter were: 30, 60, 90 and 120 hours and the rotation speed in all the experiments was 350 rpm. The milling process was done using milling balls with diameter of 3mm and 10 grams of powder was milled in all cases. In order to prevent the milling media from overheating during the mechanical alloying process and the powder getting cold welded, we put 10 minutes pauses in between the 10 minutes milling periods. An experiment was done on the $Fe_{73.5}Si_{13.5}B_9Cu_1Nb_3$ composition using the same mechanical alloying parameters as mentioned for finemet before, using benzene as the process control agent in order to find out which PCA (benzene or stearic acid) is more effective for amorphization of finemet-type alloys. Spark plasma sintering was done under argon atmosphere using packing pressure of 20 MPa, sintering temperature of 550°C, maximum pressure of 600 MPa and heating rate of 30°C/min and pressure ramping speed of 100 MPa/min. 10 mm dies, and punches were made of tungsten carbide and were covered by graphite foil to prevent contact between the powder and dies and punches as well as to increase the conductivity. The powder was held at the maximum temperature and pressure for five minutes. One sample was sintered from each of the powder alloys prepared by mechanical alloying giving us 4 samples milled with BPR 10:1 (30, 60, 90 and 120 h) and one sample with BPR 15:1 with milling duration of 120 hours. The sintered samples were then mounted and polished using grinding papers 250-1200 grit followed by 30-45 minutes of polishing using colloidal silica on a micro cloth followed by 12 hours of vibromet polishing. Scanning electron microscopy was done on all the sintered and polished samples using a FEI-Quanta Nova-SEM with magnifications ranging from 100x to 5000x. phase and microstructural analysis on the samples were done by X-ray diffraction. X-ray diffraction was done using a X-ray diffraction (XRD)

machine using a Rigaku Ultima III X-Ray diffractometer (Cu Kα radiation, 1.54 Å) and 2θ range of 30° to 90° for all of the powder alloys milled with BPR 10:1 and samples sintered from powders milled with BPR 10:1. The crystallite sizes of the samples were measured using the XRD results with the help of the Scherrer Equation [80]. Microhardness of the sintered samples was measured using a standard Wilson Vickers microhardness tester. The measurements were taken under a load of 5N and dwell time of 10 seconds. For each sample microhardness readings of 10 different spots were taken into account and the average value was reported. Magnetic properties of the samples were measured using a magnetometer (VSMLakeshore 7404) with maximum magnetic field of 1T.

4.4 Results and discussion

4.4.1 X-ray diffraction of finemet alloys

Figure 4.1 depicts the XRD patterns of mechanically alloyed finemet powders with milling durations of 30, 60, 90 and 120 hours and the samples sintered from the respective powders. From the XRD patterns it can be observed that the α-Fe_3Si phase is the primary phase found in both powder and sintered samples. In case of the milled finemet powders it can be observed that the Fe_3Si peak located at 2θ = 45° has been broadened with increasing milling duration from 30 hours to 120 hours. The increase in full width at half maximum (FWHM) and broadening of the peak is a due to the decrease in the size of the crystallites (Figure 4.4 depicts the crystallite size measurements) as the milling duration increases. It appears that the increase in milling duration from 30 to 120 hours is still in the stage of crystallite size reduction in the mechanical alloying process. Increase in the milling time any further than 120 hours could have resulted in complete

stop in size reduction or even an increase in the size of the crystallites. The XRD pattern (figure 4.1-a) of the 120 hours milled finemet alloy shows no sharp peaks which can be associated with the amorphization process. The α-Fe_3Si phase peaks at $2\theta = 85^\circ$, $2\theta = 65^\circ$ and $2\theta = 45^\circ$ almost disappear after 120 hours of mechanical alloying. This observation indicates that a high level of amorphization has taken place in case of samples with longer milling durations. Different studies done on magnetic alloys with iron and silicon in their composition have shown the formation of α-Fe_3Si phase happens at different stages of mechanical alloying. Raja et al. [74] studied the microstructure of soft magnetic finemet alloys and observed formation of α-Fe_3Si phase at very early stages of milling (as early as 6 hours of milling) and stated that further milling only reduces the grain sizes. However, Yang et al. [69] who also studied the mechanical alloying of finemet alloys only observed formation of α-Fe_3Si crystallites (with grain size of 10 nm) after 80 hours of milling and did not find any trace of the phase at earlier stages of mechanical alloying. In our study of mechanically alloyed finemet powder we observed peaks of α-Fe(Si) at milling durations as early as 30 hours (Figure 1-a). As mentioned before, finemet alloy is consist of iron, silicon, boron, copper and niobium. Iron which has the highest weight percentage acts as the matrix and other elements diffuse into the Fe-matrix completely or partially at different stages of mechanical alloying. Out of the above-mentioned elements boron diffuses into the Fe matrix first. The x-ray diffraction patterns of both powder and sintered alloys show traces of the boron rich phases. Peaks at 2θ value of 36.92° present in the 60 and 90 hour milled samples indicates the existence of boron phase Fe_2B. According to Neamtu et al. [124] as the milling progresses, after the boron atoms, silicon, which has a bigger atomic radius as compared to boron starts to dissolve into the Fe

matrix. Traces of silicon phases are observed in all of the samples.

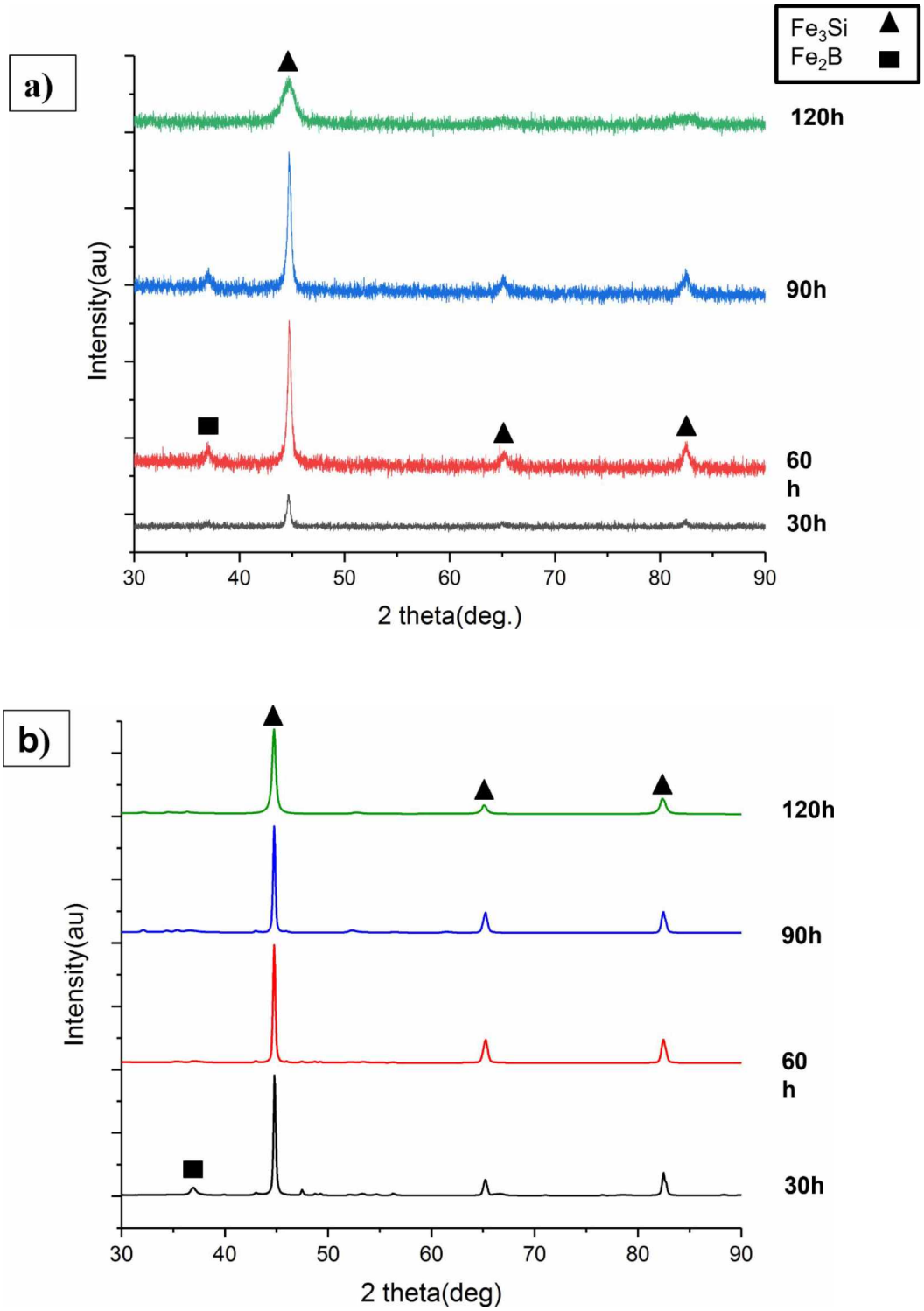

Figure 4.1 XRD patterns of a) Finemet powder b) sintered alloy for 30,60,90 and 120h milled powders

4.4.2 magnetic properties of finemet alloys

Fig. 4.2 shows the magnetization versus applied magnetic field curves for mechanically alloyed finemet alloy milled at different milling durations at room temperature and Table 4.1 shows the saturation magnetization and coercivity values of the finemet alloys.

Table 4.1 Saturation magnetization and coercivity values for finemet alloy milled for 30, 60, 90 and 120 hours

Milling time (hrs.)	Saturation Magnetization Ms (emu/g)	Coercivity Hc (A/m)
30	132.3	5928.5
60	130.5	7997.5
90	122.0	7074.4
120	166.8	8689.8

Samples sintered from the 30, 60 and 90 hour milled powders show saturation magnetization values in the same range. However, the sample sintered from the 120-hour milled powder alloy shows a significantly higher saturation magnetization value. Based on the x-ray diffraction patterns of the finemet alloy this increase in the saturation magnetization value can be attributed to the larger volume fractions of α-Fe(Si) phase that is present in this sample as compared to lower milling duration finemet samples. The reason for this difference in the volume fractions of the Fe(Si) phase is the progress of bonding between larger silicon atoms with the iron matrix as the milling progresses and formation of more Fe(Si) phase with longer milling durations. Another reason for observing a higher value for saturation magnetization in case of the 120-hour milled finemet alloy is due to the higher level of amorphization of the powder from which the

sample was sintered in comparison to the 30-, 60- and 90-hour samples. The grain refinement that occurs due to longer milling durations can play an important role in reduction of magneto crystalline anisotropy that eases the rotation of the domain walls and consequently increases the saturation magnetization of the alloy [125].

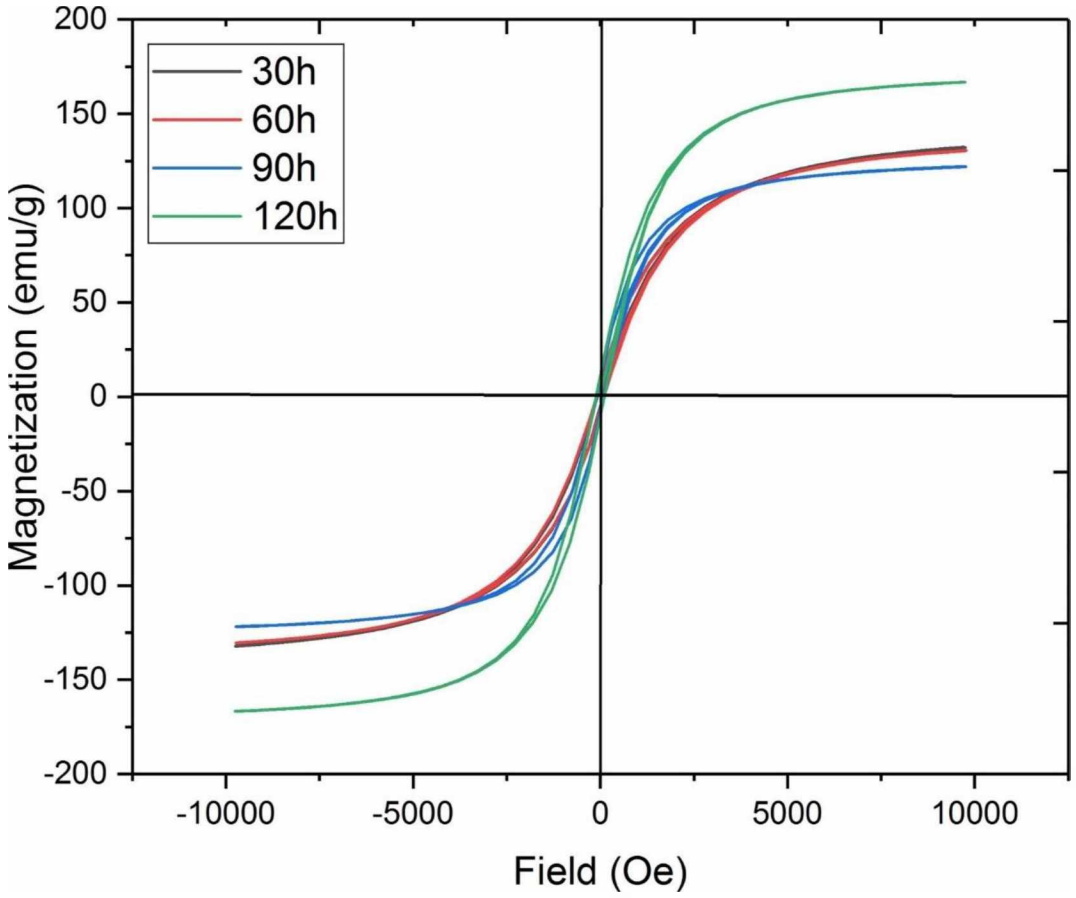

Figure 4.2 VSM results of SPS processed Fe-Si-B-Cu-Nb alloys milled for different durations.120h (a),90h (b), 60h (c), 30h (d)

Other than the phases present in the sample, microstructure is another important factor that effects the magnetic properties of the alloy. According to Alleg et al [126] this dependence of magnetic properties to the microstructure arises from morphology.

4.4.3 Scanning electron microscopy of finemet alloys

Figure 4.3 shows the SEM images of SPS-processed finemet alloys sintered from powders milled for 30, 60, 90 and 120 hours. From this figure it can be observed that the 120 hours milled sample has a homogeneous and much more refined microstructure as compared to coarser structures of other samples which is another reason for better saturation magnetization in case of this sample. From fig. 4.3 it can also be observed that samples sintered from powder alloys milled for different milling durations show a decrease in the size of the grains as well as more uniformity in the microstructure as the milling time increases. It should be mentioned that same spark plasma sintering parameters (550 °C, 600 MPa and 5 min holding time) were used for sintering all the samples depicted in figure 4.3 however, different levels of alloying can be observed for samples sintered from powders with different milling durations. In case of sample sintered from the 30-h milled powder it can be seen that the microstructure is very coarse and not much alloying has taken place. This observation from the SEM images of the sintered samples can confirm that milling duration has an important effect on microstructural refinement and uniformity as well as the level of alloying that takes place during mechanical milling of metals and metal composites.

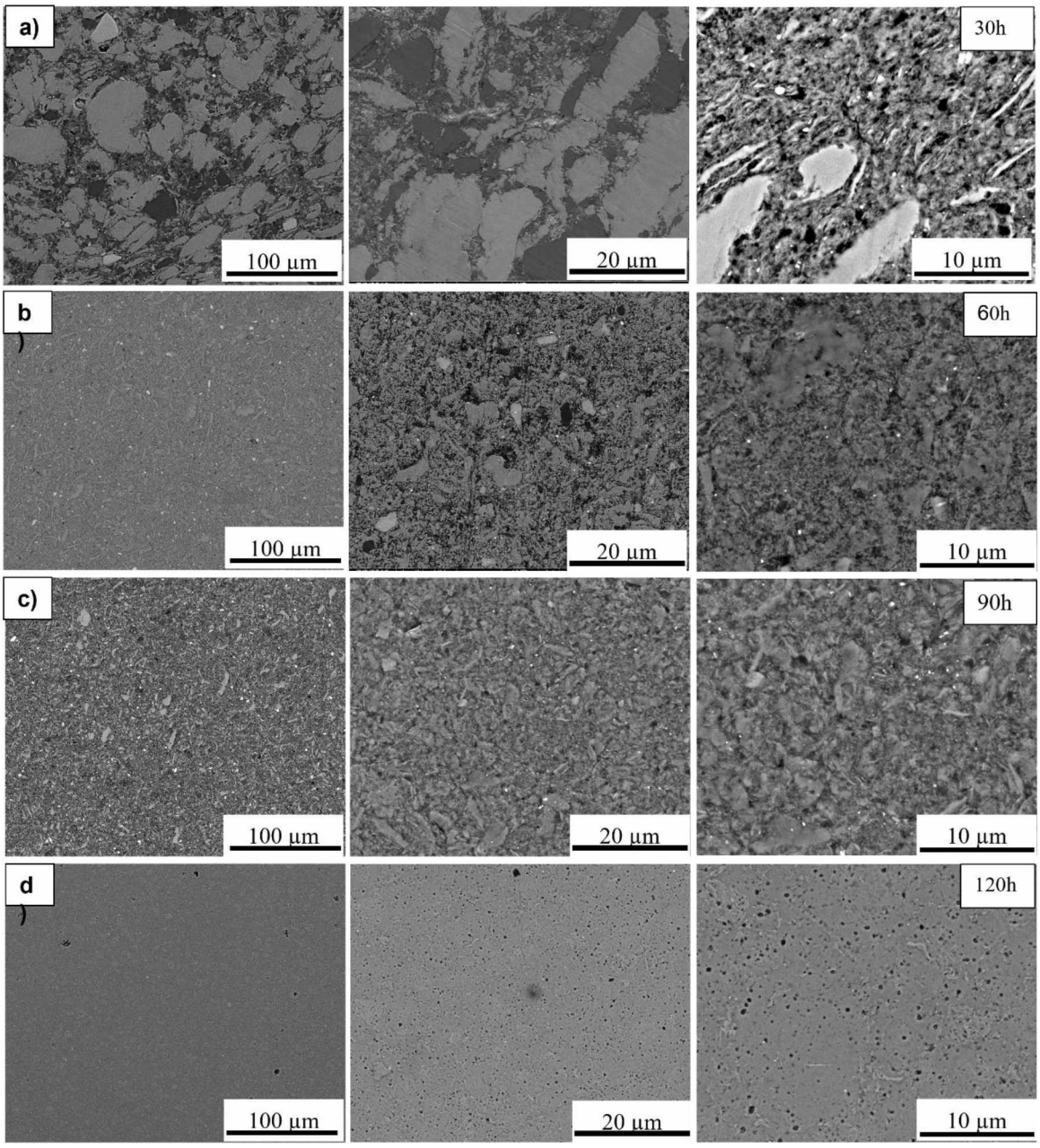

Figure 4.3 SEM images of sintered alloys for (a) 30h, (b) 60h, (c) 90h and (d)120h of milled samples at different magnifications

Even though bulk FeSiB-based alloys processed with mechanical alloying and solidified by spark plasma sintering show very good saturation magnetizations, and they have a potential in producing magnetic components in complex shapes, they show relatively higher coercivity values. Suzuki et al. [127] who studied the nanostructures of advanced magnetic alloys, reported that in order to keep the magnetostriction near zero

certain amount of α-Fe_3Si crystallites needs to be dispersed in the amorphous Fe matrix. They predicted this amount to be about 75 to 80% and stated that the higher volume fractions of α-Fe_3Si crystallites can result in increased magnetostriction and therefore increase the coercivity values. All the sintered samples in our experiments show high volume fractions of α-Fe(Si) phase, specifically the 120 hour finemet sample, and consequently the coercivity values are high for our samples specially for 120 h finemet alloy. Moreover, powder particles processed by mechanical alloying tend to have more irregularity and are usually not spherical in shape in comparison to alloy prepared by other methods such as melt spinning [54]. More pining of the domain walls tends to happen when particles have irregularities on the surface. The irregularity of the shape and the higher roughness results in higher coercivity in mechanically alloyed magnetic alloys in comparison to melt-spun ribbons and magnetic alloys processed with other similar techniques [128]. The higher coercivity values can be reduced to some extend since coercivity is partly due to the strain during the mechanical alloying process which can be eliminated or minimized by annealing heat treatment

4.4.4 crystallite size and microhardness of finemet alloys

Figure 4.4 depicts the correlation between the microhardness of finemet alloys (left axis, black squares) and their crystallite size (right axis, blue squares) sintered from powders milled for 30, 60, 90 and 120 hours. It can be observed that the microhardness value of sintered finemet alloys increased from around 340 HV in case of sample sintered from the 30h milled powder to 950 HV in case of sample sintered from 120h milled powder. The mechanical alloying processing parameters are proven to have an effect on the particle size of the powder alloy and even the microstructure of the alloy that is being

sintered from a mechanically alloyed powder. The crystal size of the finemet alloy went from 20.5 nm in case of sample milled for 30 hours to 18.4 nm in case of the sample milled for 60 hours. The crystallite size further decreased until it reached 90 hours of milling but did not have a significant change going from 90 hours of milling to 120 hours. These changes in the crystallite sizes in the initial stages of mechanical alloying is due to the fact that at these early stages particle sizes decrease due to multiple collisions between milling balls and the powder which occurs constantly. However, the increased in the grain boundaries as a result of these collisions will eventually increase the particles' tendency to fuse together and form bigger particles. At some point these two tendencies become almost equal where the size of the particles will not change significantly. This is in line with our findings depicted in figure 4.4 for milled finemet alloy going from 30 h to 120 h of milling.

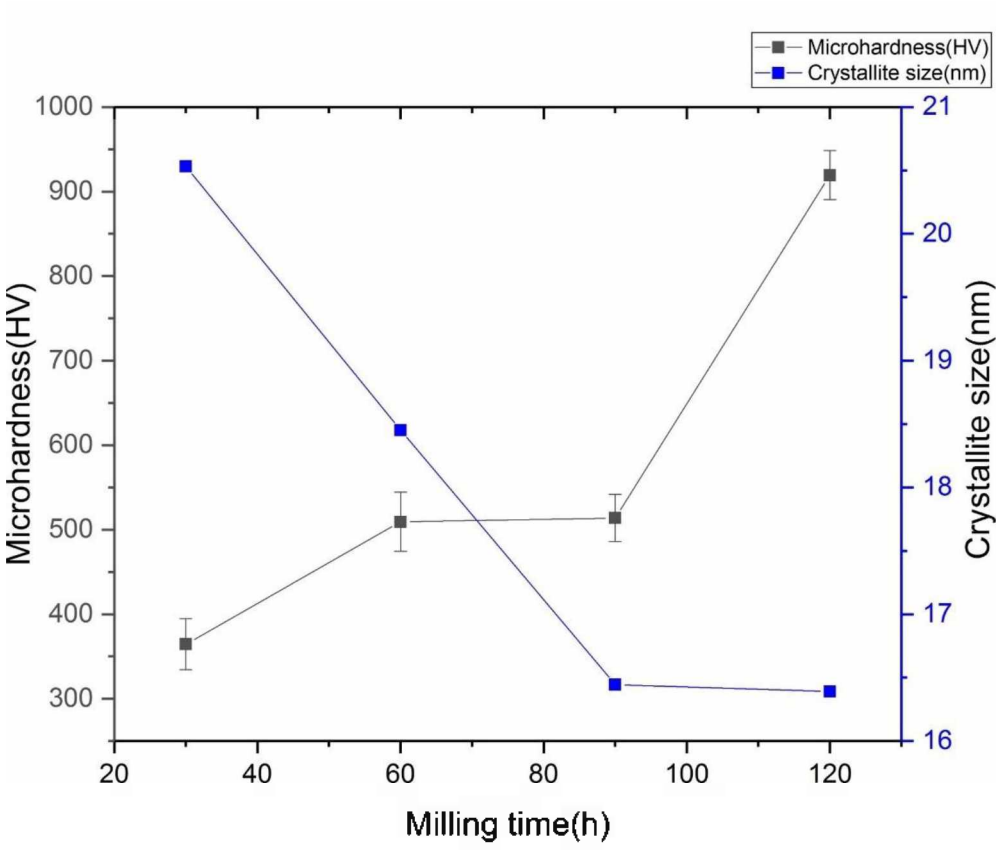

Figure 4.4 Microhardness and crystal size of sintered alloys for 30,60,90 and 120h

One of the most important mechanical alloying processing parameters is ball to powder weight ratio (BPR). BPR plays an important role in defining the microstructure and mechanical properties of the milled alloy. In our initial studies we used ball to powder weight ratio of 10:1 for finemet alloys and observed broadening of the main Fe_3Si XRD peaks and amorphization after 120 hours of milling. Therefore, we decided to investigate the effect of BPR on microstructure and crystallite size of the milled alloys by performing the experiment where other than the BPR the rest of the mechanical alloying processing parameters were kept the same and milling was done on powder alloys with the same composition. Two different BPRs (10:1 and 15:1) were used for mechanically alloying of finemet using 350 rpm as the rotation speed, stearic acid as PCA, milling balls

with diameter of 3mm and milling duration of 120 hours. Since the same amount of powder was used in both cases (10 g) and the milling balls used in both processes had the same diameter and were made from the same material (tungsten carbide) difference in the ball to powder weight ratio was translated to difference in number of milling balls. From these experiments we witnessed a reduction in the crystallite size for samples milled with higher a BPR even though the milling duration was kept the same in both cases. Figure 4.5 depicts the crystallite size of finemet alloy sintered from 120 hours milled powder with BPRs of 10:1 and 15:1. The main reason for this reduction of crystallite size is the increase in the number of collisions that happen during the mechanical alloying process due to higher number of balls which consequently increases the energy transferred to the powder [72]. Suryanarayana [72] who studied mechanical alloying and milling processes stated that the energy required for the physical process of size reduction in grains of powders being mechanically alloyed can be shown by **E** which is equal to $\gamma . \Delta S$, where γ is the specific surface energy and ΔS is the change in the surface area. For this process γ can be considered constant therefore according to the formula ($E = \gamma . \Delta S$) by increasing the energy during the alloying process, the surface area is going to increase. Higher surface area can be translated into smaller and finer powder grains. Moreover, the time required to achieve alloying of the elemental powders as well as to achieve the amorphous phase will decrease by increasing the ball to powder weight ratio due to the increase in the energy and the heat generated during the mechanical alloying process [124]. After this set of experiments, we used the ball to powder weight ratio of 15:1 for mechanical alloying of our FeSiB, FeSiBNb and FeSiBCu powder compositions.

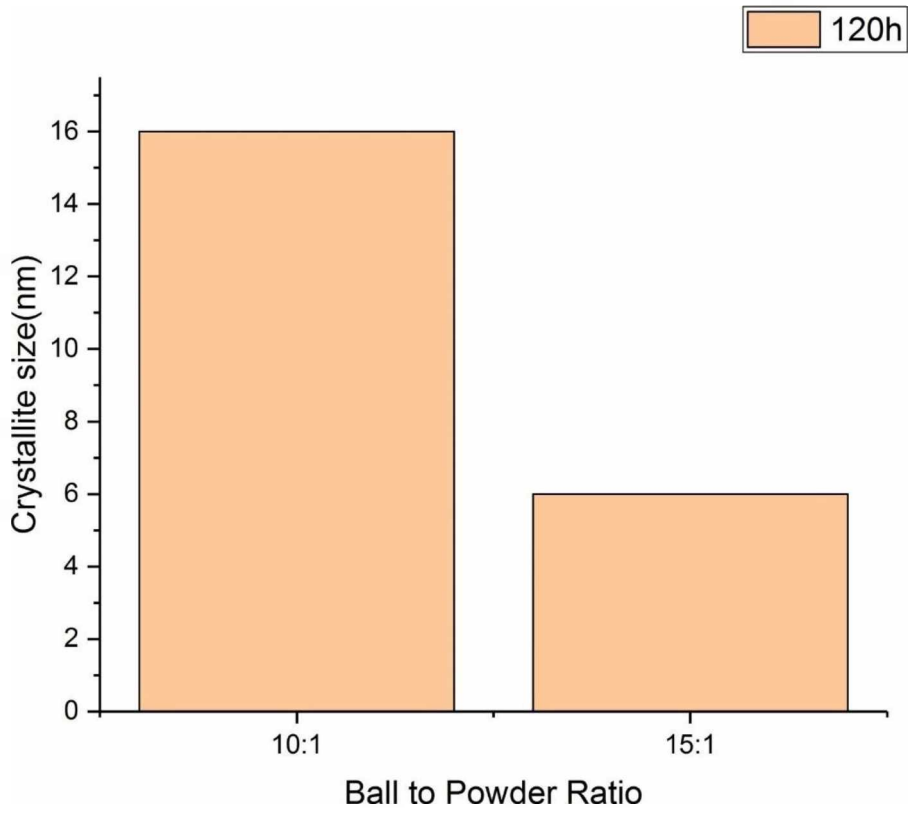

Figure 4.5 Crystal size of 120h sintered alloy with ball to powder ratio of 10:1 and 15:1

4.5 Conclusions

FeSiBCuNb alloys were processed via mechanical alloying followed by spark plasma sintering. Effect of ball to powder weight ratio and milling duration on amorphization, microstructure, crystallite size and mechanical and magnetic properties of the alloy were studied. All the sintered samples showed very good magnetic properties with the finemet alloy sintered from the 120-hour milled powder showing the highest saturation magnetization of 166.8 emu/g. This high saturation magnetization in case of the 120-hour sample can be attributed to the high-volume fraction of α-Fe_3Si phase present in this sample according to the XRD results. The x-ray diffraction patterns of powder finemet alloy mechanically alloyed for different milling durations as well as

finemet alloy consolidated from these powders vis SPS showed α-Fe_3Si phase as the primary phase present. A significant broadening of (110) peak of Fe_3Si was observed with longer milling durations which was attributed to the amorphization process as well as a decrease in the Fe(Si) crystallite size. Traces of secondary boron phases were found in the sample sintered from the 30h milled powder. The decrease in the crystallite size of α-Fe_3Si due to longer milling duration and/or increased ball to powder weight ratio cased an increase in the microhardness value of the spark plasma sintered finemet alloy. Scanning electron microscopy analysis of the samples further proved the grain size reduction with longer milling durations as well as finer and more uniform microstructure in case of samples sintered from powers milled for longer times (comparing between 2 samples with the same SPS and milling parameters except for milling duration). Sample with the longest milling duration showed the highest volume fraction of α-Fe_3Si phase which led to the highest saturation magnetization value in case of this sample. However, this very high volume fraction of Fe(Si) phase also led to comparatively higher coercivity value in case of the sample sintered from the 120h milled powder due to increased magnetostriction. The higher coercivity value in case of the 120h sintered sample can also be attributed to the longer milling duration which due to the nature of the mechanical alloying process results in higher residual stress in the powder alloy from which the sample is sintered.

CHAPTER V

ENERGY MAPS AND AMORPHIZAION OF MECHANICALLY ALLOYED FeSiB ALLOYS AND THE EFFECT OF SPARK PLASMA SINTERING ON MECHANICAL AND MAGNETIC PROPERTIES

5.1 Abstract

During the mechanical alloying process the kinetic energy of the rotating milling balls gets introduced to the powder being milled. The amount of energy introduced to the powder during the mechanical alloying process can impact the amorphization of the resultant powder alloy. The impact energy of each ball and the total energy of the milling process for mechanically alloyed FeSiB-based samples were calculated and an energy map was drawn for samples milled with different milling processing parameters. The minimum energy required for a single ball and the window of energy in which the resultant powder alloy would have amorphous structure is defined. Moreover, effect of spark plasma sintering processing parameters on mechanical properties and magnetic behavior of the sintered FeSiB-based alloys are reported. Comparison between samples that were spark plasma sintered from the same powder alloy but sintered at two different temperatures showed an improvement in saturation magnetization values as the sintering

temperature increased. Coercivity of samples mechanically alloyed with the same condition and sintered with 470 °C and 510 °C were examined and it was observed that increasing the sintering temperature increases the coercivity value. Effect of heat-treatment (annealing) on magnetic and mechanical properties of the sintered alloys was also studied. The comparison between samples, one annealed and one not annealed, both processed with the same mechanical alloying and spark plasma sintering processing parameters showed that saturation magnetization of the alloys increases with the annealing heat treatment. However, an increase in the coercivity value was also observed in the heat-treated samples. Microhardness of samples processed with higher sintering temperature showed an improvement in comparison to samples sintered at lower temperatures. A coarser microstructure was observed in case of samples sintered at higher temperatures. Samples processed with our methods (mechanical alloying followed by spark plasma sintering) show high saturation magnetizations as compared to magnetic alloys with similar compositions fabricated with other methods. Saturation magnetization values as high as 174.6 and 182.8 emu/g were observed for samples milled with rotation speeds of 700 rpm, ball size of 3 and 5mm, ball to powder ratios of 5:1 and 10:1 and milling durations of 10 and 30 respectively. The first sample was sintered with sintering temperature of 470 °C and maximum pressure of 600 MPa with holding time of 5 minutes and the second sample was in powder format (not sintered).

5.2 Introduction

As a result of constant collision between the milling balls and the powder during the mechanical alloying process kinetic energy is introduced to the powder that is being milled. Mechanical alloying processing parameters can affect the milling and

amorphization process as well as the total energy that is introduced to the powder and the energy of each single ball. Mechanical alloying processing parameters such as milling duration, ball to powder weight ratio, size of the milling balls and the rotation speed are among these processing parameters. In this research work we have looked into all of these processing parameters and their effect on the amorphization process of FeSiB-based powder alloys as well as their impact on the total energy of the process and the energy of each single milling ball. Previous studies that were done on amorphization of FeSiB-based magnetic alloys gave us a base for our own experiments. Other researchers who worked with similar composition alloys reached amorphization with mechanical milling of their alloys anywhere between 30 hours [129] to 300 hours [130] with ball to powder weight ratio ranging from 5:1 [129] to 16:1 [130]. Higher ball to powder weight ratio and higher rotation speed are among the milling parameters that increase the total energy of the process. Eckert et al. [131] who studied the effect of milling intensity on mechanical alloying of niobium-zirconium alloys concluded that increasing the intensity of alloying will decrease the window in which the alloy shows amorphous structure. This means that if the milling intensity or the amount of energy that is induced to the powder during the milling process is higher than a certain value the amorphous phase will diminish, and the structure will go back to crystallite. The reason for this can be attributed to the higher temperature that is generated in case of the high intensity ball milling which in turn can aid the crystallization. One of the ways to reduce the temperature that is generated during the milling process is to use process control agents. Some studies have shown that without the help of a PCA, amorphization often cannot happen during the mechanical alloying process [132]. Other researchers have shown that using a PCA during the

process increases the amorphization window for ball milled alloys [133-134]. However, some studies have shown that contamination of the milled powder with the PCA has reduced the glass forming rage of the alloy [135]. Therefore, it is important to choose the PCA agent that is appropriate for mechanical alloying of each individual alloy composition. In our studies we compared benzene and stearic acid as PCA for our FeSiB-based alloys. In our experiments we used benzene and stearic acid as PCA for samples with the same composition that were mechanically alloyed using the same parameters and after XRD analysis we observed a higher level of carbon contamination from the sample with benzene as PCA even though the 2 wt% PCA was used in both cases. Furthermore, for the same milling parameters we observed higher levels of amorphization for samples that were milled using stearic acid as PCA as compared to samples that were milled using benzene.

El-Eskandarani et al. [71] who studied the mechanical alloying of Ti-Al alloys came to the conclusion that higher ball to powder weight ratio results in higher rates of amorphization in these alloys. Burgio et al. [136] also studied the effect of ball to powder weight ratio on amorphization of powders via ball milling. However, in their study on mechanically alloying of iron-zirconium Burgio et al. [136] kept the number of milling balls the same and change the amount of powder that is being milled instead. From their experiments Burgio et al. [136] realized that the higher amount of powder being milled will result in less amorphization during the mechanical alloying process. A higher total energy and higher energy of a single milling ball does not always result in crystallization. In fact, increasing the energy of a single ball increases the defects generated in the powder particles which results in higher amorphization. Therefore, it is important to

know the range in which amorphization takes place [131]. Our goal in this chapter was to find the glass forming range and the window of total energy of the mechanical alloying process in which amorphization takes place for FeSiB-based alloys. We also aimed to find the minimum energy of a single ball that is required for amorphization to take place in order to be able to generate a working energy map for mechanically alloyed FeSiB-based magnetic alloys.

Spark plasma sintering is a process in which a direct current (DC) and a uni-axial pressure is used in order to densify powder material. The spark plasma sintering technique can be used for processing ceramics, metallic, composite powders etc. [132-133]. The main advantage of the spark plasma sintering process in comparison to conventional sintering processes is its higher speed. The faster sintering process prevents grains from growing aggressively and helps to retain the nanocrystalline structure. In the spark plasma sintering technique sintering happens when high temperature is generated as a result of spark discharge in the gaps or contact points in between the particles of the powder that is placed in between the die and punches. This local high temperature causes melting on the surface of the particles and the combination of pressure in the SPS process accompanied by the high temperature helps in formation of fully dense components. One of the greatest advantages of the spark plasma sintering process is that it can be used for many different powder materials with wide range of particle sizes. The ability to process a large range of materials and particles sizes is why spark plasma sintering has gained a lot of attention for processing amorphous and nanocrystalline materials. The spark plasma sintering technique is also capable of fabricating near-net shape components with symmetrical and simple geometries in a single step. Spark plasma sintering uses an on

and off direct pulse for heating up the powder homogeneously from inside and outside. This results in faster heating and consequently shorter sintering process which prevents grain growth and crystallization [64]. According to Joule's heating law, the current has a tendency to pass through an area with the least resistance. In case of the powder trapped in between the die and punches in an SPS machine the areas of least resistance are the particle borders and boundaries. The electrical field passing through the particle boundaries generates enough heat that causes sintering [134]. Magnetic alloys fabricated using the SPS technique show high densities and homogeneous microstructures. The high density and homogeneous grain structure of magnetic samples processed with spark plasma sintering results in high saturation magnetization and permeability for these alloys [135]. Although there are several processing parameters that can affect the samples fabricated with sintering process, temperature has the most effect on mechanical and magnetic properties of SPS-processed magnetic alloys. Very few research has been done on SPS-processed soft magnetic alloys and therefore the effect of the sintering parameters on magnetic alloys is not yet fully understood. Holding time and temperature have the most effect on the microstructure of the SPS-fabricated samples. Xio et al. [66] who studied the iron-based magnetic alloy proved that sintering temperature affects the magnetic properties of the alloy. In their studies Xio et al. [66] stated that saturation magnetization as well as coercivity are affected by sintering temperature and higher temperature improves the saturation magnetization and the coercivity of the magnetic components (increased Ms and decreased Hc). Composition of alloys from the above-mentioned study is different than the base composition of the samples studied in this research work. The effect of sintering temperature on SPS-processed iron-based magnetic

alloys was also studied by Neamtu et al. [67] who used low pressures and high sintering temperatures for their process. In this study [67] utilization of graphite dies, and punches prohibited achieving higher pressures during the SPS process therefore, in order to obtain fully dense parts at lower pressures Neamtu at al [67] increased the sintering temperature to high temperature of 800 °C and they observed an enhancement in magnetic properties of the sintered parts due to higher levels of densification. However, choosing graphite dies and punches for this study [67] might have just been due to the fact that these dies and punches are capable of enduring higher temperatures than tungsten carbide dies and punches and reaching temperatures as high or higher than 800 °C with tungsten carbide dies and punches is practically impossible. Gheiratmand et al. [136] studied the sintering of two types of Finemet powder alloys (amorphous and semi-crystallite) at high holding times and low pressures. From their research on amorphous and semi-crystallite powders they concluded that the density of the sintered alloy depends on the initial sate of the powder and samples sintered from amorphous powders tend to show higher densities as compared to samples fabricated from partially crystallized powders. Another important factor that impacts the SPS-processed alloys is the maximum pressure. Xio et al. [66] stated that if the loading pressure during the SPS process is less than 500 MPa the powders would not be properly consolidated or may require longer holding times to achieve full densification which might result in grain growth and crystallization. Therefore, it is important to choose a maximum pressure that would help reduce the sintering time. Since we could use tungsten carbide dies and punches for our experiments, we were able to increase the maximum pressure to 600 MPa. Another important factor in the SPS process is the holding time which is the time that the powder

is kept inside the die and in between the punches under the maximum pressure and the highest temperature in the process while sintering is taking place. Spark plasma sintering of FeSiB composition was done by Neamtu at al. [71] who sintered the samples with holding time ranging from 1 to 15 minutes using different sintering temperatures and loading pressure of 30 MPa. The range for the sintering temperature of their experiments were from 450 °C to 900 °C. Neamtu at al. [67] only observed full densification of the FeSiB alloy at temperatures higher than 800 °C due to a very low loading pressure. They achieved higher levels of densification with longer holding times [67]. However, choosing higher holding times will increase the chance of crystallization and grain growth. Therefore, in this research work we have used the high compaction pressure of 600 MPa to avoid increasing the holding time or sintering temperature in order to achieve full densification. Different sintering temperatures were used to determine the effect of this parameter on magnetic, mechanical and microstructural properties of FeSiB magnetic alloys.

5.3 Experimental procedures

The $Fe_{77.5}Si_{13.5}B_9$ composition was milled with ball to powder weight ratios of 5:1, 10:1 and 15:1 with rotation speed of 700 rpm and milling duration of 10, 20 and 30 hours with ball sizes of 3 and 5 mm from Fe, Si and B elemental powders. Stearic acid was used as PCA, and 10-minute pauses were put in between 10-minute milling cycles in order to prevent excessive heating. Spark plasma sintering process was done under controlled argon filled atmosphere. The powder was pre-compacted with 20 MPa pressure and the maximum pressure during the sintering process was at 600 MPa. The holding time of 5 minutes was used for all the experiments and the heating rate was kept

at 30°C/min and the pressure was increased at the rate of 100 MPa/min. Different sintering temperatures were selected in order to study the role of sintering temperature on microstructure, mechanical properties and magnetic behavior of the FeSiB magnetic alloys. The dies and punches used for the SPS process were made of tungsten carbide and were covered with graphite foil in order to prevent direct contact between the powder alloy and the dies and punches as well as for better electrical conductivity. Differential scanning calorimetry (DSC) was performed in order to find the crystallization temperatures of different phases in the alloy powder and 2 temperatures of 470 °C and 510 °C were chosen, one bellow and one above the crystallization temperature of the alloy that was found to be 500 °C from the DSC experiment results. Annealing heat treatment was done on FeSiB sample milled with BPR 10:1, ball size of 3mm, milling duration of 30 hours and rotation speed of 700 rpm which showed the highest level of amorphization among all our ball milled samples. Annealing was done in an oven furnace at the temperature of 200 °C for duration of 2 hours in order to relieve the residual stress induced to the powder during the mechanical alloying process. The oven furnace was not inert atmosphere therefore in order to prevent the alloy from oxidizing a glove box filled with argon atmosphere was used. After the milling process the milling vials were placed inside the glovebox and powder was taken out of the vial, weighed and placed in a secure container with a sealed lid for annealing. The mechanical and magnetic properties as well as the microstructure of the sample sintered from the annealed powder was then compared with sample sintered from the same powder batch (milled with the same parameters) but un-annealed. The micro hardness values of the SPS consolidated samples were measured using a standard Wilson Vickers microhardness tester. The

measurements were taken under a load of 5N and dwell time of 10 seconds. For each sample microhardness readings of 10 different spots were taken into account and the average value was reported. For microstructural analysis, the spark plasma sintered samples were mounted and polished using an automatic polisher. polishing was done on different grit polishing papers ranging from rough to soft (250 to 1200 grit) and a final polishing was done using colloidal silica on a micro cloth. Vibrometer was used for the final polishing stage in order to get a clearer view of the microstructure. After the polishing steps the samples were viewed and characterized with a FEI-Quanta Nova-SEM. Both secondary and backscattered images were taken at magnifications ranging from 100x to 5000x. grain sizes of the alloys were measured using the SEM images. Magnetic properties of the mechanically alloyed as well as spark plasma sintered alloys were measured using a magnetometer (VSMLakeshore 7404) with maximum magnetic field of 1T. The structure and phases of powder and consolidated samples were determined with a X-ray diffraction (XRD) using a Rigaku Ultima III X-Ray diffractometer (Cu Kα radiation, 1.54 Å).

5.4 Results and discussion

5.4.1 Mechanical alloying and x-ray diffraction of FeSiB-based alloys

Mechanical alloying is a simple process that has gained attention for obtaining amorphous phase through solid state amorphization of powder instead of conventional rapid solidification processes [137-138]. In this research work we have studied the amorphization of FeSiB-based magnetic alloys prepared by mechanical alloying. In the past, scientists have achieved amorphization via mechanical alloying for other alloy compositions. Researchers such as kotch et al. [138] who reported the first amorphous

alloy, prepared by mechanical alloying, which contained nickel and niobium, Hellstern et al. [139] who studied the amorphization of zirconium alloys and Veltl et al. [140] who explored the amorphization of copper and tantalum-based alloys have all studied the amorphization of alloys via mechanical alloying in the past. The reason for choosing the mechanical alloying process is due to the fact that this technique is known to have a much wider glass forming range in comparison to conventional methods of making amorphous alloys [105] therefore it is preferred for obtaining powder alloys in amorphous state. During the mechanical alloying process, several different processing parameters can affect the alloying process. These parameters include the ball to powder weight ratio, milling duration, rotation speed, size of the milling balls and even the PCA that is used during the process. In this research work we have studied all the above-mentioned parameters for FeSiB-based magnetic alloys processed via the mechanical alloying process followed by Spark Plasma Sintering (SPS) technique. Experiments were designed in a way that one MA parameter was changed at a time while the rest of the parameters were kept the same in order to find the role of each particular parameter on amorphization of the alloyed powder. From our previous experiments with FeSiB, FeSiBCu, FeSiBNb and FeSiBCuNb we found that we can reach amorphization after 120 hours of milling using 3mm milling balls, rotation speed of 350 rpm and 10:1 BPR as milling parameters. For the next step of our research work we decided to study the amorphization of FeSiB alloys under higher rotation speeds but shorter milling durations. Therefore, we chose 700 rpm as the rotation speed and 10 to 30 hours as milling durations. Moreover, for understanding the role that size of the milling balls plays in the amorphization process 2 different ball sizes were looked into: 3 mm balls and 5 mm balls.

Figure 1 shows the XRD patterns of 10 different samples that were mechanically alloyed with the same rotation speed of 700 rpm, milling durations of 10 to 30hours with ball sizes of 3 and 5mm and ball to powder ratios of 5:1, 10:1 and 15:1. Based on the results from our experiments increasing the BPR higher than 15:1 is not advised since a great amount of powder will end up sticking to the milling bowl, consequently decreasing the powder yield and it would also increase the chance of contaminating the powder with the milling media. Additionally, a very high BPR might result in crystallization of the powder due to excess kinetic energy that can be converted into heat during the process.

From fig. 5.1 it can be observed that the best result in terms of amorphization is obtained from the sample that was milled for 30 hours with BPR 10:1 and ball size of 3mm. From the x-ray diffraction patterns of the powder alloys the other amorphous samples with the broadest XRD peaks and smallest crystallite sizes were: BPR 10:1and milling duration of 20h with 3mm balls, BPR 10:1 and milling duration of 10h with 5mm balls, BPR 15:1 and milling duration of 10h with 3mm, BPR 15:1 and milling duration of 10 with 5mm balls and finally BPR 5:1 and milling duration of 20h with 5mm balls in sequence. As it can be seen, using ball to powder ratio of 5:1 does not necessarily result in a completely amorphous powder or a complete crystalline structure. It can also be seen that in comparison between powders mechanically alloyed with the same milling duration and ball size, powders with BPR 10:1 show the most promising results in terms of amorphization.

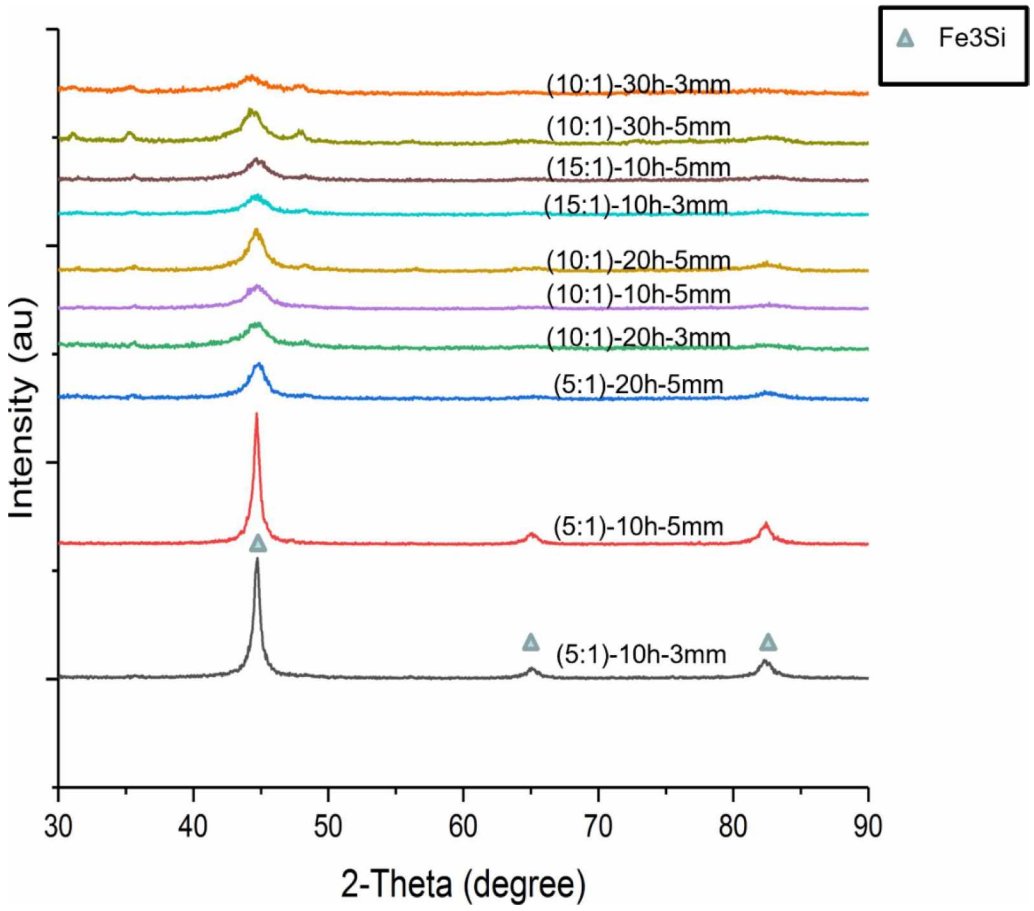

Figure 5.1 XRD patterns of FeSiB powder mechanically alloyed with Rotation Speed of 700rpm and different milling duration, ball to powder ratio and ball size

Figure 5.2 depicts the XRD results from powders that were milled with the same rotation speed and ball size but different milling durations and BPRs. By comparing samples with milling duration of 10 hours it can be concluded that even though both samples show an almost amorphous structure, the 10:1 sample depicts a broader peak and lower crystallite size. It can be concluded that when the ball to powder ratio is too high, (in our case BPR 15:1), or too low (BPR 5:1), it can negatively affect the amorphization process. The increased number of collisions during the milling process and generation of

more energy can produce excessive heat which results in powder alloy with more crystalline phase present [140]. On the other hand, if not enough total energy is transferred to the powder during the milling process, amorphization does not take place.

In order to understand the role of ball size in amorphization of FeSiB alloys, we studied samples milled with the same rotation speed of 700 rpm and 3 different BPRs, 3 different milling durations and 2 different ball sizes. When we compared samples with the same BPR and milling time in 4 different cases we observed that the powder milled with ball size of 3mm showed more amorphization as compared to powders milled with 5mm balls. This comparison can be observed form XRD patterns depicted in figure 5.2. In case of samples with BPR 10:1 and 30h milling time, samples with BPR 15:1 and 10h milling time, samples with BPR 10:1 and milling time 20h and samples with BPR 5:1 and milling time 10h all milled with 2 ball sizes of 3 and 5 mm, it can be observed that the powders milled with the 3mm balls are showing more promising results in terms of level of amorphization. According to Suryanarayna et al. [141], during the mechanical alloying process the smaller balls create more intense friction action which consequently enhances the amorphization process. From the figure 5.2 it can also be concluded that increasing the milling duration can improve the amorphization. In comparison between samples milled with 3mm balls with BPR 10:1 and 30 and 20 hours of milling as well a 5mm balls with BPR 5:1 and 10 and 20 hours of milling, it can clearly be seen that higher milling duration results in more amorphization.

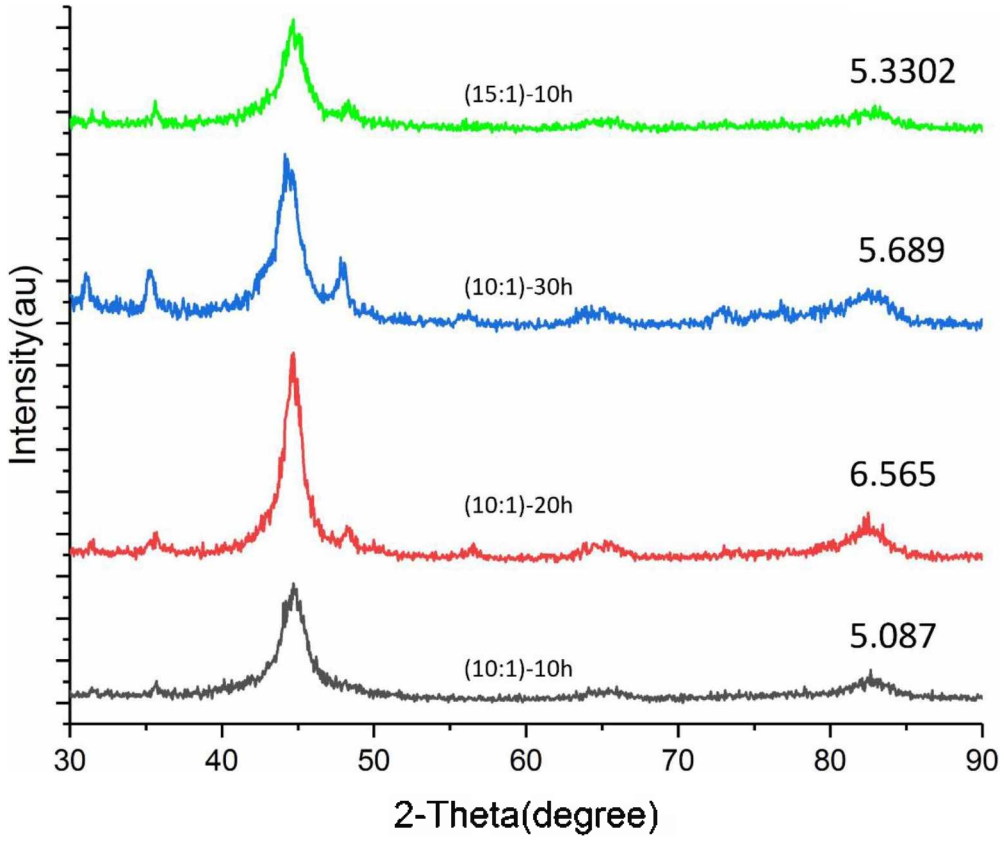

Figure 5.2 XRD patterns and crystallite sizes of FeSiB powder mechanically alloyed with Rotation Speed of 700rpm, 5mm ball size and ball to powder ratio of 10:1 with different milling duration

From figure 5.3 it can be observed that in case of the powder milled with BPR 10:1 and rotation speed of 700 rpm for 20 hours the peaks have started to become broader which is a sign that amorphization has begun but the sample does not reach full amorphization until 30 hours. As it can be seen in XRD patterns of figure 5.2, we obtained an amorphous powder after 30 hours of milling and therefore did not continue the process for longer milling durations, however, it is worth mentioning that if the milling duration is too long the microstructure can go from amorphous back to crystalline state which was not what we intended for our investigations.

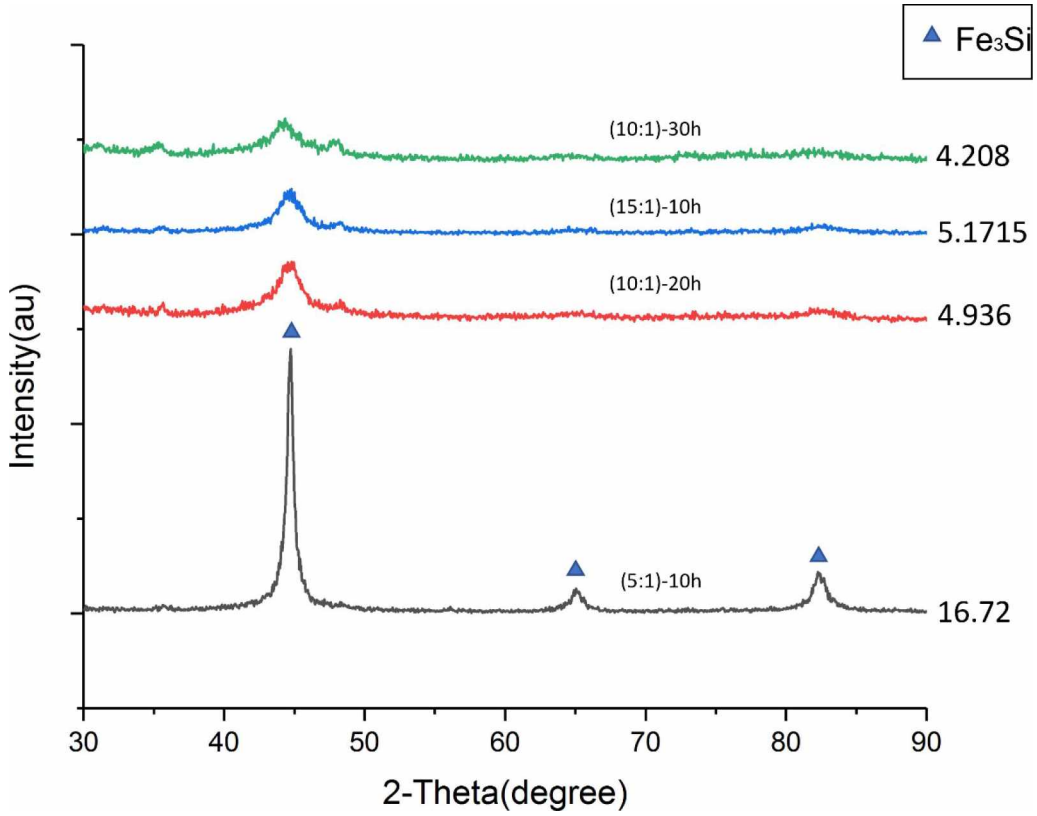

Figure 5.3 XRD patterns and crystallite sizes of FeSiB powder mechanically alloyed with Rotation Speed of 700rpm and 3mm ball with different milling duration and ball to powder ratios

This phenomenon was observed in our previous investigation on FeSiB samples milled with ball size 3mm, BPR 10:1 and rotation speed of 30, 60 and 90 hours. While the 30h sample did not show any sign of amorphization the 60 and 90h samples had somewhat more promising results. However, it can be seen in figure 5.4 that the 60h sample has the highest amorphization level while the 90h sample is almost back to crystalline structure.

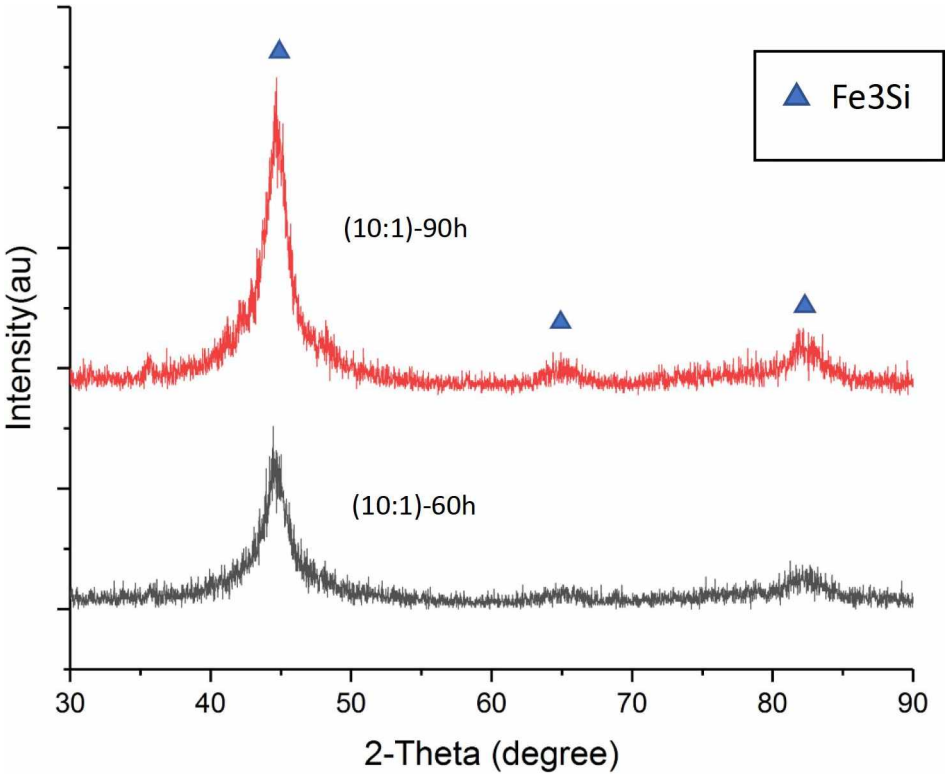

Figure 5.4 XRD patterns and crystallite sizes of FeSiB powder mechanically alloyed with Rotation Speed of 700rpm, BPR 10:1 and 3mm balls with different milling duration

In the past we have investigated mechanical alloying of FeSiB-based alloys such as FeSiBCu, FeSiBNb and FeSiBCuNb (finemet), with lower rotation speeds of 350 rpm and 500 rpm and longer milling durations of up to 120h. We only observed amorphization in one finemet sample milled for 120 hours with rotation speed of 350 rpm and BPR 10:1. This is the reason we decided to study higher rotation speeds with shorter milling duration for the rest of our experiments. Furthermore, as discussed in the literature review section the PCA has a significant effect on the amorphization process. The 2 control agents available for this study were stearic acid and benzene. These 2 PCAs

were examined in order to find the best option for amorphization. After comparing the XRD patterns of samples that were mechanically alloyed using a powder with the same composition (FeSiB) and the same BPR, rotation speed, ball size and milling duration, we observed much better results in terms of amorphization in samples that used stearic acid as PCA than samples that used benzene. Since cold welding can reduce the powder yield specially in higher rotation speeds, we chose stearic acid as our PCA for our experiments with 700 rpm rotation speed.

5.4.2 Energy maps of FeSiB-based alloys

The amount of energy that is induced to the powder during mechanical alloying affects the amorphization process and the glass forming ability of blend of elemental powder composition. Ball to powder weight ratio, milling duration, size of the milling balls, number of balls, rotation speed etc. directly impacts the amount of energy that is introduced to the powders during the milling process. In order to understand the role of these parameters on the mechanically alloyed powders these processing parameters were converted into two parameters: the impact energy of a single ball and the total energy of the mechanical alloying process [142]. A milling map based on these two parameters have been prepared for FeSiB-based powder alloys in many different milling conditions. Based on the energy map our goal was to find out whether there is a minimum or maximum impact energy of a single ball which is required for amorphization to take place and if so, what are these values, as well as a window of total energy value in which milled samples will be amorphous. There is few research done on the effect of mechanical alloying processing parameters on formation of amorphous phase in ball milled powders however, researchers such as Magini el al., [143-145], Murty et al. [105-

142-146] and Burgio et al. [136] have studied the mechanical alloying process of other alloys with different compositions, which was a basis for our research and energy calculations. Eckert et al. [131] who studied the glass forming range of mechanical alloyed Ni-Zr have reported a very narrow range when no PCA was used during the process. Therefore, in an effort to increase this range we tried wet mechanical alloying with help of stearic acid as PCA which reduces the overall temperature during the process and prevents crystallization. We also experimented with different milling/pause time ratios and came up with the best milling/pause time that would give us the highest amount of amorphous phase (based on XRD results) in any given experiment. We used 3 different BPRs of 5:1, 10:1 and 15:1 and used the same amount of powder for all of our experiments, we also used the same rotation speed and same milling duration and we realized that increasing the ball to powder weight ratio from 5:1 to 10:1, increases the amorphization. This can be explained by the increase in the kinetic energy that is induced to the powder in case of higher BPR [147]. However, further increase in the BPR results in a decrease in the amorphous phase which is due to excess energy during the process that can be converted into heat and cause formation of small amounts of crystalline phases. Based on amorphization information from XRD graphs, samples with BPR 5:1 have levels of kinetic energy that are too low to be sufficient for converting the crystalline phases into amorphous phase. Another factor that can affect the amorphization process is the degree by which the milling bowl is filled with powder. Filling level is a separate parameter than ball to powder weight ratio. In order to understand the role of powder amount on amorphization we experimented with 2 separate but identical milling bowls each filled with balls and powder with weight ratio of 10:1 and concluded that with

the same BPR the powder from the experiment with higher level of filling in the bowl showed less amorphization compared to the powder from the bowl with less powder in. This is explainable by the fact that the impact energy that each milling ball has is affected by the level by which the bowl is filled [148]. Moreover, Murty et al. [142] showed that the contamination of the milled powder that might occur during the milling process depends on the number of balls and not the BPR. This means that increasing the number of balls to keep the BPR the same can harm the resultant alloy powder in terms of contamination with the milling media.

The energy of a single ball and the total energy of the milling process have been calculated by Joardar et al. [149] who used a milling machine with similar mechanism to our Fritsch Pulverisette 7 high energy planetary ball milling machine. The energy of each milling ball is altered when it interacts with other milling balls in the vial. According to Burgio et al. [136] the energy of each ball is reduced by a factor when it interacts with other balls. The basic formula for kinetic energy is $K=0.5mv^2$ which in this case can be written as:

$$E_b=0.5m_bv_b^2$$

Where Eb is the energy of a single ball, mb is the mass of a ball and vb is the absolute velocity of the ball. As mentioned before, when multiple balls are used during the milling process energy of each ball is a factor of energy of it if it was alone in the milling bowl. This equation can be written as:

$$E_b'=Q_b E_b \text{ [142]}$$

Where:

$$Q_b=1-n_v^{\xi} \text{ [142]}$$

The variable Q_b depends on nv which is called the packing fraction. The packing fraction is dependent upon the ratio of number of balls used in an experiment and the total number of balls that can fit in the milling bowl. Therefore, nv can be written as:

$$nv=\frac{nb}{nb.v}$$

where nb is the number of balls that are used in an experiment and $n_{b.v}$ is the total number of balls that can fit inside the bowl. In order to calculate the total number of balls that can fit in the bowl we can divide the total volume of the milling bowl, which is in shape of a cylinder, to the volume of a single spherical milling ball. Assuming that π=3, nb.v can be written as:

$$n_{b.v}=\frac{\pi D^2 H}{4d}$$

where D and H are the diameter and height of the milling bowl and d is the diameter of each ball. The ξ factor is equal to 1.193 for 3mm balls and 1.462 for 5mm balls. Next, we need to calculate the total amount of energy that is transferred to the powder during the milling process per unit mass of powder that is being milled. The total energy per unit mass depends on the energy of a single ball (Eb´) the number of balls (n_b) the frequency by which the balls collide (f) and the total milling duration (t).

$$Et=\frac{ftnbEb'}{mp}\ [142]$$

Where m_p is the mass of the milled powder. Iasonna and Magini [143] have calculated the frequency of impact for a single ball:

$$F=K(\Omega-\omega)$$

Where Ω is the rotation speed of the disk, ω is the rotation speed of the vial and k is equal to 1.5.

For our milling machine, Fritsch Pulverisette 7, the ratio of rotation speed of the disk to the rotation speed of the vial is $\frac{\Omega}{\omega}$=2. The total energy per unit mass and energy of a single ball have been calculated for 19 different powders milled under different conditions. The BPR, ball size, rotation speed and milling durations of these conditions are listed in table 5.1.

Table 5.1 Energy of a single ball and the total energy of the milling process for mechanically alloyed FeSiB-based alloys with different BPR, ball size, rotation speed and milling duration

Ball Size (mm)	BPR	Rotation Speed (RPM)	Milling Duration (h)	Eb	Et
5	10:01	700	10	0.0227	2462.13
5	5:01	700	10	0.02289	1249.81
3	5:01	700	10	0.0043	1137.02
3	5:01	700	20	0.0043	2274.05
5	10:01	700	20	0.0227	4924.26
5	5:01	700	20	0.02289	2499.62
3	10:01	700	10	0.00401	2094.94
3	10:01	700	20	0.00401	4189.89
5	15:01	700	10	0.0226	3678.93
3	10:1	700	30	0.004	6284.83
5	10:1	700	30	0.0227	7386.39
3	15:01	700	10	0.00362	2837.03
3	15:01	700	20	0.00362	5674.07
3	10:1	350	30	0.001	785.604
3	10:1	350	60	0.001	1571.209
3	10:1	350	90	0.001	2356.81
3	10:1	350	120	0.001	3142.418
3	15:1	350	60	0.0009	2127.77
3	15:1	350	90	0.0009	3191.66
3	15:1	350	120	0.0009	4255.55
3	10:1	500	60	0.002	4580.78
3	10:1	500	90	0.002	6871.17

Figure 5.1 shows the XRD patterns of the first 4 samples which all show amorphous structures. The point that these samples have in common is their higher rotation speed accompanied by shorter milling times of only up to 30 hours. However, the best result was observed after 30 hours of milling. According to Murty et al. [142] at longer milling times, as the powder particles become finer, the diffusion distance between them becomes smaller which aids the amorphization process and therefore observing more amorphous phase in samples with longer milling times can be explained. Furthermore Murty et al. [142] studied the morphology of mechanically alloyed powder particles with different milling durations and found that powder particles are more uniform and spherical shaped in case of longer milling durations which can have a positive effect on the amorphization process. According to XRD patterns obtains from all the powder alloys, samples with the following mechanical alloying processing parameters showed amorphous structure: with rotation speed of 700 rpm and BPR, milling duration and ball size as follows: 10:1-30h-3mm, 10:1-20h-3mm, 10:1-10h-5mm, 15:1-10h-3mm, 15:1-10h-5mm, 10:1-30h-5mm, 10:1-20h-5mm and 5:1-20h-5mm as well as one sample from our previous study [150] with rotation speed of 350 rpm, 10:1 BPR, 120 hour of milling with ball size of 3 millimeters. We have located the energy of a single ball as well as the total energy transferred to the powder for each of the conditions that our amorphous alloys were milled with on the energy map depicted in figure 5.5.

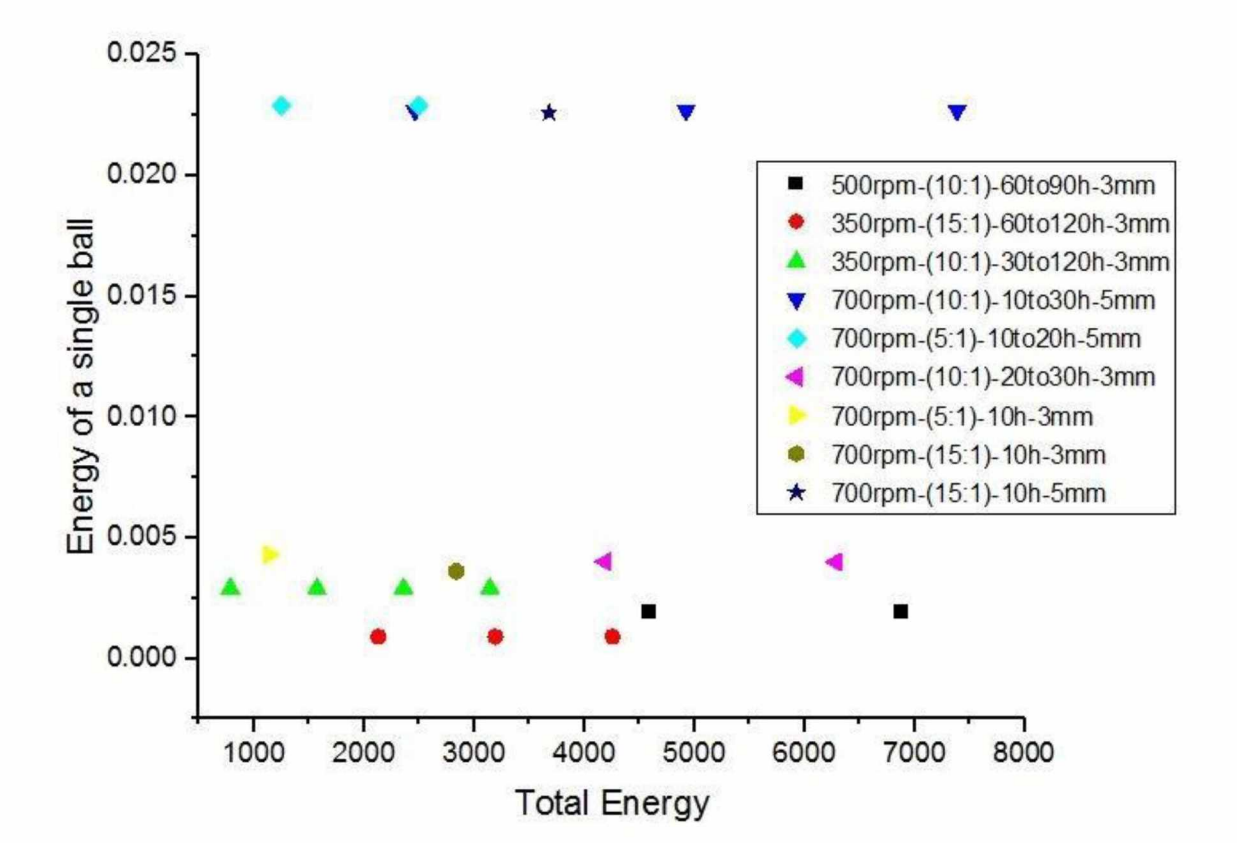

Figure 5.5 Graph of Total energy and Energy of a Single Ball for Different Milling Conditions

From this energy map it can be observed that all the samples that show amorphous structure fall between total energies of 2462.13 and 7386.3. The XRD patterns of mechanically alloyed powders that were milled with rotation speed of 500 rpm and BPR of 10:1 are depicted in figure 5.4. From this figure it can be observed that even though these samples fall within the amorphization range of the energy map they do not show amorphous structure. The same can be said for samples milled with rotation speed of 350 rpm with BPR of 15:1 and ball size of 3mm with 90- and 120-hours milling duration.

From this we concluded that there is a minimum impact energy for a single ball that is needed for amorphization to take place and these powders were all milled with energy of

a single ball less than that amount. From the energy map (fig. 5.5) we can see that any sample that shows amorphous structure falls above the line of impact energy of 0.0029 J for each single ball. This phenomenon was also observed by Murty at al. [142] who found out that there is a minimum milling intensity needed in order to obtain amorphous TiNi and TiCu powders via mechanical alloying. Using this milling map we can make a clear prediction about the minimum Eb needed for amorphization of FeSiB-based powder via mechanical alloying. The importance of this milling map is that it is the result of many experiments on the FeSibB-based compositions, and they can predict the amorphization of the alloy powder with any given milling parameter using the formulas.

5.4.3 Annealing

Powder alloys processed by mechanical alloying are prone to residual stress induced by the milling media [151]. In this research work one of goals was to investigate how residual stress can alter the magnetic properties of the milled alloy by reducing it via the annealing process. During their experiments, Neamtu et al. [98] realized that the saturation magnetization values for their mechanically alloyed magnetic alloys increased from ~131 emu/g to ~141 emu/g after the annealing process. Similar results were observed by Sinha et al. [152] who studied the role of annealing on magnetic properties of finemet alloys. Therefore, we investigated the level by which the annealing process improves the magnetic properties of FeSiB alloy milled with high rotation speed of 700 rpm. In order to do so, we chose a powder that was milled for 30 hours using 3mm balls and BPR 10:1, which had the highest level of amorphization amongst all our samples, and annealed it for 2 hours with temperature 200 °C. The coercivity and saturation magnetization values of the 2 amorphous powders, one annealed and not annealed, can be

seen in figure 5.9. As it can be observed, the coercivity value is decreased in case of the annealed sample and the saturation magnetization is increased which proves that the annealing process and release of residual stress in fact improves the magnetic properties of the mechanically alloyed magnetic alloys. We then sintered our amorphous powder alloys (annealed and un annealed) in 2 different temperatures of 470 °C and 510 °C. We then studied the role of annealing on magnetic properties of both sintered samples. Interestingly the coercivity value was increased in both cases of samples sintered at 470 °C and 510 °C. As can be observed in fig. 5.6 even though the coercivity values of samples sintered from annealed and regular powders were close, the sample sintered from the annealed powder showed slightly higher coercivity. These higher coercivity values can be explained by the higher intensity of the Fe_2B and $Fe_{23}B_6$ peaks (from the XRD patterns) and presence of slightly larger volume fractions of these 2 phases in these samples.

We also compared the microhardness and crystallite sizes of samples sintered from annealed and regular (not-annealed) powders. From table 5.2 it can be seen that the crystallite size of the annealed samples is slightly larger than the samples that did not go through annealing. According to the Hall-Petch relationship microhardness and crystallite size have an inverse correlation. This can explain the fact that the microhardness of the annealed samples is slightly lower than the samples sintered from regular powder. Kotan et al. [153] have stated that when the crystallite sizes are smaller (in range of nanometers) the slope on their Hall-Petch plot is also smaller. This can explain why we do not observe drastic changes in the microhardness values of our samples.

Table 5.2 Microhardness and crystallite values for FeSiB sintered samples

Condition	Crystallite Size (nm)	Microhardness (HV)
10h-3mm-470-5to1	14.8	694.2
10h-5mm-470-5to1	11.2	974.5
30h-3mm-470-10to1	6.3	1176
30h-3mm-470-10to1 (HT)	7.7	1167
30h-3mm-510-10to1	8.4	1127
30h-3mm-510-10to1 (HT)	9.1	1122

5.4.4 Magnetic properties of heat treated and not heat treated powder FeSiB alloys

There are several parameters that can be altered in the SPS process. The most important of these parameters includes packing pressure, holding time and the maximum heating temperature. In this research work we aimed to discover if and how SPS processing parameters can affect the magnetic, mechanical, and microstructural behavior of the consolidated magnetic powders. Studies have shown in the SPS process higher packing pressure, higher temperature and higher holding times will produce samples with higher density [142]. Therefore, in order to be able to keep the short holding time of 5 minutes along with lower sintering temperatures we have used 600 MPa packing pressure for all of our experiments. There are 2 types of dies and punches that can be used in the SPS process. The ones that are made of graphite and the ones that are made of tungsten carbide. The graphite dies and punches are good choices when it comes to higher temperatures however, they cannot endure pressures higher than 60 MPa for a 20mm die and 200 MPa for a 10mm die. On the contrary, dies and punches made of tungsten carbide can tolerate pressure up to 250 MPa for a 20mm die and 1200 MPa for 10mm

dies but are incapable of enduring temperatures higher than 600 °C whereas graphite dies, and punches can endure temperatures up to and even higher than 1000 °C. For this research work we choose 10 mm tungsten carbide dies and punches that can go up to 600 MPa pressure and 510 °C temperature which is our highest target temperature. From our previous experiments [37][150], we had observed that Fe_2B, Fe_3B and $Fe_{23}B_6$ phases appear after the SPS process. The 470 and 510 °C sintering temperatures were chosen based on DSC data acquired for the powder in order to find the crystallization temperatures of each of the phases mentioned. Based on this data the major exothermic crystallization temperature peak was found to be at about 500 °C so we chose 470 °C as one of our target sintering temperatures, which is a temperature bellow the crystallization point to preserve the microstructure as much as we can, and 510 °C as another target sintering temperature, which is a temperature slightly above the crystallization point, for studying the role of altering the temperature on mechanical, microstructural and magnetic properties of our samples. We studied 4 types of powder alloys for our SPS experiments. We used our most amorphous powder in 2 types, one heat-treated and one not heat-treated as well as 2 non-amorphous powders from our mechanical alloying experiments (10h_3mm_5:1 and 10h_5mm_5:1) for comparison. From figure 5.6 and table 5.3 we can observe that, in case of the regular and heat-treated amorphous powders increasing the sintering temperature has a positive effect on saturation magnetization but it also increases the coercivity value significantly.

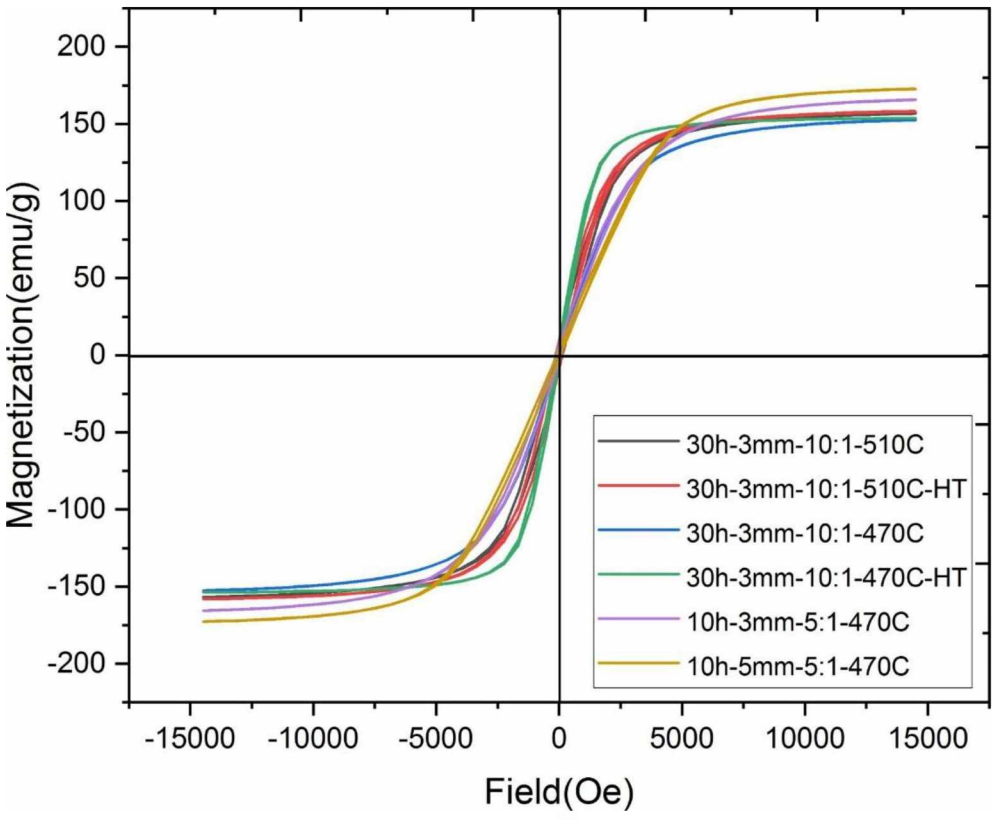

Figure 5.6 Magnetization and coercivity graph for mechanically alloyed FeSiB samples under different milling and SPS conditions for heat treated and non-heat-treated samples

Table 5.3 Magnetization and coercivity values for mechanically alloyed FeSiB samples under different milling and SPS conditions for heat treated and non-heat-treated samples

SPS Sample	Ms (emu/g)	Hc (Oe)
1. 30h_3mm_10:1_510 °C	156.9	137.0
2. 30h_3mm_10:1_510 °C_HT	158.1	139.1
3. 30h_3mm_10:1_470 °C	152.6	33.4
4. 30h_3mm_10:1_470 °C_HT	153.7	46.5
5. 10h_3mm_5:1_470 °C	165.6	99.7
6. 10h_5mm_5:1_470 °C	172.7	65.6

According to Gheiratmand et al. [68] higher density as well as uniformity of the grains can increase the permeability and saturation magnetization values in magnetic alloys. It has been proven that increasing the sintering temperature increases the density of the SPS-fabricated samples [154] therefore it can be concluded that the samples sintered at higher temperature will have higher saturation magnetization. The mechanically alloyed 30h_3mm_10:1 (heat treated and not heat treated) powder as well as 10h_3mm_5:1 and 10h_5mm_5:1 powders that were all sintered with temperature of 470 °C have coercivity values in range of 33.4 to 99.7 Oe with average value of 61.3 Oe which is considerably lower than 137.0 and 139.1 Oe values observed for samples sintered at 510 °C. From the XRD patterns depicted in figure 5.7 it can be seen that samples that were sintered at 510 °C show more intense peaks of Fe_2B and $Fe_{23}B_6$. These peaks are broader in case of amorphous samples sintered at 470 °C and almost non-existent in case of non-amorphous samples sintered at 470 °C. Formation of these secondary phases can be attributed to higher sintering temperature which has given rise to crystallization of theses 2 phases. Formation of Fe_2B and $Fe_{23}B_6$ for temperatures higher

than 500 °C can be expected since α-Fe_2B forms between 496 ° and 642 °C [59] and $Fe_{23}B_6$ can form at temperatures even lower than that [58]. Moreover, the crystallite size and microhardness of samples sintered at different temperatures is depicted in table 5.2. It can be observed that for powders that were mechanically alloyed under the same condition, the higher sintering temperature resulted in bigger crystallite size and lower microhardness values which can be explained by the Hall-Petch relation.

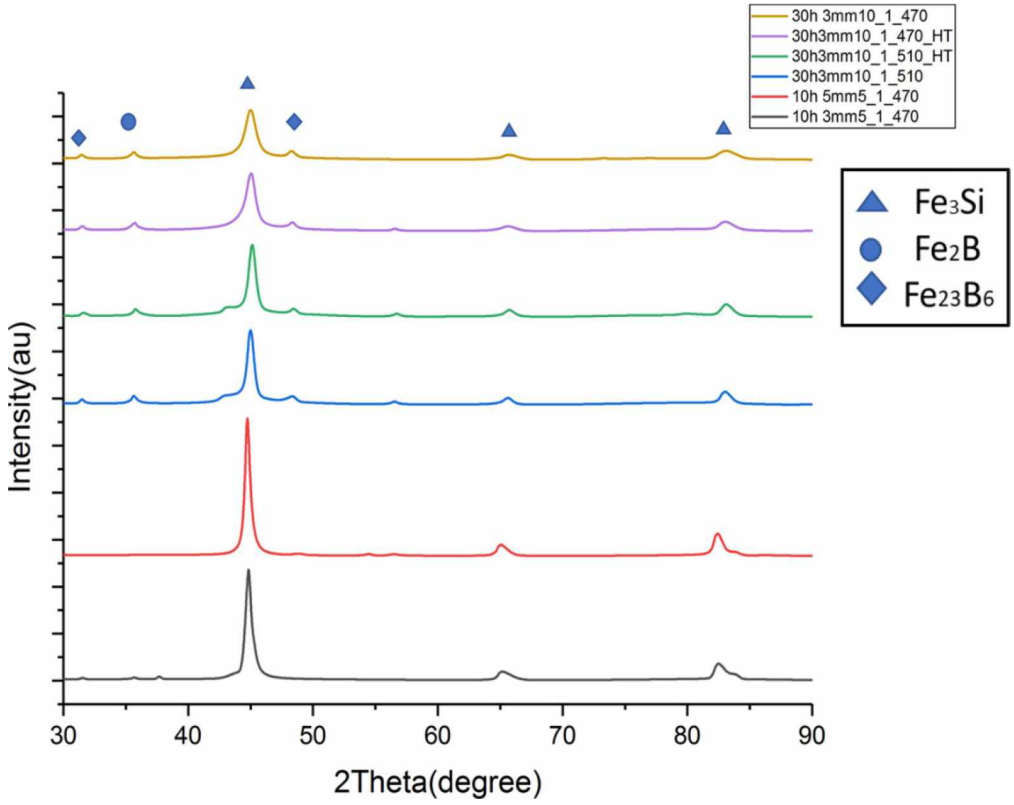

Figure 5.7 XRD pattern of spark plasma sintered samples milled and sintered under different conditions

5.4.5 Scanning electron microscopy analysis of heat treated and not heat treated sintered FeSiB alloys

Figure 5.8 shows the SEM images of SPS processed samples milled and sintered under the following conditions: 30h_3mm_10:1_sintered at 510 °C, 30h_3mm_10:1 heat treated then sintered at 510 °C, 30h_3mm_10:1 sintered at 470 °C, 30h_3mm_10:1, heat treated then sintered at 470 °C, 10h_3mm_5:1 sintered at 470 °C and 10h_5mm_5:1 sintered at 470 °C with the same magnification.

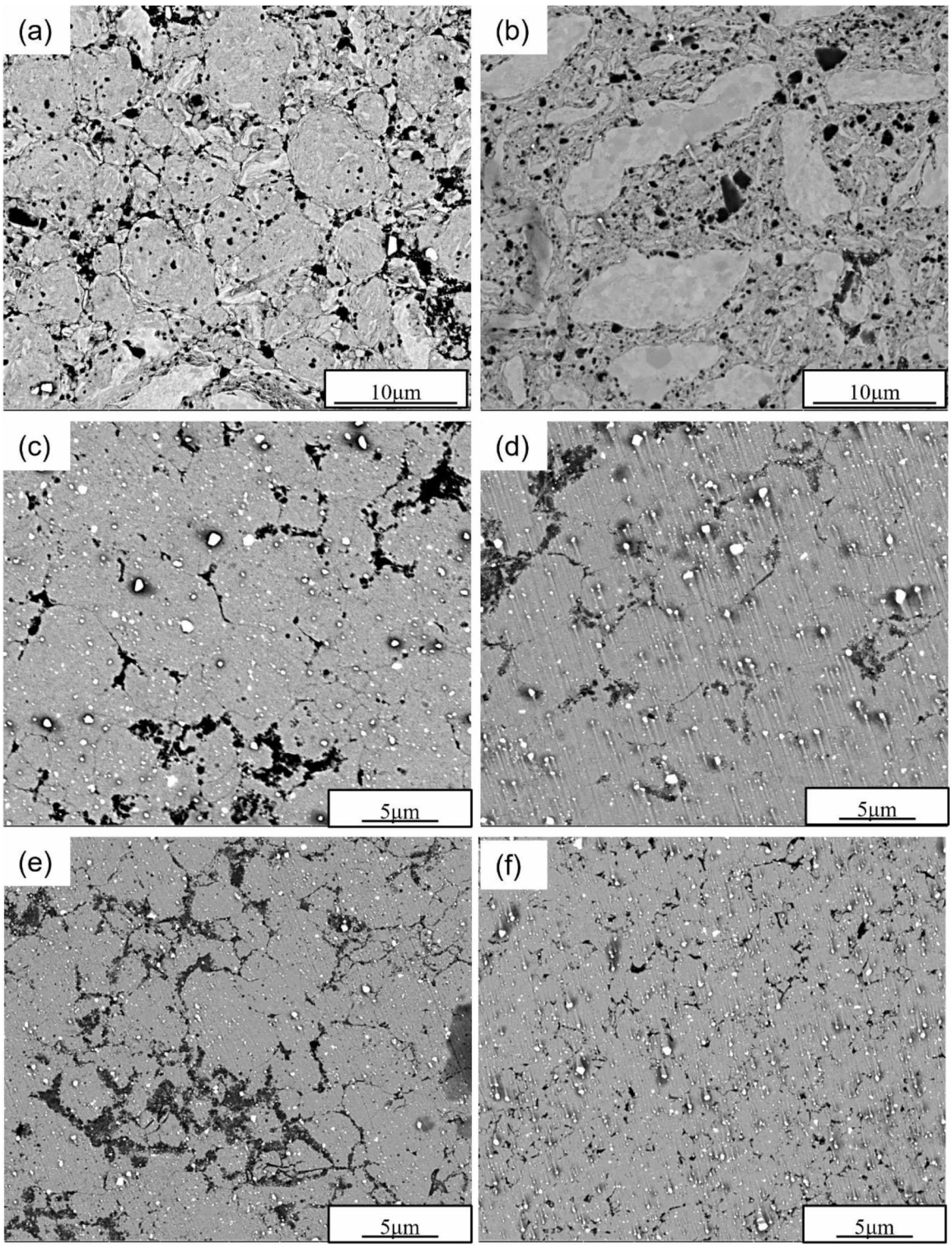

Figure 5.8 SEM images of spark plasma sintered samples with the following conditions for milling duration, ball size, BPR and sintering temperature: (a) 30h, 3mm, 10:1, sintered at 510 °C; (b) 30h, 3mm, 10:1 heat treated then sintered at 510 °C, (c) 30h, 3mm, 10:1 s

It can clearly be observed that samples that were only milled for 10 hours have much rougher microstructure compared to 30h samples which can be attributed to fined powder particles that the samples were sintered from due to longer milling duration. The coarse and non-homogenous microstructure in case of 10h-milled samples also shows that a lower level of alloying has taken place in these alloys compared to the 30h-milled alloys due to the limited milling time. In terms of difference in grain size and homogeneity of the microstructure it can be seen that heat treatment only makes slight changes to the microstructure when 2 samples sintered at the same temperature are compared. On the other hand, a coarser microstructure is observed for both heat-treated and non-heat-treated samples sintered at temperature of 510 °C compared to 470 °C samples even though the initial powder for both 510°C and 470°C samples were the same (heat treated or not). This difference is due to higher sintering temperature which ultimately increases the grain sizes and coarsens the microstructure. These observations can confirm that while milling duration of a powder alloy plays an important role in the microstructure of the sample that is sintered from it, heat treatment is almost un effective on the resultant sample.

5.4.6 Magnetic properties of heat treated and not heat treated sintered FeSiB alloys

Magnetic properties of a magnetic alloy can be influenced by various factors such as the chemical composition of the alloy, the magnetostriction and magnetic anisotropy [155]. Vibrating sample magnetometer results for powder and sintered samples are shown in Figures 5.9 and 5.10 as well as tables 5.4 and 5.5.

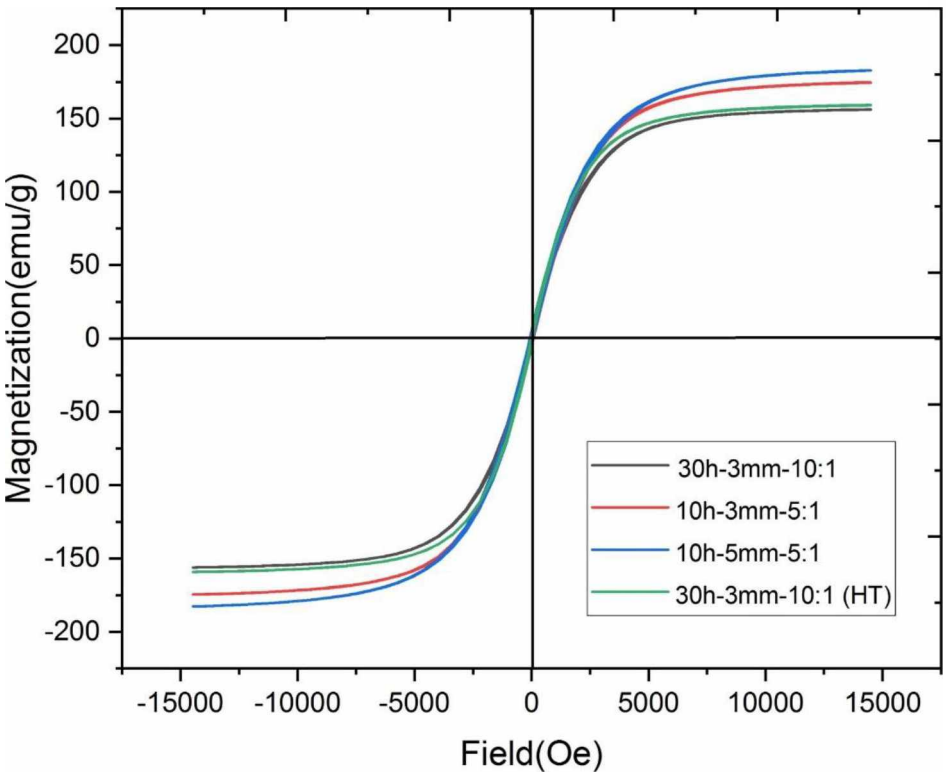

Figure 5.9 Magnetization and coercivity graphs for mechanically alloyed FeSiB samples under different milling conditions

Table 5.4 Magnetization and coercivity values for mechanically alloyed FeSiB samples under different milling conditions

Powder Sample	Ms (emu/g)	Hc (Oe)
7. 30h_3mm_10:1	156.1	56.9
8. 10h_3mm_5:1	174.6	74.2
9. 10h_5mm_5:1	182.8	78.7
10. Heat treated (30h-3mm-10:1)	159.2	44.9

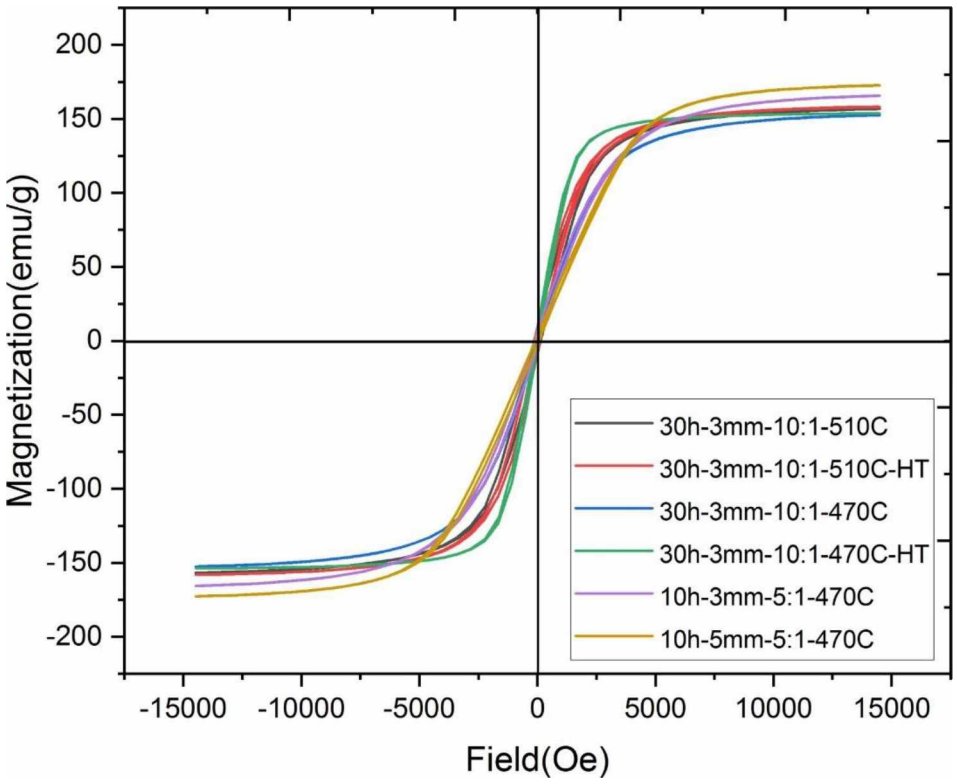

Figure 5.10 Magnetization and coercivity graph for mechanically alloyed FeSiB samples under different milling and SPS conditions

Table 5.5 Magnetization and coercivity values for mechanically alloyed FeSiB samples under different milling and SPS conditions

SPS Sample	Ms (emu/g)	Hc (Oe)
1. 30h_3mm_10:1_510 °C	156.9	137.0
2. 30h_3mm_10:1_510 °C_HT	158.1	139.1
3. 30h_3mm_10:1_470 °C	152.6	33.4
4. 30h_3mm_10:1_470 °C_HT	153.7	46.5
5. 10h_3mm_5:1_470 °C	165.6	99.7
6. 10h_5mm_5:1_470 °C	172.7	65.6

These curves depict the magnetization versus applied magnetic field measured at room temperature for all the samples. The saturation magnetization values from our experiments are high in comparison to the findings of other researchers and the coercivity values are reasonable. For instance, the highest saturation magnetizations observed in our experiments are 182.8 and 172.7 emu/g for powder and sintered samples respectively which are both higher than the highest saturation magnetization value that we obtained from our amorphous powder in our previous studies for mechanical alloying processing parameters of 120h, 350rpm, 10:1 [37][150] and coercivity values as low as 44.9 and 33.4 Oe which are lower than the lowest coercivity value that we have previously observed which was 62.4 Oe. The highest saturation magnetization observed by Gheiratmand et al. [68] who got Ms of 124 emu/g by mechanically alloying amorphous ribbons and consolidating them by spark plasma sintering, Neamtu et al. [98] who got Ms of 131 emu/g for their mechanically alloyed samples and Ms of 141 emu/g after annealing as well as Alleg et al. [196] who observed *Ms* of 14.3 emu/g after 150h of milling their finemet alloy are also lower than our maximum saturation magnetization. The reason for higher saturation magnetization observed from our experiments is due to alloying with optimized parameters as well as refinement of powder grains resulted from mechanical alloying which in turn reduces the magneto crystalline anisotropy which eases the rotation of domain walls and therefore increases the saturation magnetization [156]. From our experiments we observed that the saturation magnetization values for samples sintered from the same powder were proven to be close together. Samples sintered from the amorphous powder that was milled for 30 hours with 700 rpm and 10:1 BPR had saturation magnetization in the range of 152.6 to 158.1 emu/g. Similarly, un-

sintered samples from the amorphous powder, one heat treated and one not heat treated showed magnetic properties close to each other. However, there is a bigger change in magnetic properties when it comes to samples mechanically alloyed with different processing parameters. By changing the milling duration and ball to powder ratio the saturation magnetization changes from the range of 152 to 158 emu/g to 174 to 182 emu/g. Even the change in ball size between the 2 samples milled with 10h and BPR 5:1 are more significant than the changes between two powders milled under the same condition with the only difference being the heat-treatment. Therefore, it can be concluded that mechanical alloying processing parameters have a more significant effect on the magnetic properties of FeSiB-based alloys than heat-treatment. Fig. 5.9 shows the coercivity values for the mechanically alloyed samples. The results show that the coercivity of samples milled for 10h, 5:1 BPR with 5mm balls are very close to 3mm balls sample with the 5mm ball milled sample slightly higher. This is due to the fact that the intensity of the boron phases (Fe_2B and $Fe_{23}B_6$) is higher in case of 5mm powder alloy compared to the 3mm powder alloy. Boron phases that are present in the sample act as pinning sites for magnetic domains and therefore deteriorate the magnetization value. The saturation magnetization of the 10h, 5:1 sample is higher than the 30h and 10:1 sample which might be due to presence of more Fe_3Si phase in the samples sintered from these powder alloys. The same can be said for the comparison between the 10h, 5:1, 5mm and the 10h, 5:1, 3mm samples where the saturation magnetization value is higher in case of the 5mm sample. From the XRD patterns it can be seen that these 2 samples have higher volume fraction of Fe_3Si phase. The higher saturation magnetization in case of 10h_3mm_5:1 and 10h_5mm_5:1 samples sintered at 470 °C can be attributed to

dispersion of large volume fraction of Fe_3Si particles in the amorphous matrix which results in increased saturation magnetization [33].

5.5 Conclusions

FeSiB alloys were fabricated with different processing parameters via mechanical alloying and consolidated via spark plasma sintering at different sintering temperatures. Additionally, the energy induced by a single ball and the total energy of the mechanical alloying process was calculated to determine at what window of energy amorphization of FeSiB-based magnetic alloys takes place. The conclusions from our experiments are as follows:

1) Samples sintered from a heat-treated powder showed higher saturation magnetization but also higher coercivity values.
2) In case of powder alloys, heat treatment helped with decreasing the coercivity, but this was not the case with the sintered samples
3) Using bigger milling balls resulted in higher magnetization and lower coercivity
4) Too low or too high ball to powder ratio hinders the amorphization process. The ideal BPR was found to be 10:1
5) In order to reach amorphization a minimum energy for a single ball is required even if the total energy of the process is in the amorphization window.
6) Mechanical alloying processing parameters have a more significant effect on the magnetic properties of FeSiB-based alloys than heat-treatment.

CHAPTER VI

CONCLUSIONS AND FUTURE WORK

A novel way of processing bulk FeSiB-based alloys was presented in this study. Mechanical alloying process was successfully used for producing amorphous FeSiB-based alloys and spark plasma sintering was used for consolidating the amorphous as well as partially crystalline powder alloys into bulk format.

Effects of different mechanical alloying processing parameters (ball to powder weight ratio and milling duration) were studied on $Fe_{73.5}Si_{13.5}B_9Cu_1Nb_3$ (finemet) alloys. Finemet was milled with relatively low rotation speed of 350 rpm, with milling durations of 30, 60, 90 and 120 hours with ball to powder weight ratio of 10:1 in order to study the effect of milling duration on amorphization, phase transformation, microstructure and mechanical and magnetic properties of the alloy. The main phase observed in all the milled finemet alloys was Fe_3Si. Dispersion of α- Fe_3Si nano crystals in the iron matrix was responsible for the high saturation magnetization values observed in all the finemet alloys. Full amorphization of finemet powder was observed after 120 hours of milling using 3mm milling balls, 10:1 ball to powder ratio and 350 rpm rotation speed. In order to investigate the effect of ball to powder ratio finemet powder was milled for 120 hours using 3mm milling balls, 15:1 ball to powder ratio and 350 rpm rotation speed. The

results showed refinement in crystallite size with an increase in ball to powder weight ratio. Finemet powder milled for 30 to 120 hours using 10:1 ball to powder ratio were then consolidated using the spark plasma sintering technique. The crystallite size of the samples was calculated using the Scherrer method based on the x-ray diffraction data. A significant decrease in the crystallite size of the samples was observed for samples going from 30h milled to 90h milled however, the crystallite size did not decease significantly from 90h to 120h which is in line with grain size changes occurring during the mechanical alloying process where the grains get smaller significantly in the beginning of the milling process but then the rate of particles getting fused together slows down the size reduction speed. The microhardness of finemet samples increased with increase in milling time which is in line with the Hall-Petch relationship which states that the crystallite size and microhardness are inversely correlated.

Effect of adding two elements of copper and niobium to the base FeSiB alloy was studied. Microstructure, mechanical properties, and magnetic behavior of FeSiB, FeSiBCu, FeSiBNb and FeSiBCuNb alloys were studied. Copper containing samples showed both higher saturation magnetization and coercivity values in comparison to niobium containing samples. Both FeSiBCu and FeSiBNb samples had lower saturation magnetization values in comparison to finemet alloy which shows that simultaneous addition of these two elements to the base FeSiB alloy enhances the magnetic properties. According to XRD data the main phase present in FeSiBCu and FeSiBNb samples was Fe_3Si however, some secondary boron phases did appear after the spark plasma sintering process. Crystallite size of the sample containing niobium was smaller than copper containing sample and finemet sample which is due to niobium's ability to prevent grain

growth. Consequently, the microhardness values of the FeSiBNb sample were higher than both FeSiBCu and Finemet sample. FeSiB alloys were mechanically alloyed for 30, 60 and 90 hours with rotation speed of 350 rpm and broadening of α-Fe(Si) peaks was observed as the milling progressed however, full amorphization was not achieved for FeSiB alloy. The magnetic properties of FeSiB improved with longer milling duration with higher saturation magnetization and coercivity almost the same as 60h sample.

Amorphization process and influential mechanical alloying processing parameters of FeSiB alloys were studied in depth in chapter 5. Mechanical alloying processing parameters such as size of the milling balls, ball to powder weight ratio, the degree of filling the milling bowl, rotation speed, PCA and milling duration were investigated. Higher rotation speed of 700 rpm was chosen and in return milling durations were much shorter than our previous experiments from chapters 3 and 4. Bal to powder ratios of 5:1, 10:1 and 15:1 and milling durations of 10, 20 and 30 hours were examined. Two different sizes of milling balls were considered. Milling balls with diameter of 3mm and milling balls with diameter of 5mm. The best result in terms of amorphization was observed with ball to powder weight ratio of 10:1 and milling duration of 30 hours with 3mm milling balls.

Effect of heat treatment on magnetic properties of parts fabricated from annealed and not-annealed powder alloys was studied. The results showed a decrease in the coercivity value of heat-treated powder alloy compared to its not-heat treated counterpart. An improvement in saturation magnetization was observed for heat treated powder alloy and SPS-fabricated alloy sintered from heat treated alloy in comparison to not heat-treated powder alloy and the alloy sintered from powder that was not heat treated. Effect

of spark plasma sintering maximum temperature on magnetic properties of alloys sintered from amorphous FeSiB powder alloy was studied and the results showed an improvement in saturation magnetization in case of sample sintered at higher temperature. However, the coercivity value also increased in case of samples sintered at higher temperatures.

The amount of energy introduced to the milled powder was calculated in chapter 5 based on various mechanical alloying processing parameters. The total energy induced to the powder and energy of a single rotating ball was calculated for three rotation speeds of 350, 500 and 700 rpm, milling ball sizes of 3mm and 5mm, ball to powder weight ratios of 5:1, 10:1 and 15:1 and milling durations of 10, 20, 30, 60, 90 and 120 hours. The x-ray diffraction data from all the milled samples was then studied in order to corelate the amorphization with total energy of the process and the energy of a single milling ball. The result was a milling map designed to depict a window of total energy and a minimum energy for a single ball in which the FeSiB-based alloys will show amorphous structure.

FeSiB-based alloys are proven to have outstanding magnetic properties and very good mechanical properties. The volume fraction of different phases in the material depends on the alloy composition. Fe(Si) phases are known to enhance the saturation magnetization of the FeSiB-based alloys while secondary boron phases are known to increase the coercivity values. The next follow up task would be to study various compositions of iron, silicon and boron processed by mechanical alloying followed by spark plasma sintering in order to discover the optimum composition for milled-SPSed magnetic alloys. Moreover, it has been proven that addition of elements such as copper and niobium improves the magnetic properties of the FeSiB-based alloys. However, mechanical properties, thermal stability, corrosion resistance and other qualities of the

FeSiB-based alloys need more in-depth research. Given the wide application of FeSiB-based alloys in different industries, it is important to improve their properties for use in different environments. Elements such as chromium are known to improve the corrosion resistance of iron-based alloys however, their role on magnetic behavior of iron-based magnetic alloys remains un-known. Effect of addition of elements such as chromium, molybdenum, and phosphorus, which can each improve the mechanical properties of iron-based alloy in some way on magnetic properties of spark plasma sintered amorphous FeSiB-based alloys can be studied in detail in the future.

REFRENCES

[1] R. Hasegawa, Present status of amorphous soft magnetic alloys, J. Magn. Magn Mater. 215 (2000) 240–245.

[2] T. Liu, M. Wang, Z. Zhao, High frequency properties of Fe73.5Cu1Nb3Si13.5B9/ Zn0.5Ni0.5Fe2O4 soft magnetic composite with micro-cellular structure, Sci. China Phys. Mech. Astron. 55 (12) (2012) 2392–2396.

[3] S. Lee, H. Kato, T. Kubota, A. Makino, A. Inoue, Fabrication and soft-magnetic properties of Fe–B–Nb–Y glassy powder compacts by spark plasma sintering technique, Intermetallics 17 (4) (2009) 218–221.

[4] S. Sharma, R. Vaidyanathan, C. Suryanarayana, Criterion for predicting the glass forming ability of alloys, Appl. Phys. Lett. 90 (11) (2007) 111915.

[5] B. Movahedi, M.H. Enayati, C.C. Wong, Study on nano crystallization and amorphization in Fe–Cr–Mo–B–P–Si–C system during mechanical alloying, Mater. Sci. Eng., B 172 (1) (2010) 50–54.

[6] Chen, Q. J., Fan, H. B., Ye, L., Ringer, S., Sun, J. F., Shen, J., & McCartney, D. G. (2005). Enhanced glass forming ability of Fe–Co–Zr–Mo–W–B alloys with Ni addition. *Materials Science and Engineering: A*, *402*(1-2), 188-192.

[7] Suryanarayana, C., & Inoue, A. (2013). Iron-based bulk metallic glasses. *International Materials Reviews*, *58*(3), 131-166

[8] Wang, M., Zan, Z., Deng, N., & Zhao, Z. (2014). Preparation of pure iron/Ni–Zn ferrite high strength soft magnetic composite by spark plasma sintering. *Journal of magnetism and magnetic materials*, *361*, 166-169.

[9] Shen, J., Chen, Q., Sun, J., Fan, H., & Wang, G. (2005). Exceptionally high glass-forming ability of an FeCoCrMoCBY alloy. *Applied Physics Letters*, *86*(15), 151907.

[10] Ouyang, Y., Zhang, J., Chen, H., Liao, S., & Zhong, X. (2008). Crystallization study of amorphous Al82Fe5Ni5Ce8 alloy. *Journal of alloys and compounds*, *454*(1-2), 359-363.

[11] Z. Li, K. Yao, D. Li, X. Ni, Z. Lu, Core loss analysis of Finemet type nanocrystalline alloy ribbon with different thickness, Prog. Nat. Sci.: Materials International 27 (5) (2017) 588–592.

[12] R. Jha, D.R. Diercks, A.P. Stebner, C.V. Ciobanu, Metastable Phase Diagram and Precipitation Kinetics of Magnetic Nanocrystals in FINEMET Alloys, 2017 arXiv preprint arXiv:1709.08306.

[13] R. Alben, J.J. Becker, M.C. Chi, Random anisotropy in amorphous ferromagnets, J. Appl. Phys. 49 (3) (1978) 1653–1658

[14] Y.R. Zhang, R.V. Ramanujan, A study of the crystallization behavior of an amorphous Fe77. 5Si13. 5B9 alloy, Mater. Sci. Eng., A 416 (1–2) (2006) 161–168.

[15] R.V. Ramanujan, Y.R. Zhang, Solid state dendrite formation in an amorphous magnetic Fe77.5Si13.5B9 alloy observed by in situ hot stage transmission electron microscopy, Appl. Phys. Lett. 88 (18) (2006) 182506.

[16] G. Herzer, Grain size dependence of coercivity and permeability in nanocrystalline ferromagnets, IEEE Trans. Magn. 26 (5) (1990) 1397–1402.

[17] V.A. Kataev, Y.N. Starodubtsev, K.O. Bessonova, November). Magnetizing of Finemet-type alloys by magnetization rotation in weak fields, No. 1, J Phy: Confer Series vol. 1389 (2019), 012120. IOP Publishing.

[18] C.C. Koch, Amorphization by mechanical alloying, J. Non-Cryst. Solids 117 (1990) 670–678.

[19] M.H. Enayati, F.A. Mohamed, Application of mechanical alloying/milling for synthesis of nanocrystalline and amorphous materials, Int. Mater. Rev. 59 (7) (2014) 394–416.

[20] McHenry, M. E., Johnson, F., Okumura, H., Ohkubo, T., Ramanan, V. R. V., & Laughlin, D. E. (2003). The kinetics of nanocrystallization and microstructural observations in FINEMET, NANOPERM and HITPERM nanocomposite magnetic materials. *Scripta Materialia*, *48*(7), 881-887

[21] Moya, J. A. (2015). Improving soft magnetic properties in FINEMET-like alloys. A study. *Journal of Alloys and Compounds*, *622*, 635-639.

[22] Alam, T., Borkar, T., Joshi, S. S., Katakam, S., Chen, X., Dahotre, N. B., Ramanujan, R. V., & Banerjee, R. (2015). Influence of niobium on laser de-vitrification of Fe–Si–B based amorphous magnetic alloys. *Journal of Non-Crystalline Solids*, *428*, 75-81

[23] Ponpandian, N., Narayanasamy, A., Chattopadhyay, K., Raja, M. M., Ganesan, K., Chinnasamy, C. N., & Jeyadevan, B. (2003). Low-temperature magnetic properties and the crystallization behavior of FINEMET alloy. *Journal of applied Physics*, *93*(10), 6182-6187.

[24] Singhal, R., & Majumdar, A. K. (1992). Crystallization of glassy Fe80B20-xSix (0⩽ x⩽ 12) alloys. *Journal of magnetism and magnetic materials*, *115*(2-3), 245-249

[25] Cremaschi, V., Avram, I., Perez, T., & Sirkin, H. (2002). Electrochemical studies of amorphous, nanocrystalline, and crystalline FeSiB based alloys. *Scripta materialia*, *46*(1), 95-100.

[26] Okumura, H., Laughlin, D. E., & McHenry, M. E. (2003). Magnetic and structural properties and crystallization behavior of Si-rich FINEMET materials. *Journal of magnetism and magnetic materials*, *267*(3), 347-356.

[27] Marin, P., Vázquez, M., Olofinjana, A. O., & Davies, H. A. (1998). Influence of Cu and Nb on relaxation and crystallization of amorphous FeSiB (CuNb) wires. *Nanostructured materials*, *10*(2), 299-310.

[28] Yoshizawa, Y. A., Oguma, S., & Yamauchi, K. (1988). New Fe-based soft magnetic alloys composed of ultrafine grain structure. *Journal of applied Physics*, *64*(10), 6044-6046.

[29] Zhang, X., del Real, R. P., Vázquez, M., Liang, W., Mesa, J., Jimenez, A., & Lewis, L. H. (2022). Controlling devitrification in the FeSiB system without alloying additions. *Journal of Non-Crystalline Solids*, *576*, 121277.

[30] Xu, J., Liu, X., Wang, Y., Wang, G., Wang, J., Zhou, L., & Yang, Y. (2021). Nanocrystallization, magnetic properties and bending ductility of antiferromagnetic Mn-doped FeSiBCuPC alloys induced by micro-compressive stress annealing. *Journal of Alloys and Compounds*, *882*, 160746.

[31] Duan, L., Wang, K., Wang, E., & Jia, P. (2021). Precipitation of α-Fe from Fe84−xSi4B12+ x (x= 1, 3) Amorphous Alloys Under High Magnetic Field Annealing. *Acta Metallurgica Sinica (English Letters)*, *34*(8), 1163-1172.

[32] Saad, M., & Poulain, M. (1987). Glass forming ability criterion. In *Materials Science Forum* (Vol. 19, pp. 11-18). Trans Tech Publications Ltd.

[33] AR, Y., & Drbohlav, O. (1995). Thermodynamics and kinetics of nanostructure formation in soft-magnetic nanocrystalline alloys (overview). *Materials Transactions, JIM*, *36*(7), 896-902.

[34] Duhaj, P., Mat'ko, I., Švec, P., & Janičkovič, D. (1995). Structural characterization of the finemet type alloys. *Journal of non-crystalline solids*, *192*, 561-564

[35] Jha, R., Diercks, D. R., Chakraborti, N., Stebner, A. P., & Ciobanu, C. V. (2019). Interfacial energy of copper clusters in Fe-Si-B-Nb-Cu alloys. *Scripta Materialia*, *162*, 331-334

[36] Jiang, D., Zhou, B., Jiang, B., Ya, B., & Zhang, X. (2017). Study on soft magnetic properties of Finemet-type nanocrystalline alloys with Mo substituting for Nb. *physica status solidi (a)*, *214*(10), 1700074

[37] T. Larimian, V. Chaudhary, J. Christudasjustus, R.V. Ramanujan, R. Gupta, T. Borkar, Bulk-nano spark plasma sintered Fe-Si-B-Cu-Nb based magnetic alloys, Intermetallics 124 (2020) 106869.

[38] Graf, T., Hampel, G., Korus, J., Hesse, J., & Herzer, G. (1995). Influence of Nb concentration on structure and crystallization onset of amorphous Fe (Cu, Nb) SiB FINEMET alloys. *Nanostructured Materials*, *6*(1-4), 469-472.

[39] Ruckman, M. W., Levy, R. A., Kessler, A., & Hasegawa, R. (1980). Mössbauer and X-ray studies of the kinetics of crystallization in glassy Fe□ B alloys. *Journal of Non-Crystalline Solids*, *40*(1-3), 393-406.

[40] M.A. Gibson, G.W. Delamore, Nucleation kinetics of primary crystallization products in FeSiB metallic glasses, J. Mater. Sci. 27 (13) (1992) 3533–3538.

[41] I. Mat'ko, E. Illekova, ´ P. Svec, ˇ P. Duhaj, Crystallization characteristics in the FeSiB glassy ribbon system, Mater. Sci. Eng., A 225 (1–2) (1997) 145–152.

[42] H. Chiriac, C.S. Marinescu, New position sensor based on ultra-acoustic standing waves in FeSiB amorphous wires, Sensor Actuator Phys. 81 (1–3) (2000) 174–175.

[43] C. Smith, S. Katakam, S. Nag, Y.R. Zhang, J.Y. Law, R.V. Ramanujan, N.B. Dahotre, R. Banerjee, Comparison of the crystallization behavior of Fe-Si-B-Cu and Fe-Si-BCu-Nb-based amorphous soft magnetic alloys, Metall. Mater. Trans. 45 (7) (2014) 2998–3009.

[44] Y.R. Zhang, R.V. Ramanujan, The effect of niobium alloying additions on the crystallization of a Fe–Si–B–Nb alloy, J. Alloys Compd. 403 (1–2) (2005) 197–205.

[45] M. Matsuura, M. Nishijima, K. Takenaka, A. Takeuchi, H. Ofuchi, A. Makino, Evolution of fcc Cu clusters and their structure changes in the soft magnetic Fe85.2Si1B9P4Cu0.8 (NANOMET) and FINEMET alloys observed by X-ray absorption fine structure, J. Appl. Phys. 117 (17) (2015) 17A324.

[46] Rixecker, G., Schaaf, P., & Gonser, U. (1992). Crystallization behaviour of amorphous Fe73. 5Cu1Nb3Si13. 5B9. *Journal of Physics: Condensed Matter*, *4*(50), 10295.

[47] Inoue, A., & Gook, J. S. (1995). Multicomponent Fe-based glassy alloys with wide supercooled liquid region before crystallization. *Materials Transactions, JIM*, *36*(10), 1282-1285.

[48] Enomoto, M., & Aaronson, H. I. (1986). Nucleation kinetics of proeutectoid ferrite at austenite grain boundaries in Fe-CX alloys. *Metallurgical Transactions A*, *17*(8), 1385-1397.

[49] Suslick, K. S., Choe, S. B., Cichowlas, A. A., & Grinstaff, M. W. (1991). Sonochemical synthesis of amorphous iron. *nature*, *353*(6343), 414-416..

[50] Maeland, A. J. (1978). Comparison of hydrogen absorption in glassy and crystalline structures. In *Hydrides for Energy Storage* (pp. 447-462). Pergamon.

[51] Chen, H. S. (1980). Glassy metals. *Reports on Progress in Physics*, *43*(4), 353

[52] Shirzadi, A. A., Kozieł, T., Cios, G., & Bała, P. (2019). Development of Auto Ejection Melt Spinning (AEMS) and its application in fabrication of cobalt-based ribbons. *Journal of Materials Processing Technology*, *264*, 377-381.

[53] E. Fechova, P. Kollar, J. Füzer, J. Kov ac, P. Petrovic, V. Kavecansky, The influence of the long time milling on the structure and magnetic properties of the Fe–Cu–Nb–Si–B powder, Mater. Sci. Eng., B 107 (2) (2004) 155–160

[54] J. Intrater, Mechanical Alloying and Milling, c. Suryanarayana, 2007

[55] A.W. Weeber, H. Bakker, Amorphization by ball milling. A review, Phys. B Condens. Matter 153 (1–3) (1988) 93–135.

[56] Hu, Z. Q., Wang, A. M., & Zhang, H. F. (2017). Amorphous Materials. In *Modern Inorganic Synthetic Chemistry* (pp. 641-667).

[57] Y. Zhang, Nanyang Technological University, Ph.D. thesis, 2007.

[58] J. Long, P.R. Ohodnicki, D.E. Laughlin, M.E. McHenry, T. Ohkubo, K. Hono, Structural studies of secondary crystallization products of the Fe 23 B 6-type in a nanocrystalline FeCoB-based alloy, J. Appl. Phys. 101 (9) (2007), 09N114.

[59] E.C. Passamani, J.R.B. Tagarro, C. Larica, A.A.R. Fernandes, Thermal studies and magnetic properties of mechanical alloyed Fe2B, J. Phys. Condens. Matter 14 (8) (2002) 1975.

[60] Schwarz, R. B., & Johnson, W. L. (1983). Formation of an amorphous alloy by solid-state reaction of the pure polycrystalline metals. *Physical Review Letters*, *51*(5), 415.

[61] Zhao, Y. H. (2006). Thermodynamic model for solid-state amorphization of pure elements by mechanical-milling. *Journal of Non-Crystalline Solids*, *352*(52-54), 5578-5585

[62] Schultz, L. (1988). Formation of amorphous metals by mechanical alloying. *Materials Science and Engineering*, *97*, 15-23.

[63] T. Voisin, L. Durand, N. Karnatak, S. Le Gallet, M. Thomas, Y. Le Berre, A. Couret, Temperature control during spark plasma sintering and application to up-scaling and complex shaping, J. Mater. Process. Technol. 213 (2) (2013) 269–278.

[64] Liu, Y. J., Chang, I. T. H., & Bowen, P. (2001). Amorphization and microstructural evolution in multicomponent $(FeCoNi)_{70}Zr_{10}B_{20}$ alloy system by mechanical alloying. *Materials Science and Engineering: A*, *304*, 389-393.

[65] Cavaliere, P., Sadeghi, B., & Shabani, A. (2019). Spark plasma sintering: process fundamentals. In *Spark plasma sintering of materials* (pp. 3-20). Springer, Cham.

[66] Xiao, Z., Tang, C., Zhao, H., Zhang, D., & Li, Y. (2012). Effects of sintering temperature on microstructure and property evolution of Fe81Cu2Nb3Si14 soft magnetic materials fabricated from amorphous melt-spun ribbons by spark plasma sintering technique. *Journal of non-crystalline solids*, *358*(1), 114-118.

[67] Neamţu, B. V., Marinca, T. F., Chicinaş, I., Isnard, O., Popa, F., & Pâşcuţă, P. (2014). Preparation and soft magnetic properties of spark plasma sintered compacts based on Fe–Si–B glassy powder. *Journal of alloys and compounds*, *600*, 1-7.

[68] Gheiratmand, T., Hosseini, H. M., Davami, P., & Sarafidis, C. (2016). Fabrication of FINEMET bulk alloy from amorphous powders by spark plasma sintering. *Powder Technology*, *289*, 163-168.

[69] Yang, Z. H., Jia, D. C., Zhou, Y., & Yu, C. Q. (2007). Fabrication and characterization of amorphous SiBCN powders. *Ceramics international*, *33*(8), 1573-1577.

[70] Aydinbeyli, N., Celik, O. N., Gasan, H., & Aybar, K. (2006). Effect of the heating rate on crystallization behavior of mechanically alloyed Mg50Ni50 amorphous alloy. *International journal of hydrogen energy*, *31*(15), 2266-2273.

[71] El-Eskandarany, M. S., Aoki, K., Itoh, H., & Suzuki, K. (1991). Effect of ball-to-powder weight ratio on the amorphization reaction of Al50Ta50 by ball milling. *Journal of the Less common Metals*, *169*(2), 235-244.

[72] Suryanarayana, C. (2001). Mechanical alloying and milling. *Progress in materials science*, *46*(1-2), 1-184.

[73] Herzer, G. (1997). Nanocrystalline soft magnetic alloys. *Handbook of magnetic materials*, *10*, 415-462.

[74] Raja, M. M., Chattopadhyay, K., Majumdar, B., & Narayanasamy, A. (2000). Structure and soft magnetic properties of Finemet alloys. *Journal of Alloys and Compounds*, *297*(1-2), 199-205.

[75] Tong, X., Zhang, Y., Wang, Y., Liang, X., Zhang, K., Zhang, F., ... & Wang, W. (2022). Structural origin of magnetic softening in a Fe-based amorphous alloy upon annealing. *Journal of Materials Science & Technology*, *96*, 233-240.

[76] Carr, G. E., Davies, H. A., & Buckley, R. A. (1988). Crystallite size determinations for melt-spun Fe-Nd-B permanent magnet alloys. *Materials Science and Engineering*, *99*(1-2), 147-151

[77] Hartridge, A., Bhattacharya, A. K., Sengupta, M., Majumdar, C. K., Das, D., & Chintalapudi, S. N. (1997). Crystallite size dependence on the magnetic properties of nanocrystalline magnetite powders. *Journal of magnetism and magnetic materials*, *176*(2-3), L89-L92

[78] Berkowitz, A. E., & Schuele, W. J. (1959). Magnetic properties of some ferrite micropowders. *Journal of Applied Physics*, *30*(4), S134-S135

[79] Zhang, Y. F., Lu, L., & Yap, S. M. (1999). Prediction of the amount of PCA for mechanical milling. *Journal of Materials Processing Technology*, *89*, 260-265.

[80] P. Scherrer, R. Zsigmondy, Gottinger " Nachrichten, Kolloidchemie (3rd, 1920, p. 394, 1918)

[81] Heiman, N., Hempstead, R. D., & Kazama, N. (1978). Low-coercivity amorphous magnetic alloy films. *Journal of Applied Physics*, *49*(11), 5663-5667.

[82] M.E. McHenry, M.A. Willard, D.E. Laughlin, Amorphous and nanocrystalline materials for applications as soft magnets, Prog. Mater. Sci. 44 (4) (1999) 291–433.

[83] Yoshizawa, Y. (1999). Magnetic properties and microstructure of nanocrystalline Fe-based alloys. In *Materials Science Forum* (Vol. 307, pp. 51-62). Trans Tech Publications Ltd.

[84] Murugaiyan, P., Mitra, A., Jena, P. S. M., Mahato, B., Ghosh, M., Roy, R. K., & Panda, A. K. (2021). Grain refinement in Fe-rich FeSiB (P) NbCu nanocomposite alloys through P compositional modulation. *Materials Letters*, *295*, 129852.

[85] López-Sánchez, J., Navarro, E., Rodríguez-Granado, F., Serrano, A., & Marín, P. (2021). Multiphase materials based on the Fe73. 9Si15. 5Cu1Nb3B6. 6 alloy obtained by dry and wet high-energy ball milling processes. *Journal of Alloys and Compounds*, *864*, 158136.

[86] Meng, Y., Pang, S., Chang, C., Bai, X., & Zhang, T. (2021). Nanocrystalline Fe83Si4B10P2Cu1 ribbons with improved soft magnetic properties and bendability prepared via rapid annealing of the amorphous precursor. *Journal of Magnetism and Magnetic Materials*, *523*, 167583.

[87] Sharma, P., & Gupta, A. (2006). Ion beam sputtered thin films of finemet alloy for soft magnetic applications. *Nuclear Instruments and Methods in Physics Research Section B: Beam Interactions with Materials and Atoms*, *244*(1), 105-109.

[88] Zhang, Z., Jiang, Z., Meng, L., Yu, H., Ma, H., & Guan, L. (2021). The Magnetic Properties and Glass Formation Ability of the Fe80Si8B6Nb5Cu Amorphous-

Nanocrystalline Alloys with Different Phosphorus Addition. *Journal of Superconductivity and Novel Magnetism*, *34*(2), 519-523.

[89] J.M. Borrego, A. Conde, Nanocrystallization behaviour of FeSiBCu (NbX) alloys, Mater. Sci. Eng., A 226 (1997) 663–667.

[90] Y.R. Zhang, R.V. Ramanujan, Characterization of the effect of alloying additions on the crystallization of an amorphous Fe73. 5Si13. 5B9Nb3Cu1 alloy, Intermetallics 14 (6) (2006) 710–714.

[91] R.V. Ramanujan, Y.R. Zhang, Quantitative transmission electron microscopy analysis of the nanocrystallization kinetics of soft magnetic alloys, Phys. Rev. B 74 (22) (2006) 224408.

[92] Livingston, J. D. (1981). A review of coercivity mechanisms. *Journal of Applied Physics*, *52*(3), 2544-2548.

[93] Zhai, X. B., Wang, Y. G., Zhu, L., Zheng, H., Dai, Y. D., Chen, J. K., & Pan, F. M. (2019). Influence of Ni substitution for B on crystallization behavior, microstructure and magnetic properties of FeBCu alloys. *Journal of Magnetism and Magnetic Materials*, *480*, 47-52.

[94] D.H. Ping, K. Hono, H. Kanekiyo, S. Hirosawa, Microstructural evolution of Fe 3 B/ Nd 2 Fe 14 B nanocomposite magnets microalloyed with Cu and Nb, Acta Mater. 47 (18) (1999) 4641–4651.

[95] Czyż, O., Kusiński, J., Radziszewska, A., Liao, Z., Zschech, E., Kąc, M., & Ostrowski, R. (2020). Study of Structure and Properties of Fe-Based Amorphous Ribbons after Pulsed Laser Interference Heating. *Journal of Materials Engineering and Performance*, *29*(10), 6277-6285.

[96] S. Alleg, S. Kartout, M. Ibrir, S. Azzaza, N.E. Fenineche, J.J. Sunol, Magnetic, ~ structural and thermal properties of the Finemet-type powders prepared by mechanical alloying, J. Phys. Chem. Solid. 74 (4) (2013) 550–557

[97] E.Y. Kang, Y.B. Kim, K.Y. Kim, Y.H. Chung, H.K. Baik, vacuum hot pressing of Fe–Si–B–Nb-based amorphous powder cores and their high-frequency magnetic properties, J. Appl. Phys. 99 (8) (2006), 08F111.

[98] B.V. Neamt¸u, H.F. Chicinas¸, T.F. Marinca, O. Isnard, O. Pana, I. Chicinas¸, Amorphisation of Fe-based alloy via wet mechanical alloying assisted by PCA decomposition, Mater. Chem. Phys. 183 (2016) 83–92.

[99] Vaidya, M., Muralikrishna, G. M., & Murty, B. S. (2019). High-entropy alloys by mechanical alloying: A review. *Journal of Materials Research*, *34*(5), 664-686.

[100] Mucsi, G. (2019). A review on mechanical activation and mechanical alloying in stirred media mill. *Chemical Engineering Research and Design*, *148*, 460-474.

[101] Benjamin, J. S., & Volin, T. E. (1974). The mechanism of mechanical alloying. *Metallurgical Transactions*, *5*(8), 1929-1934.

[102] Benjamin, J. S. (1976). Mechanical alloying. *Scientific American*, *234*(5), 40-49.

[103] Lü, L., & Lai, M. O. (1997). *Mechanical alloying*. Springer Science & Business Media.

[104] Benjamin, J. S. (1992). Fundamentals of mechanical alloying. In *Materials Science Forum* (Vol. 88, pp. 1-18). Trans Tech Publications Ltd.

[105] B.S. Murty, S. Ranganathan, Novel materials synthesis by mechanical alloying/ milling, Int. Mater. Rev. 43 (3) (1998) 101–141.

[106] Calka, A., & Radlinski, A. P. (1991). Universal high performance ball-milling device and its application for mechanical alloying. *Materials Science and Engineering: A, 134*, 1350-1353.

[107] C. Suryanarayana, A. Inoue, Bulk Metallic Glasses, CRC press, 2017.

[108] L. Xie, A. Wang, S. Yue, A. He, C. Chang, Q. Li, C.T. Liu, Significant improvement of soft magnetic properties for Fe-based nanocrystalline alloys by inhibiting surface crystallization via a magnetic field assisted melt-spinning process, J. Magn. Magn Mater. 483 (2019) 158–163.

[109] Kase, S., & Matsuo, T. (1965). Studies on melt spinning. I. Fundamental equations on the dynamics of melt spinning. *Journal of Polymer Science Part A: General Papers*, *3*(7), 2541-2554.

[110] Karpe, B., Kosec, B., & Bizjak, M. (2012). Analyses of the melt cooling rate in the melt-spinning process. *J. Achiev. Mater. Manuf. Eng*, *51*(2), 59-65.

[111] Bryant, Y. G. (1999, November). Melt spun fibers containing microencapsulated phase change material. In *ASME International Mechanical Engineering Congress and Exposition* (Vol. 16431, pp. 225-234). American Society of Mechanical Engineers.

[112] Fair, G. H., & Wood, J. V. (1994). Mechanical alloying of Fe-Al intermetallics in the DO3 composition range. *Journal of materials science*, *29*(7), 1935-1939.

[113] J. Torrens-Serra, P. Bruna, S. Roth, J. Rodriguez-Viejo, M.T. Clavaguera-Mora, Bulk soft magnetic materials from ball-milled Fe77Nb7B15Cu1 amorphous ribbons, Intermetallics 17 (1–2) (2009) 79–85.

[114] El-Eskandarany, M. S., Bahgat, A. A., Gomaa, N. S., & Eissa, N. A. (1999). Kinetics and formation mechanism of amorphous Fe52Nb48 alloy powder fabricated by mechanical alloying. *Journal of Alloys and compounds*, *290*(1-2), 181-190.

[115] Zaitsev, A. I., Natal'ya, E. Z., Alexeeva, J. P., Dunaev, S. F., & Nechaev, Y. S. (2003). Thermodynamics and amorphization of the copper–zirconium alloys. *Physical Chemistry Chemical Physics*, *5*(19), 4185-4196.

[116] W.L. Johnson, Thermodynamic and kinetic aspects of the crystal to glass transformation in metallic materials, Prog. Mater. Sci. 30 (2) (1986) 81–134.

[117] Delogu, F., & Cocco, G. (2007). Kinetics of amorphization processes by mechanical alloying: a modeling approach. *Journal of alloys and compounds*, *436*(1-2), 233-240.

[118] Li, X., Wen, X., Zhao, H., Ma, Z., Yu, L., Li, C., ... & Liu, Y. (2019). The formation and evolution mechanism of amorphous layer surrounding Nb nano-grains in Nb-Al system during mechanical alloying process. *Journal of Alloys and Compounds*, *779*, 175-182.

[119] S.W. Du, R.V. Ramanujan, Mechanical alloying of Fe–Ni based nanostructured magnetic materials, J. Magn. Magn Mater. 292 (2005) 286–298.

[120] Schwarz, R. B., & Koch, C. C. (1986). Formation of amorphous alloys by the mechanical alloying of crystalline powders of pure metals and powders of intermetallics. *Applied Physics Letters*, *49*(3), 146-148.

[121] E. Hellstern, L. Schultz, Progress of the amorphization reaction during mechanical alloying in Fe-Zr, J. Appl. Phys. 63 (5) (1988) 1408–1413.

[122] Yurkova, A. I., Cherniavsky, V. V., Bolbut, V., Krüger, M., & Bogomol, I. (2019). Structure formation and mechanical properties of the high-entropy AlCuNiFeCr alloy prepared by mechanical alloying and spark plasma sintering. *Journal of Alloys and Compounds*, *786*, 139-148.

[123] H.F. Li, R.V. Ramanujan, Microstructural evolution and nanocrystalline formation kinetics in FeCo based alloys during mechanical alloying, in: Journal of Metastable

[124] B.V. Neamt¸u, T.F. Marinca, I. Chicinas¸, O. Isnard, Structural, magnetic and thermal characterization of amorphous FINEMET powders prepared by wet mechanical alloying, J. Alloys Compd. 626 (2015) 49–55.

[125] Chang, J., Zhan, T., Peng, X., Li, J., Yang, Y., Xu, J., ... & Ge, H. (2021). Improved permeability and core loss of amorphous FeSiB/Ni-Zn ferrite soft magnetic composites prepared in an external magnetic field. *Journal of Alloys and Compounds*, *886*, 161335.

[126] Alleg, S., Drablia, R., & Fenineche, N. (2018). Effect of the Laser Scan Rate on the Microstructure, Magnetic Properties, and Microhardness of Selective Laser-Melted FeSiB. *Journal of Superconductivity and Novel Magnetism*, *31*(11), 3565-3577.

[127] Suzuki, K., & Herzer, G. (2006). Soft magnetic nanostructures and applications. In *Advanced Magnetic Nanostructures* (pp. 365-401). Springer, Boston, MA.

[128] Rong, C., & Shen, B. (2018). Nanocrystalline and nanocomposite permanent magnets by melt spinning technique. *Chinese Physics B*, *27*(11), 117502.

[129] Neamțu, B. V., Chicinaş, H. F., Ababei, G., Gabor, M., Marinca, T. F., Lupu, N., & Chicinaş, I. (2017). A comparative study of the Fe-based amorphous alloy prepared by mechanical alloying and rapid quenching. *Journal of Alloys and Compounds*, *703*, 19-25.

[130] Surinach, S., Baró, M. D., Segura, J., Clavaguera-Mora, M. T., & Clavaguera, N. (1991). Amorphization of soft magnetic alloys by the mechanical alloying technique. *Materials Science and Engineering: A*, *134*, 1368-1371.

[131] Eckert, J., Schultz, L., Hellstern, E., & Urban, K. (1988). Glass-forming range in mechanically alloyed Ni-Zr and the influence of the milling intensity. *Journal of applied physics*, *64*(6), 3224-3228

[132] Watanabe, R., Hashimoto, H., & Lee, G. G. (1995). Computer simulation of milling ball motion in mechanical alloying (overview). *Materials Transactions, JIM*, *36*(2), 102-109.

[133] Ghobrial, S., Kirk, D. W., & Thorpe, S. J. (2018). Solid state amorphization in the Ni-Nb-Y system by mechanical alloying. *Journal of Non-Crystalline Solids*, *502*, 1-8.

[134] Kochetov, N. A., Rogachev, A. S., Shchukin, A. S., Vadchenko, S. G., & Kovalev, I. D. (2019). Mechanical alloying with the partial amorphization of the Fe–Cr–Co–Ni–Mn multicomponent powder mixture and its spark plasma sintering to produce a compact high-entropy material. *Russian Journal of Non-Ferrous Metals*, *60*(3), 268-273.

[135] Gaffet, E. (1991). Planetary ball-milling: an experimental parameter phase diagram. *Materials Science and Engineering: A*, *132*, 181-193.

[136] Burgio, N., Iasonna, A., Magini, M., Martelli, S., & Padella, F. (1991). Mechanical alloying of the Fe– Zr system. Correlation between input energy and end products. *Il nuovo cimento D*, *13*(4), 459-476.

[132] Mamedov, V. (2002). Spark plasma sintering as advanced PM sintering method. *Powder Metallurgy*, *45*(4), 322-328.

[133] Guillon, O., Gonzalez-Julian, J., Dargatz, B., Kessel, T., Schierning, G., Räthel, J., & Herrmann, M. (2014). Field-assisted sintering technology/spark plasma sintering: mechanisms, materials, and technology developments. *Advanced Engineering Materials*, *16*(7), 830-849.

[134] Hulbert, D. M., Anders, A., Andersson, J., Lavernia, E. J., & Mukherjee, A. K. (2009). A discussion on the absence of plasma in spark plasma sintering. *Scripta Materialia*, *60*(10), 835-838.

[135] Yue, M., Zhang, J. X., Liu, W. Q., & Wang, G. P. (2004). Chemical stability and microstructure of Nd-Fe-B magnet prepared by spark plasma sintering. *Journal of magnetism and magnetic materials*, *271*(2-3), 364-368.

[136] Gheiratmand, T., Hosseini, H. M., & Reihani, S. S. (2017). Iron-borosilicate soft magnetic composites: The correlation between processing parameters and magnetic properties for high frequency applications. *Journal of Magnetism and Magnetic Materials*, *429*, 241-250.

[137] Sundaresan, R., & Froes, F. H. (1987). Mechanical alloying. *JOM*, *39*(8), 22-27.

[138] Soni, P. R. (2000). *Mechanical alloying: fundamentals and applications*. Cambridge Int Science Publishing.

[138] Koch, C. C., Cavin, O. B., McKamey, C. G., & Scarbrough, J. O. (1983). Preparation of ''amorphous''Ni60Nb40 by mechanical alloying. *Applied Physics Letters*, *43*(11), 1017-1019.

[139] Hellstern, E., & Schultz, L. (1986). Amorphization of transition metal Zr alloys by mechanical alloying. *Applied physics letters*, *48*(2), 124-126.

[140] Veltl, G., Scholz, B., & Kunze, H. D. (1991). Amorphization of Cu Ta alloys by mechanical alloying. *Materials Science and Engineering: A*, *134*, 1410-1413.

[141] Suryanarayana, C., Chen, G. H., Frefer, A., & Froes, F. H. (1992). Structural evolution of mechanically alloyed Ti□ Al alloys. *Materials Science and Engineering: A*, *158*(1), 93-101.

[142] Murty, B. S., Rao, M. M., & Ranganathan, S. (1995). Milling maps and amorphization during mechanical alloying. *Acta Metallurgica et Materialia*, *43*(6), 2443-2450.

[143] Magini, M., & Iasonna, A. (1995). Energy transfer in mechanical alloying (overview). *Materials Transactions, JIM*, *36*(2), 123-133.

[144] Magini, M., Iasonna, A., & Padella, F. (1996). Ball milling: an experimental support to the energy transfer evaluated by the collision model. *Scripta Materialia*, *34*(1).

[145] Magini, M., Colella, C., Iasonna, A., & Padella, F. (1998). Power measurements during mechanical milling—II. The case of "single path cumulative" solid state reaction. *Acta materialia*, *46*(8), 2841-2850.

[146] Bhatt, J., & Murty, B. S. (2008). On the conditions for the synthesis of bulk metallic glasses by mechanical alloying. *Journal of Alloys and Compounds*, *459*(1-2), 135-141.

[147] Suryanarayana, C., Ivanov, E., & Boldyrev, V. V. (2001). The science and technology of mechanical alloying. *Materials Science and Engineering: A*, *304*, 151-158.

[148] Kumar, A., Swarnakar, A. K., & Chopkar, M. (2018). Phase evolution and mechanical properties of AlCoCrFeNiSi x high-entropy alloys synthesized by mechanical alloying and spark plasma sintering. *Journal of Materials Engineering and Performance*, *27*(7), 3304-3314.

[149] Joardar, J., Pabi, S. K., & Murty, B. S. (2007). Milling criteria for the synthesis of nanocrystalline NiAl by mechanical alloying. *Journal of Alloys and Compounds*, *429*(1-2), 204-210.

[150] Larimian, T., Chaudhary, V., Khan, M. U. F., Ramanujan, R. V., Gupta, R. K., & Borkar, T. (2021). Spark plasma sintering of Fe–Si–B–Cu–Nb/Finemet based alloys. *Intermetallics*, *129*, 107035.

[151] Peng, J., Yang, J., Zhang, T., Song, X., & Chen, Y. (2004). Preparation and characterization of Fe substituted CoSb3 skutterudite by mechanical alloying and annealing. *Journal of alloys and compounds*, *381*(1-2), 313-316.

[152] A.K. Sinha, M.N. Singh, A. Upadhyay, M. Satalkar, M. Shah, N. Ghodke, S.N. Kane, L.K. Varga, A correlation between the magnetic and structural properties of isochronally annealed Cu-free FINEMET alloy with composition Fe72B19.2Si4.8Nb4, Appl. Phys. A 118 (1) (2015) 291–299

[153] Kotan, H., Saber, M., Koch, C. C., & Scattergood, R. O. (2012). Effect of annealing on microstructure, grain growth, and hardness of nanocrystalline Fe–Ni alloys

prepared by mechanical alloying. *Materials Science and Engineering: A*, *552*, 310-315.

[154] Mo, W., Zhang, L., Shan, A., Cao, L., Wu, J., & Komuro, M. (2007). Microstructure and magnetic properties of NdFeB magnet prepared by spark plasma sintering. *Intermetallics*, *15*(11), 1483-1488.

[155] Nagesha, K., Rajanish, M., & Shivappa, D. (2013). A review on mechanical alloying. *change*, *3*.

[156] R.C. O'handley, Modern Magnetic Materials: Principles and Applications, Wiley, 2000.

APPENDIX

PUBLICATIONS

- Christudasjustus, J., **Larimian, T.**, Esquivel, J., Gupta, S., Darwish, A. A., Borkar, T., & Gupta, R. K. (2022). Aluminum alloys with high elastic modulus. *Materials Letters*, *320*, 132292.
- **Larimian, T.,** Chaudhary, V., Khan, M. U. F., Ramanujan, R. V., Gupta, R. K., & Borkar, T. (2021). Spark plasma sintering of Fe–Si–B–Cu–Nb/Finemet based alloys. *Intermetallics*, *129*, 107035.
- **Larimian, T.,** AlMangour, B., Grzesiak, D., Walunj, G., & Borkar, T. (2021). Effect of Laser Spot Size, Scanning Strategy, Scanning Speed, and Laser Power on Microstructure and Mechanical Behavior of 316L Stainless Steel Fabricated via Selective Laser Melting. *Journal of Materials Engineering and Performance*, 1-20.
- Farooq Khan, M. U., **Larimian, T.,** Borkar, T., & Gupta, R. K. (2021). Corrosion behavior and hardness of binary Mg alloys produced via high-energy ball-milling and subsequent spark plasma sintering. *Corrosion*, *77*(2), 228-241.
- Walunj, G., Bearden, A., Patil, A., Larimian, T., Christudasjustus, J., Gupta, R., & Borkar, T. (2021). The Effect of Titanium Carbide and Spark Plasma Sintering Processing on Nickel–Titanium Carbide Composites. In *Metal-Matrix Composites* (pp. 65-73). Springer, Cham.
- **Larimian, T.,** Chaudhary, V., Christudasjustus, J., Ramanujan, R. V., Gupta, R., & Borkar, T. (2020). Bulk-nano spark plasma sintered Fe-Si-B-Cu-Nb based magnetic alloys. *Intermetallics*, *124*, 106869.

- Walunj, G., Bearden, A., Patil, A., **Larimian, T.,** Christudasjustus, J., Gupta, R. K., & Borkar, T. (2020). Mechanical and Tribological Behavior of Mechanically Alloyed Ni-TiC Composites Processed via Spark Plasma Sintering. *Materials*, *13*(22), 5306.
- **Larimian, T.,** Kannan, M., Grzesiak, D., AlMangour, B., & Borkar, T. (2020). Effect of energy density and scanning strategy on densification, microstructure and mechanical properties of 316L stainless steel processed via selective laser melting. *Materials Science and Engineering: A*, *770*, 138455.
- **Larimian, T.,** & Borkar, T. (2019). Additive manufacturing of in situ metal matrix composites. In *Additive Manufacturing of Emerging Materials* (pp. 1-28). Springer, Cham.
- Mavros, N., **Larimian, T.,** Esqivel, J., Gupta, R. K., Contieri, R., & Borkar, T. (2019). Spark plasma sintering of low modulus titanium-niobium-tantalum-zirconium (TNTZ) alloy for biomedical applications. *Materials & Design*, *183*, 108163.